

2019

## Detection of Mercury Through Surface Plasmon Resonance of Immobilized Gold Nanorods

Khang Trieu  
*University of Central Florida*

 Part of the [Chemistry Commons](#)

Find similar works at: <https://stars.library.ucf.edu/etd>

University of Central Florida Libraries <http://library.ucf.edu>

This Doctoral Dissertation (Open Access) is brought to you for free and open access by STARS. It has been accepted for inclusion in Electronic Theses and Dissertations by an authorized administrator of STARS. For more information, please contact [STARS@ucf.edu](mailto:STARS@ucf.edu).

---

### STARS Citation

Trieu, Khang, "Detection of Mercury Through Surface Plasmon Resonance of Immobilized Gold Nanorods" (2019). *Electronic Theses and Dissertations*. 6390.  
<https://stars.library.ucf.edu/etd/6390>

DETECTION OF MERCURY THROUGH SURFACE PLASMON  
RESONANCE OF IMMOBILIZED GOLD NANORODS

by:

KHANG TRIEU

B.S. in the University of Central Florida, 2012

A dissertation submitted in partial fulfillment of the requirements  
for the degree of Doctor of Philosophy  
in the Department of Chemistry  
in the College of Sciences  
at the University of Central Florida  
Orlando, Florida

Spring Term  
2019

Major Professor: Andres D. Campiglia

© 2019 Khang Trieu

## ABSTRACT

Mercury is a known environmental pollutant that can damage the brain, heart, kidney and lungs upon exposure. Emissions from fossil fuel plants can release mercury into the air, where it can settle into the water supply and be exposed to human and aquatic life. The use of gold nanorods functionalized on solid substrates as a mercury sensor in tap water samples is investigated herein. The functionalization of the substrates involves the physical immobilization of the nanorods onto the solid surface through the use of (3-mercaptopropyl)trimethoxysilane (MPTMS). The immobilization of the nanorods drastically increases their stability, allowing for use in complicated sample matrices. When gold nanorods are exposed to mercury in aqueous samples, their amalgamation to mercury metal causes a reduction of the effective aspect ratio of the nanoparticles and a blue shift of their maximum longitudinal surface plasmon resonance (SPR) absorption wavelength. Quantitative analysis is made possible due to the linear correlation that exists between the concentration of mercury and the wavelength shift of the maximum SPR absorption wavelength. In order to achieve the quantitative amalgamation of Hg (II) with the nanorods, it is necessary to reduce the mercury ions to mercury metal, which is accomplished herein via chemical or electrochemical processes. Chemical reduction of mercury was been carried out with a strong reducing agent, specifically sodium borohydride. Electrochemical reduction has been accomplished with gold nanorods immobilized on Indium Tin Oxide (ITO) substrates. Mercury determination in tap water using the immobilized gold nanorods was successfully conducted, with further experiments on improving selectivity with potential control, and improving sensitivity through flow injection analysis.

## **ACKNOWLEDGMENTS**

I would like to foremost thank my research adviser, Dr. Andres Campiglia for giving me the opportunity for me pursue a higher education within his research group. I would also like to acknowledge the late Dr. Anthony Moore for not only introducing me to the research group but also for being my mentor and friend throughout my undergraduate and graduate studies at UCF. My research would not be possible without the assistance of post-doctorates such as Dr. Emily Heider and Dr. Stacy Wise, as well as my fellow colleagues that have worked alongside me in the lab: Anthony Santana, Ahmed Comas, Sadia Arif, Mohammadreza Chehelamirani, Madeleine Johnson, Hugh Hayes, and Nirvani Mujumdar.

I would also like to give a special thanks to my family for their unending support encouragement and their presence in both the good times and the hard times. In particular, I'd like to thank my mother for raising me and my brothers and sister with such love and care. Without her care none of this would be possible for me. Finally, I would like thank my committee for their time and patience: Dr. James Harper, Dr. Emily Heider, Dr. Andrew Frazer, Dr. Matthew Rex, and Dr. Aniket Bhattacharya.

## TABLE OF CONTENTS

LIST OF FIGURES .....	viii
LIST OF TABLES .....	xi
CHAPTER 1: INTRODUCTON .....	1
1.1 Relevance and Impact of Mercury .....	1
1.2 Traditional Methods of Mercury Detection .....	4
1.2.1 Cold Vapor Atomic Absorption Spectroscopy .....	4
1.2.2 Inductively Coupled Plasma Mass Spectroscopy (ICP-MS) .....	7
1.2.3 Electrochemical Methods.....	10
1.3 Gold Nanoparticles As a Sensor for Mercury .....	15
1.3.1 Localized Surface Plasmon Resonance of Gold Nanoparticles .....	15
1.3.2 Mercury Sensor using Surface Plasmon Resonance of Gold Nanorods .....	20
CHAPTER 2: PORTABLE MERCURY SENSOR FOR TAP WATER USING SURFACE PLASON RESONANCE OF IMMOBILIZED GOLD NANORODS .....	23
2.1 Introduction.....	23
2.2 Experimental .....	25
2.2.1 Chemical and Reagents.....	25
2.2.2 Instrumentation .....	25
2.2.3 Gold Nanorod Immobilization.....	26
2.2.4 Mercury Detection Measurements .....	27
2.3 Results and Discussion .....	27
2.3.1 Immobilization of Gold Nanorods onto a Solid Substrate.....	27
2.3.2 Mercury Detection .....	29
2.3.3 Analytical Figures of Merit.....	33
2.3.4 Interference Studies .....	34
2.3.5 Quantification of Mercury in Tap Water .....	35
2.4 Conclusion .....	37
CHAPTER 3: INDIUM TIN OXIDE ELECTRODE MODIFIED WITH GOLD NANORODS FOR POTENTIAL CONTROLLED SURFACE PLASMON RESONANCE STUDIES.....	39
3.1 Introduction.....	39

3.2 Experimental .....	40
3.2.1 Chemical and Reagents.....	40
3.2.2 Instrumentation .....	40
3.2.3 Preparation of MPTMS-modified ITO Electrodes .....	41
3.2.4 Attachment of Gold Nanorods to MPTMS-modified Electrodes .....	42
3.2.5 Electrochemical Characterization .....	43
3.3 Results and Discussion .....	43
3.3.1 MPTMS Surface Modification and Characterization .....	43
3.3.2 Gold Nanorod Surface Modification and Characterization .....	48
3.3.3 Response of Gold Nanorod-MPTMS-ITO Electrodes under Potential Control .....	54
3.3.4 Application of Gold Nanorod-MPTMS-ITO Electrodes to a Model System .....	59
3.4 Conclusion .....	62
CHAPTER 4: IMMOBILIZED GOLD NANORODS FOR SURFACE PLASMON RESONANCE DETECTION OF MERCURY IN FLOW INJECTION ANALYSIS .....	64
4.1 Introduction.....	64
4.2 Experimental .....	66
4.2.1 Chemical and Reagents.....	66
4.2.2 Immobilization of Gold Nanorods on a Glass Substrate .....	66
4.2.3 Instrumentation .....	67
4.3 Results and Discussion .....	69
4.3.1 Instrumental Performance and Spectral Fitting .....	69
4.3.2 Stabilization of Reference Wavelength with NaBH <sub>4</sub> .....	72
4.3.3 Effect of Ionic Strength and NOM on the Spectral Features of Gold Nanorods .....	73
4.3.4 Analytical Figures of Merit.....	77
4.3.5 Analysis of Tap Water Samples.....	81
4.4 Conclusion .....	85
CHAPTER 5: CONCLUSIONS AND FUTURE STUDIES .....	87
APPENDIX A: GOLD NANOROD TEM IMAGES .....	89
APPENDIX B: FIA PERFORMANCE .....	93
APPENDIX C: PUBLISHER PERMISSIONS .....	97

REFERENCES .....	101
------------------	-----



## LIST OF FIGURES

Figure 1. Pathways of environmental pollution to water and marine life.....	3
Figure 2. Schematic diagram of cold vapor atomic absorption spectrometer for analysis of a reduced mercury solution [CVRef].....	5
Figure 3. Schematic diagram of the instrumentation used for Inductively Coupled Plasma Mass Spectroscopy .....	8
Figure 4. Basic instrumentation setup used for electrochemical methods.....	11
Figure 5. Schematic diagram of anodic stripping voltammetry illustrating the reduction (deposition) and oxidation (stripping) of the analyte ions. ....	12
Figure 6. Schematic diagram of localized surface plasmon resonance of a spherical metal nanoparticle.....	16
Figure 7 Absorbance spectra of gold nanoparticles with localized SPR at 520 nm or higher dependent on the radius of the nanoparticle .....	17
Figure 8. (A) Schematic diagram of the two localized surface plasmon resonance modes of a metal nanorod (B) Absorbance spectrum of gold nanorods suspended in solution with a transversal SPR absorbance signal at 520 nm and a longitudinal SPR signal at 615 nm .....	19
Figure 9. Absorbance spectra of gold nanorods with varying aspect ratios (length/diameter) in aqueous solution.....	21
Figure 10. Schematic diagram of the amalgamation process of the gold nanorods with mercury and TEM images in the absence (I) and presence (II and III) of reduced mercury .....	22
Figure 11. UV-Vis spectra of gold nanorods with longitudinal SPR peak at 615 nm without (a) and with (b) aggregation .....	24
Figure 12. Schematic diagram of the procedure for the functionalization of a silica substrate with MPTMS and gold nanorods .....	28
Figure 13. Scanning electron microscope images of gold nanorod functionalized solid silica substrates at varying magnifications.....	29
Figure 14. UV-Vis spectra of gold nanorods with longitudinal SPR peak at 615 nm in solution (green), immobilized onto a solid substrate exposed to water (black) or air (red) .....	30

Figure 15. (A) Absorbance spectra of immobilized gold nanorods in aqueous solution with addition of reduced mercury. (B) Calibration curve showing the change in the SPR wavelength in the presence of mercury of the solid sensor and of gold nanorods in solution.....	32
Figure 16. Multiple standard addition curve for the quantification of mercury in tap water .....	36
Figure 17. Multiple standard addition curve for the quantification of mercury in a synthetic contaminated tap water sample .....	37
Figure 18. Cyclic voltammograms of a bare ITO slide (black line), ITO slide after reflux treatment (blue line), and room temperature treatment (red line).....	45
Figure 19. CV curves of bare ITO and MPTMS-modification with varying immersion times (a. 0 min, b. 15 min, c. 30 min, d. 45 min, e. 60 min). (B) Plot of the change in the anodic and reductive $\Delta E_{\text{peak}}$ with MPTMS reaction time. ....	46
Figure 20. Contact angle of MPTMS-modified ITO slides and peak anodic current from CV curve with respect to MTPMS reaction time .....	47
Figure 21. UV-Vis spectra of gold nanorods immobilized on ITO slides after functionalizing with MPTMS using methods 1-3 .....	49
Figure 22. Schematics showing the inter-nanorod as well as nanorod-substrate interactions under increasing ionic strength at different CTAB concentrations.....	50
Figure 23. UV-Vis spectra of centrifuged gold nanorods immobilized on ITO slides.....	51
Figure 24. UV-Vis spectra of twice-centrifuged colloidal gold nanorods in solution in the presence of varying concentrations of sodium chloride .....	52
Figure 25. UV-Vis spectra of centrifuged gold nanorods with and without a moderate concentration of NaCl immobilized on ITO slides .....	53
Figure 26. SEM images at different magnifications of gold nanorods immobilized on the MPTMS-ITO slide with surface coverage of $15 \text{ nanorods} \cdot \mu\text{m}^{-2}$ .....	54
Figure 27. Cyclic voltammogram of a bare ITO slide (dashed line), bulk gold electrode (gray line), and gold nanorod-ITO electrode (black line) in $0.5 \text{ M H}_2\text{SO}_4$ .....	56
Figure 28. Plot of the SPR wavelength maximum under applied negative or positive potential .	58
Figure 29. Cyclic voltammogram of the reduction of Hg(II) to mercury metal using the gold nanorod-MPTMS-ITO electrode .....	60

Figure 30. (A) SPR response of immobilized gold nanorods on an ITO electrode with addition of $\text{HgCl}_2$ and reduction through potential sweep voltammetry (B) Calibration curve of the change in the SPR maximum absorbance wavelength with respect to concentration of mercury per nanorod .....	61
Figure 31. Cyclic voltammograms of the reduction of various metal ions metal using the gold nanorod-MPTMS-ITO electrode .....	63
Figure 32. Cyclic voltammograms of the reduction of mercury ions and methylmercury using the gold nanorod-MPTMS-ITO electrode .....	63
Figure 33. Simplified schematic diagram of the preparation and sensing method of immobilized gold nanorods used for mercury quantification .....	65
Figure 34. Schematic diagram of the flow cell used to measure absorbance from gold nanorod substrates .....	68
Figure 35. Absorbance spectra of immobilized gold nanorod substrates with curve fitting using the GCAS function. Spectra were recorded from glass substrates with different number of nanorods on their surface: (A) $1.8 \times 10^{11}$ and (B) $2.2 \times 10^{11}$ NRs. ....	71
Figure 36. Absorbance spectra over time of the immobilized gold nanorod substrate immersed in a $10^{-3}$ M $\text{NaBH}_4$ solution. ....	72
Figure 37. (A) Absorbance spectra over time of colloidal gold nanorods in the presence of a tap water sample and 0.01 M $\text{NaBH}_4$ . (B) Absorbance spectra over time of immobilized gold nanorods on a solid substrate in the presence of a tap water sample and 0.01 M $\text{NaBH}_4$ .....	74
Figure 38. Absorbance spectra over time of immobilized gold nanorods on a solid substrate in the presence of (A) 0.5 M $\text{NaCl}$ (B) increasing concentrations of humic acid (HA) .....	76
Figure 39. (A) Absorbance spectra of the SPR response of immobilized nanorods to Hg over time under stopped flow conditions. (B) Graph of the shift in the SPR maximum wavelength over time under stopped flow conditions .....	78
Figure 40(A) Graph (B) spectra of the SPR absorbance wavelength shifts over time of immobilized gold nanorods exposed to nanomolar concentrations of Hg in a continuous flow method .....	79
Figure 41. Graph of the shift of the SPR maximum wavelength recorded after 5 min of successive exposure to 5.0 $\mu\text{M}$ concentrations of the inorganic salt .....	83
Figure 42. Graph of the shift of the SPR maximum wavelength recorded after multiple standard additions using the continuous flow method .....	85

## LIST OF TABLES

Table 1. Limits of detection of various CVAAS, ICP-MS, and ASV methods.....	15
Table 2. Analytical figures of merit for mercury detection using gold nanorods in solution or gold nanorods immobilized on a solid substrate.....	34
Table 3. Shift in the SPR absorbance maximum wavelength for the immobilized gold nanorod sensor in the presence of 5 $\mu$ M concentration of a potentially interfering species.....	35
Table 4. Reaction conditions for MTPMS-ITO monolayer self-assembly.....	42
Table 5. Reproducibility of measurements obtained with UV-Vis absorption spectrometer .....	69
Table 6. Analytical Figures of Merit for mercury detection using immobilized gold nanorod substrates using either the stop flow or continuous flow methods. ....	80
Table 7. Elements capable of forming an amalgam with Hg(0) under various conditions .....	82
Table 8. Chemical species tested for interference with immobilized gold nanorod substrates using the stopped flow method. ....	83

# **CHAPTER 1: INTRODUCTION**

## **1.1 Relevance and Impact of Mercury**

Mercury is a naturally occurring element often found in the earth's crust, including coal and other fossil fuels. In addition to its elemental or metallic form, mercury can be converted into methylmercury and other organic forms through microorganisms. While natural sources such as volcanic activity can release mercury into the environment, the majority of mercury emissions are attributed to anthropogenic sources including emissions from fossil fuel plants, mining processes, and agricultural and industrial runoff [1]. Mercury is considered a bio-accumulative pollutant that will persist in the environment as well as living tissue regardless of decomposition or chemical processes. As an example, in bodies of water mercury can accumulate in fish and other aquatic wildlife, affecting the aquatic ecosystem through neurological diseases in fish populations as well as the animals that prey upon the fish, including humans [2]. As such, since 1974 with the Safe Drinking Water Act, there has been a conscience effort by the Environmental Protection Agency (EPA) to determine the level of contaminants such as mercury that cause adverse health effects and limit them. For mercury, the maximum contamination level was determined by the EPA to be 2 ppb [3].

Mercury is an environmental pollutant that can damage the brain, heart, kidney and lungs upon exposure. Due to its ability to bioaccumulate in humans, even low amounts of exposure can build up over time and cause serious health effects on people of all ages. Ingestion of contaminated water or fish can cause including physical impairments such as renal failure or gastrointestinal bleeding, as well as mental impairments such as brain development and seizures, particularly in children [4-6]. Due to the prevalence of mercury emissions, consistent monitoring

of mercury concentrations within the environment is necessary. Determination of mercury concentrations in biological samples such as human or fish samples can be inconvenient and invasive, especially since constant monitoring may be required. Environmental samples such as in water provide a much more convenient approach to monitoring mercury concentrations. In bodies of water, mercury exists in its elemental, inorganic, or organic forms, though primarily as the aqueous inorganic ( $\text{Hg}^{2+}$  ions or complexes) or organic (methylmercury or humic acid complexes) forms [4]. Mercury analysis in water is critical as water represents a pathway for mercury through the environment and to humans as mercury can contaminate water through industrial runoff or leach into bodies of water through both air and sediment.

Water samples provide an easily accessible yet complex matrix due to the wide variety of possible contaminants, including mercury, which can differ in concentration from sample to sample through the environment that the water is exposed to. As such, it is imperative for the sensor to be able to determine the concentrations of mercury in a diversity of matrixes but also in a wide range of mercury concentrations. Generally, drinking water has concentrations generally below 2 ppb mercury due to regulations such as the Clean Water Act that monitors and treats water before human consumption [7-9]. However, in areas where drinking water is not readily available or less regulated, elevated levels of mercury can be found in the water supply. Drinking water in a mining town in Ghana was found to have mercury concentrations of 2.3 ppb [10], which is above the 1 ppb recommended by the World Health Organization (WHO) guideline for drinking water [11]. In two districts in India, drinking water was found to have an average mercury concentration of 3.55 ppb, with concentrations ranging from 0.51 – 13.58 ppb depending in location. The researchers concluded that the majority of the contamination was due

to anthropogenic sources and presented a major health risk [12]. On small coastal islands, brackish lakes present the only source of drinking water and are at risk of contamination, such as on Mljet Island near Croatia. Researchers there found total mercury levels up to 14 ppb, though the source of the high mercury concentration was theorized to be due to precipitation and bat guano rather than anthropogenic sources [13].

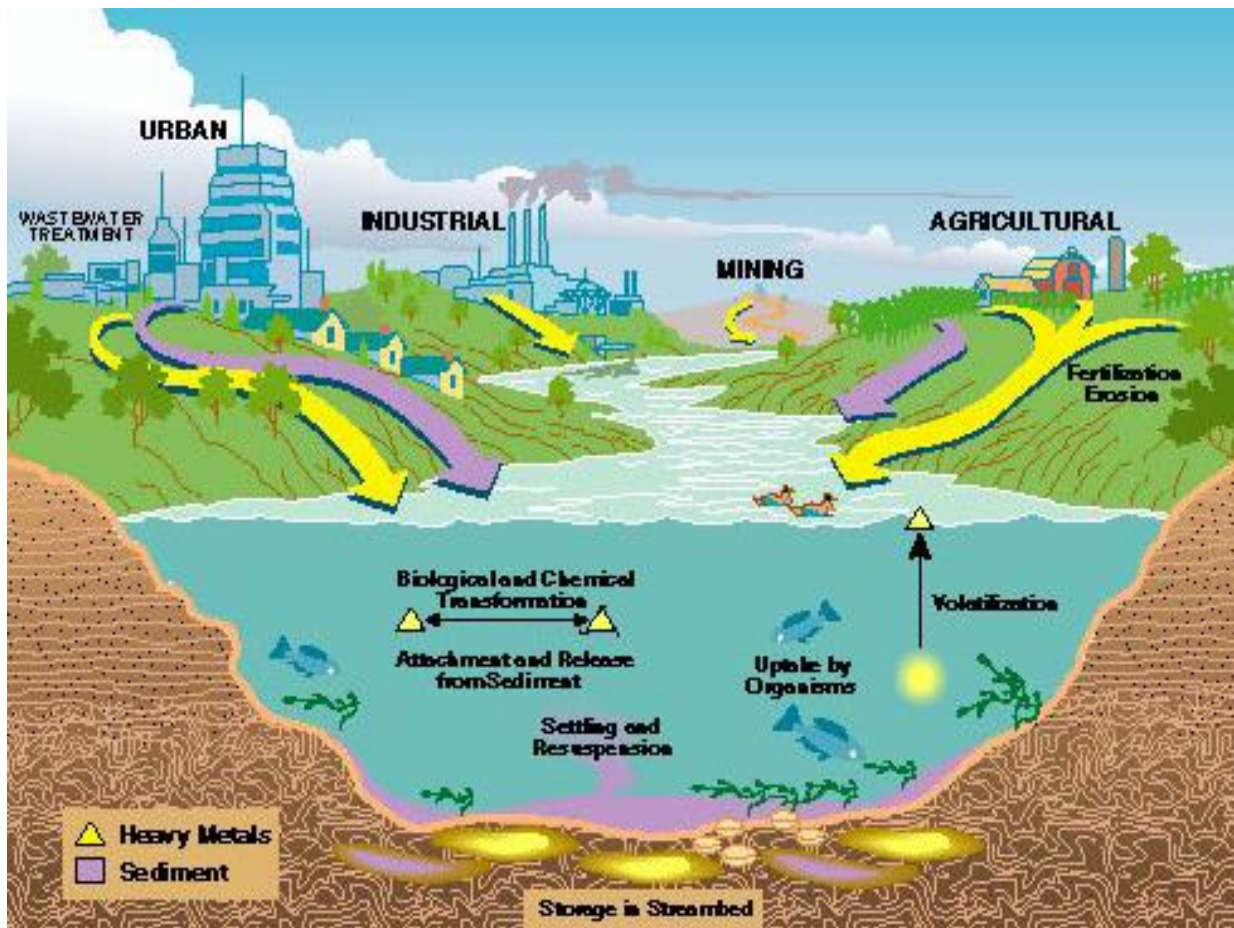


Figure 1. Pathways of environmental pollution to water and marine life

## **1.2 Traditional Methods of Mercury Detection**

### **1.2.1 Cold Vapor Atomic Absorption Spectroscopy**

One of the most common methods for mercury detection in water samples as described by the EPA is through cold vapor atomic absorption spectroscopy (CVAAS). The technique was first introduced by Hatch and Ott in 1968 [14], and since has been a staple technique for mercury detection in water samples. Atomic absorption spectroscopy (AAS) uses the absorption of optical light of free atoms of chemical elements in the gaseous state. The technique has a unique specificity to particular elements due to each element having a specific amount of energy or wavelength that it absorbs, leading to a unique profile for each element. In addition, the width of the absorption line at its corresponding wavelength is in the order of picometers, giving the technique high resolution. The radiation flux of the analyte can be measured, with the concentration determined using the Beer-Lambert law. In general, the instrumentation for AAS consists of four main components, the light source, atomizer, wavelength selector, and detector.

A common light source used for AAS is the Hollow Cathode Lamp (HCL), which is a sealed lamp filled with an inert gas with a cathode containing the element of interest and an anode. Application of a high voltage will ionize the inert gas and upon impact with the cathode, will eject particles of the element of interest which become excited through further collisions. As the excited elements decay, it will emit radiation of the particular wavelength corresponding to the element of interest. The wavelength detector is a standard monochromator, high resolution is not required of the monochromator due to the narrow line emission of the HCL providing that resolution. Detectors such as photomultiplier tubes are commonly used and are suitable to detect the emission light passed through the sample. For CVAAS, instead of a standard atomizer such



as a flame or furnace, the cold vapor technique is applied instead due to the unique properties of elemental mercury (figure 2). Elemental mercury has a very low vapor pressure of 0.0016 mbar at 20°C, allowing it to be determined directly without the use of an atomizer by passing an inert gas such as argon through the sample, effectively separating it from an aqueous matrix and carrying it to the absorbance cell already in atomic form.

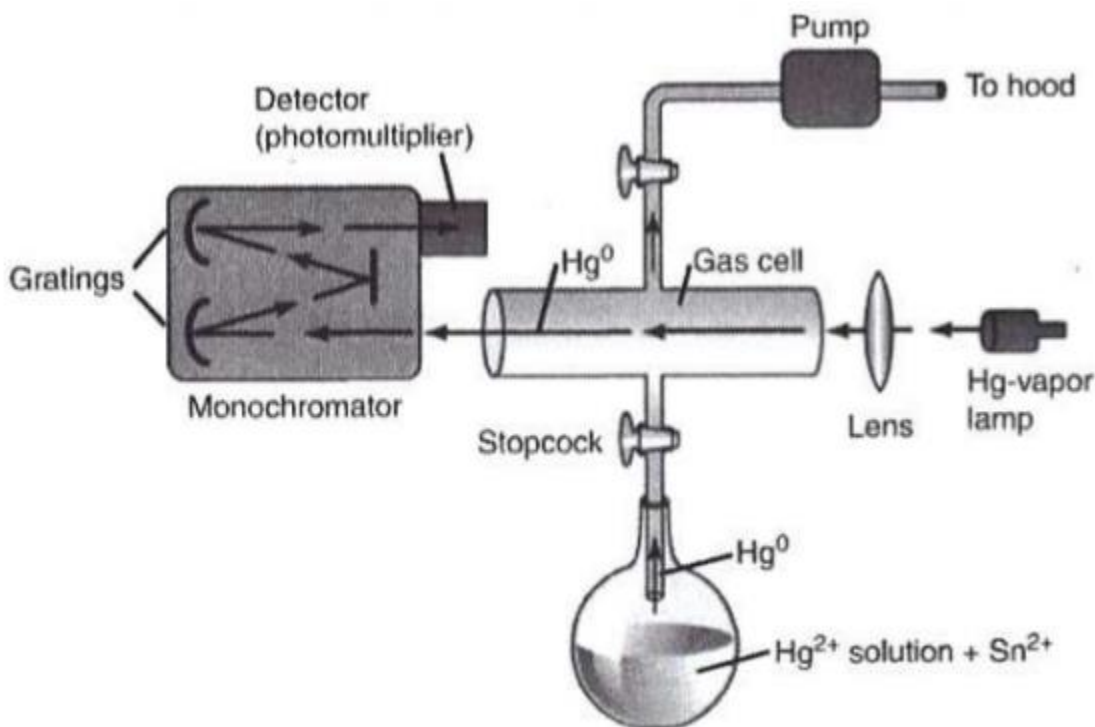


Figure 2. Schematic diagram of cold vapor atomic absorption spectrometer for analysis of a reduced mercury solution [15]

The sensitivity of CVAAS to mercury in water samples is well documented, with limits of detection in the parts-per-billion (ppb) or parts-per-trillion (ppt) range, allowing the technique to be practically used for most water samples. The selectivity and sensitivity of the technique can be enhanced further through additions such as sorbents that absorb and preconcentrate the

mercury before CVAAS analysis. Ziaei et. al. developed a mercapto-grafted graphene oxide chitosan composite for the extraction and concentration of mercury in water samples followed by determination with CVAAS. They utilized the ability of magnetic graphene/chitosan to act as an absorbent of heavy metals, with the selectivity of 3-mercaptopropyltrimethoxysilane due to the high affinity of the sulfur moiety to mercury, to obtain a limit of detection of 0.06 ppb [16]. Shibani et. al. performed speciation analysis of mercury in water samples through solid phase extraction using a column packed with dithizone supported by microcrystalline naphthalene, obtaining a limit of detection of 0.014 ppb. Dithizone forms complexes with certain metals, specifically platinum, palladium, silver, copper, and mercury under acidic conditions, making it suitable for mercury extraction. Speciation was done through selective reduction of either the inorganic or reduction of the total (inorganic and organic) mercury within solution, and the difference subtracted to determine the organic mercury concentration [17].

Research has also been done on micro or nano-extraction methods that can selectively extract mercury out of the aqueous sample and into a separate pure solvent, thereby simplifying the sample matrix while still allowing for preconcentration through control of the solvent volume. Yordanova et. al. synthesized polymeric ion-imprinted nanoparticles via dispersion copolymerization using methacrylic acid, trimethylolpropane trimethacrylate, and 1-pyrrolidinedithiocarboxylic acid. The resulting polymeric nanoparticle is imprinted during the synthesis using mercury ions as a template, allowing the nanoparticles to selectively trap mercury ions upon addition to the water sample. The nanoparticles with adsorbed mercury is extracted through centrifugation and separated from the aqueous supernatant, where the mercury itself is eluted using a thiourea solution and quantified using CVAAS. The separation and

preconcentration allowed for improved limits of detection of 0.0045 ppb [18]. Dispersive liquid-liquid microextraction was accomplished by Stanisz et. al., using microliter volumes of the task specific ionic liquid, methyltrioctylammonium thiosalicylate, utilizing the affinity of the thiol moiety for mercury. After centrifugation, the organic ionic liquid phase can be separated from the aqueous sample and the mercury quantified with CVAAS with a limit of detection of 0.03 ppb [19].

### **1.2.2 Inductively Coupled Plasma Mass Spectroscopy (ICP-MS)**

ICP-MS is a commonly used method for the detection and quantification of specific metals and non-metals through the ionization of the sample through the inductively coupled plasma followed by separation and quantification of the ions through mass spectroscopy. The plasma is formed via an argon gas flow through a loading coil connected to a radio-frequency generator. The generator provides an oscillating electromagnetic field through the coil which heats up the argon gas, and when a spark is applied, it ionizes the gas. The resulting ions are trapped within the electromagnetic field and collide with other argon atoms, creating the discharge or plasma. The plasma can reach a temperature from 6000 – 10000 K and acts as an ion source to the sample. After formation of the argon plasma, the liquid sample can be introduced as an aerosol through aspiration, where it is desolvated into a gas and ionized as it passes through the plasma.

The ionized sample is directed into the mass spectrometer, where the ions are separated by the mass-to-charge ratio, usually through the use of a quadrupole mass filter. The quadrupole mass filter is a series of four rods in which alternating AC and DC voltages are applied to in conjunction with a radio-frequency field, resulting in an electrostatic filter that only allows ions

of a certain mass-to-charge ratio to pass through. By adjusting the voltage applied, different ions can be passed through sequentially. The filtered ions are quantified through a detector that reads and displays the electrical signal (figure 3).

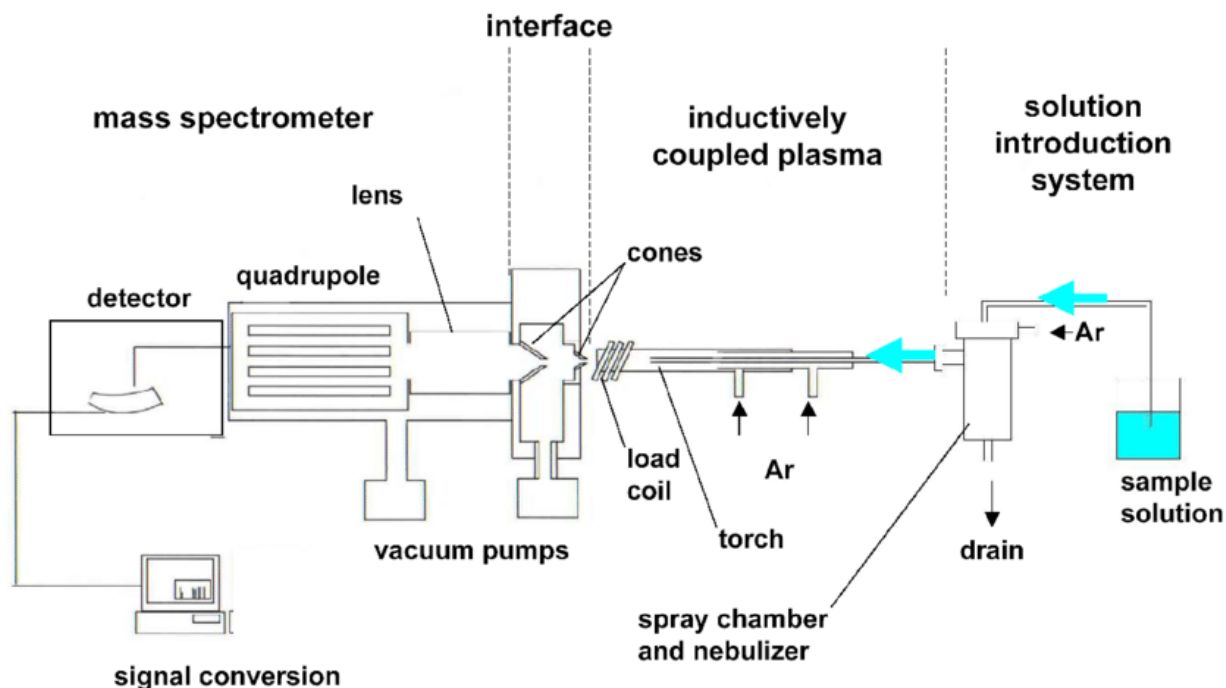


Figure 3. Schematic diagram of the instrumentation used for Inductively Coupled Plasma Mass Spectroscopy ([https://www.researchgate.net/profile/Richard\\_Gilstrap/publication/44226526/figure/fig/AS:606775002796032@1521677842621/Schematic-of-an-Inductively-Coupled-Plasma-Mass-Spectrometer-ICP-MS.png](https://www.researchgate.net/profile/Richard_Gilstrap/publication/44226526/figure/fig/AS:606775002796032@1521677842621/Schematic-of-an-Inductively-Coupled-Plasma-Mass-Spectrometer-ICP-MS.png))

ICP-MS has been used for mercury detection in water due to its extreme sensitivity, obtaining limits of detection below that of CVAAS, though at a higher operating cost [20]. ICP-MS is often paired with an extraction or separation method to clean and preconcentrate the sample as to avoid interferences from other ions. A traditional separation methods used for this purpose is column chromatography, often utilizing mercury's affinity for a particular moiety such as thiols. Column chromatography also allows for speciation of the individual mercury inorganic or organic (methylmercury, ethylmercury, and phenylmercury) through their retention

times, with inorganic mercury shortest retention time, and the organic species having longer retention times depending on their molecular weight, with longer retention times for higher molecular weight species.

Columns packed with silica particles with surfaces bound with sulfonate molecules can be used for this purpose, as demonstrated by Chen, et. al. Limits of detection of 19-22 ppt depending on the mercury species were obtained after ICP-MS using this method [21]. An alternative solution was purposed by Cheng, et. al. and Jia et. al., of which an anion exchange column conditioned with a sulfonic solution or resin was used, followed by high-performance liquid chromatography of the elutant to separate the individual mercury species further for ICP-MS analysis. This method obtained limits of detection of the various mercury species ranging from 0.009 to 0.042 ppt [22-23].

While column chromatography has many advantages, other separation methods can also be used for mercury determination and speciation. Wu et. al. used cold vapor generation after selective oxidation as a means to separate the mercury species (inorganic or methylmercury) from a liquid sample before ICP-MS analysis, taking advantage of mercury's low vapor pressure. Limits of detection were found to be 3 ppt for inorganic mercury and 75 ppt for methylmercury [24]. Another method used by Zhao et. al. is capillary electrophoresis after adding mercaptoacetic acid in order to form a complex with the mercury species, allowing for complete separation by capillary zone electrophoresis before determination with ICP-MS. With this technique, limits of detection from 0.021 – 0.032 ppt were found for the various mercury species. [25].

### **1.2.3 Electrochemical Methods**

CVAAS and ICP-MS provide exceptionally low limits of detection within the ppb or ppt range but with a high cost requirement not just in terms of instrumentation, but also professional personnel required to operate the instruments. The procedures also require sample pretreatment through digestion procedures for speciation, and external separation or extraction methods before quantitative analysis with CVAAS or ICP-MS. Overall, the methods will require a laboratory setting, with routine analysis of water samples requiring constant collection, proper storage, and shipment to laboratories for analysis. As such, there has been research focused on alternative methods that provide sufficient sensitivity and selectivity for analysis of water in mercury, while being inexpensive and portable, allowing for possible on-site monitoring.

Electrochemical methods provide an attractive alternative due to their significantly smaller instrumental size, lower costs, and ease of use. Electrochemical methods rely on the application of a potential difference, or difference in electrical voltage between the cathode and anode in the electrochemical cell. This creates an electrical current and promotes an electromotive force which attracts either cations or anions depending on the potential applied. The general setup consists of five main components (figure 4). The main component is the potentiostat, which controls the electrical potential and is connected to three electrodes – the counter, working, and reference electrodes, with the surface of the working electrode where the reduction-oxidation reaction takes place.

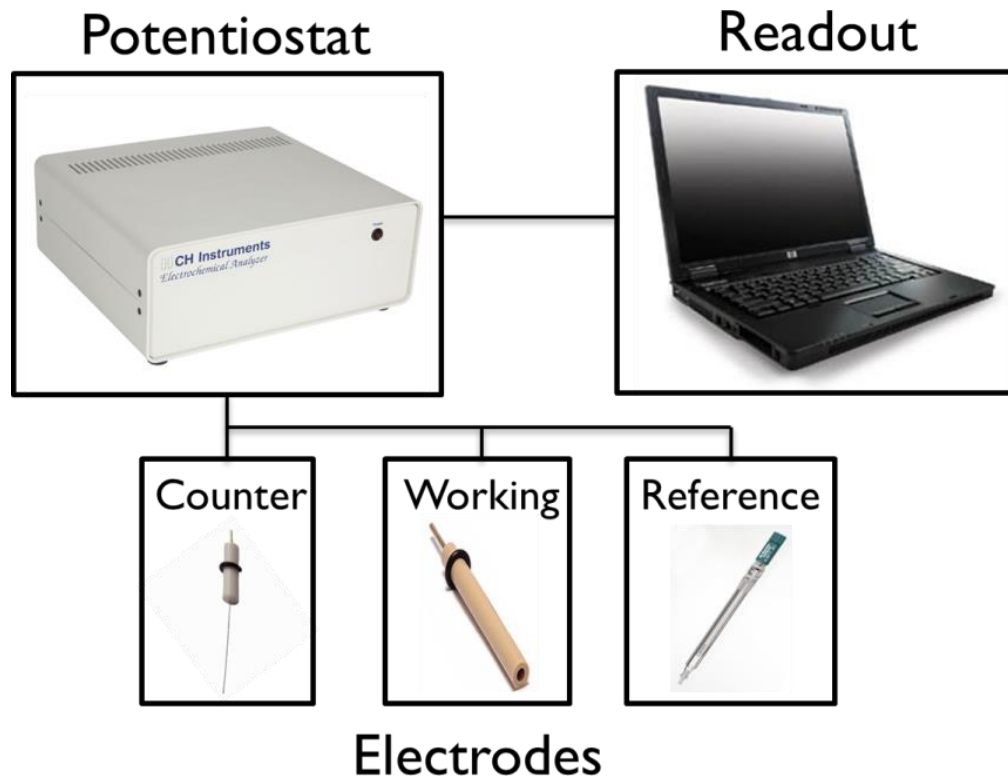


Figure 4. Basic instrumentation setup used for electrochemical methods

One area of research is through electrochemical methods such as anodic stripping voltammetry (ASV), wherein a negative potential is applied to a working electrode, causing reduction and concentration of ions onto the electrode surface. After sufficient preconcentration, the potential is reversed to more positive potentials until the oxidation and stripping of the surface ions is achieved and a current relative to the concentration is obtained (figure 5). Anodic stripping voltammetry generally makes use of potentiostats capable of either the differential pulse or square wave voltammetry technique. These techniques minimize background charging current by changing the potential through a series of steps or pulses, measuring the current at the beginning and end of a pulse. The difference in the current between these two measurements effectively subtracts the charging current generated by the polarization of the electrode with ions

in the solution forming a double layer, where certain ions are attracted to the electrode surface when the potential is changed to compensate for the charge on the electrode surface. This leaves the actual current measured to be the faradaic current caused by the actual redox process, thereby greatly increasing the sensitivity of the chosen electrochemical method compared to a standard linear sweep, particularly at low concentrations in which the charging current can obscure the faradaic signal.

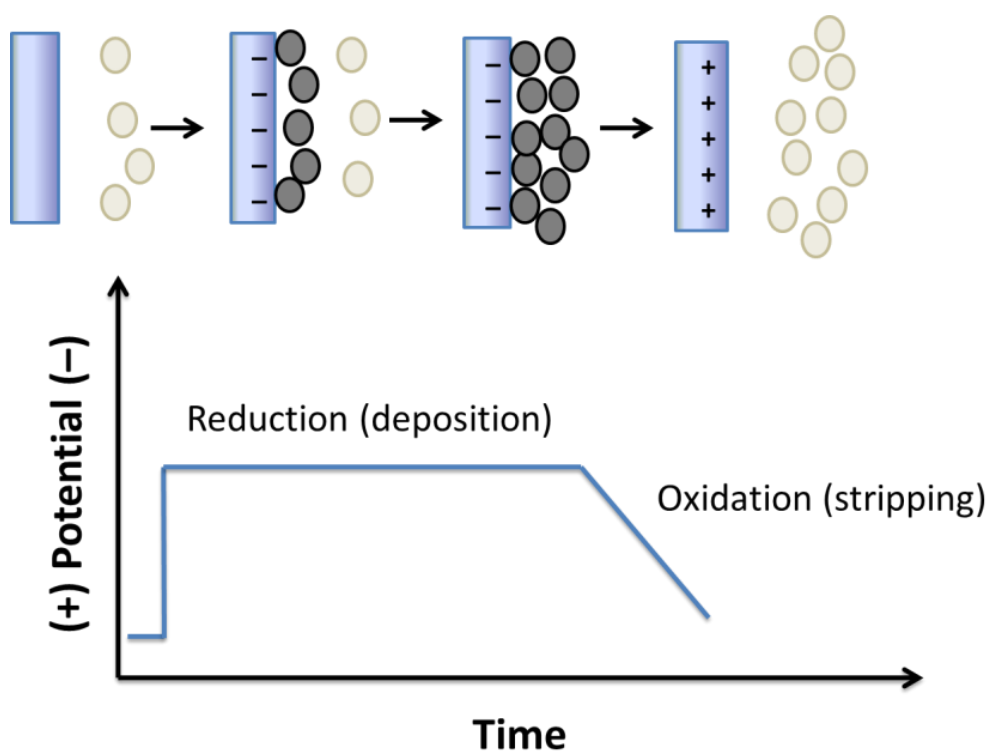


Figure 5. Schematic diagram of anodic stripping voltammetry illustrating the reduction (deposition) and oxidation (stripping) of the analyte ions.

ASV can be improved through modification or functionalization of the working electrode in order to increase its sensitivity as well as its selectivity to mercury, allowing for the method to be used in a variety of water matrices. One major modification of the working electrode is through the increase of the effective surface area, allowing a greater amount of deposition or



preconcentration onto the electrode surface, resulting in a greater sensitivity. This modification is often combined with a particular complexing/coordinating agent or other compound that will selectively target or attract mercury ions for deposition while also preventing electron fouling due to interferences from other ions.

Kempegowda et. al. functionalized a graphite based working electrode with Mercaptobenzothiozole, combining the high surface area of exfoliated graphite and the thiol moiety of the Mercaptobenzothiozole to selectively deposit mercury onto the surface. The proposed method obtained a limit of detection of 0.2 ppt through quantification using differential pulse anodic stripping voltammetry in a buffer solution with minimal sample pretreatment other than simple filtration of any suspended colloidal matter [26]. Gong et. al. synthesized a gold nanoparticle based hybrid inorganic-organic ensemble onto glassy carbon to serve as the working electrode, using a 3, 3',5,5'-Tetramethylbenzidine based nanofiber which can coordinate with transition metal ions. The nanofibers were doped with platinum ions and gold nanoparticles were electrically deposited onto the surface, forming the overall nanostructure. With a 3D porous structure, the surface area of the nanostructure is greatly enhanced, with selectivity to mercury through the strong interactions between metallic mercury and gold, allowing for limits of detection of 0.008 ppb [27]. Punrat et. al. developed an automated system based on a sequential flow injection system using an electrode compatible flow cell to allow for anodic stripping voltammetry with a gold plated screen printed working electrode. Screen printed electrodes are small disposable electrodes, fabricated through the machine “printing” of a counter, reference, and working electrode all contained within an inert strip using an “ink” composite consisting of conductive particles such as graphite. The automated injections

combined with the small disposable screen printed electrodes are viable for portable and routine analysis of mercury in water samples, with the proposed method obtaining limits of detection of 0.22 ppb [28].

Table 1 summarizes the methods and limits of detection discussed, with ICP-MS obtaining the lowest limits of detection for mercury, as well as being able to do speciation analysis. ICP-MS and CVAAS often requires significant pretreatment as well as preconcentration using a separate method or methods before quantification. Anodic stripping voltammetry uses modification of the working electrode to provide sensitivity and selectivity to the method, and while the limits of detection are not as low as in ICP-MS, they are still sufficient for the quantification of mercury in water samples based on the maximum contamination level set by the EPA for drinking water (2 ppb) or the WHO (1 ppb). Electrochemical methods also have the advantage of a much smaller instrumental requirement and minimal sample pretreatment, allowing it to be used on site, making it suitable for field analysis in areas where laboratories with the required instrumentation are not available.

Table 1. Limits of detection of various CVAAS, ICP-MS, and ASV methods

Author	Method	LOD (ppb)	Reference
Ziaie et. al.	SPE-CVAAS	0.06	[Ex Ref1]
Shabini et. al.	SPE-CVAAS	0.014	[Ex Ref2]
Yordanova et. al.	SPNE-CVAAS	0.0045	[Ex Ref3]
Stanisz et. al	LLE-CVAAS	0.03	[Ex Ref4]
Chen et. al.	CEC-ICP-MS	0.019	[ICPRef0]
Cheng et. al	CEC-HPLC-ICP-MS	0.000016	[ICPRef1]
Jia et. al	CEC-HPLC-ICP-MS	0.000042	[ICPRef2]
Wu et. al	CV-ICP-MS	0.003	[ICPRef3]
Zhao et. al.	CZE-ICP-MS	0.027	[ICPRef4]
Kempegowda et. al.	ASV	0.0002	[ECRef1]
Gong et. al	ASV	0.008	[ECRef2]
Punrat et. al.	ASV	0.012	[ECRef3]

\*SPE = Solid Phase Extraction

\*SPNE = Solid Phase Nano-extraction

\*LLE = Liquid-liquid Extraction

\*CVAAS = Cold Vapor Atomic Absorption Spectroscopy

\*CEC = Cation Exchange Chromatography

\*ICP-MS = Inductively Coupled Plasma Mass Spectroscopy

\*HPLC = High Performance Liquid Chromatography

\*CV = Cold Vapor

\*CZE = Capillary Zone Electrophoresis

\*ASV = Anodic Stripping Voltammetry

### **1.3 Gold Nanoparticles As a Sensor for Mercury**

#### **1.3.1 Localized Surface Plasmon Resonance of Gold Nanoparticles**

Gold nanoparticles are elemental gold particles in the nanoscale that are typically suspended in a solution through the use of an electrostatic surfactant to prevent aggregation and can be used as a sensor. Like other noble metal nanostructures, they possess a localized surface plasmon resonance (SPR) that was first discussed by Faraday et. al. in 1847 [29]. Surface plasmons are collective oscillations of the free electrons on the surface of a noble metal. When the surface plasmons are contained within a particle with a size smaller or comparable to

wavelengths of light, i.e. a nanoparticle, all the free electrons of the particle participate in the oscillation and will collectively oscillate in resonance with the wave of light (figure 6).

Localized surface plasmons have two unique properties, the first is the enhancement of electric fields near the nanoparticle's surface relative to how close the electric field is to the surface (close electric fields are greatly enhanced). The second is a unique optical extinction with a maximum wavelength at the nanoparticle's plasmon resonance frequency, which in noble metal nanoparticles such as gold, the maximum is within the visible wavelengths. The extinction wavelength is influenced by the physical properties of the nanoparticle such as size, shape, aspect ratio, and refractive index of the surrounding medium [30].

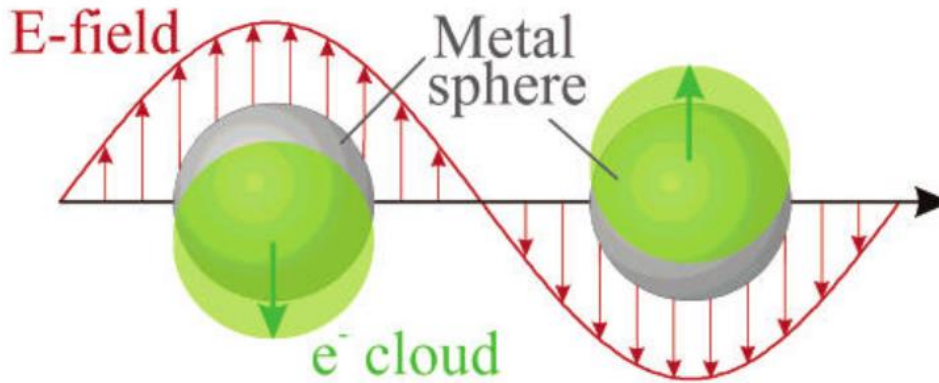


Figure 6. Schematic diagram of localized surface plasmon resonance of a spherical metal nanoparticle [32]

Following Faraday's work, Mie et. al. developed a theory for localized surface plasmon resonance through the calculation of the extinction (absorbance and scattering) cross section of a metal nanosphere using the following formula [31]:

$$C_{ext} = \frac{24\pi^2 R^3 \epsilon_m^{3/2}}{\lambda} \left[ \frac{\epsilon_i}{(\epsilon_r + 2\epsilon_m)^2 + \epsilon_i^2} \right]$$

where  $C_{\text{ext}}$  is the extinction cross section,  $R$  is the radius,  $\epsilon_m$  is the relative dielectric constant of the surrounding medium, and  $\epsilon_r$  and  $\epsilon_i$  are the dielectric properties of the metal nanoparticle relative to the excitation wavelength. The resonance condition as described by the Mie theory is when the bracketed equation approaches zero, the absorbance and scattering ( $C_{\text{ext}}$ ) will become increasingly large at a particular wavelength. Based on the formula, for this to occur, the value of  $\epsilon_r$  must approach  $-2\epsilon_m$ , which for standard dielectrics and nonmetals typically have positive  $\epsilon_r$  values [32]. This condition is most notably fulfilled by noble metals such as gold and silver which have negative  $\epsilon_r$  values as well as  $\epsilon_i$  values close to zero [33]. For example, for gold nanoparticles suspended in water ( $\epsilon_m \approx 1.7$ ), the wavelength required for  $\epsilon_r \approx -2\epsilon_m$  is at approximately 520 nm or at slightly higher wavelengths depending on the size of the nanoparticle, which can be corroborated by the absorbance spectrum (figure 7).

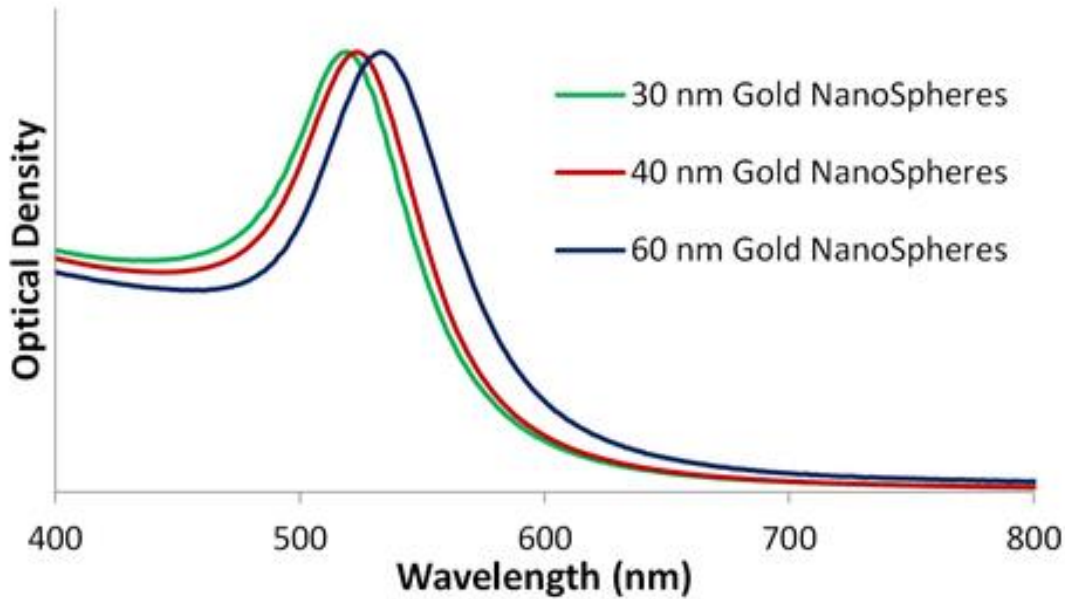


Figure 7. Absorbance spectra of gold nanoparticles with localized SPR at 520 nm or higher dependent on the radius of the nanoparticle (<https://nanohybrids.net/pages/gold-nanoparticles-for-lateral-flow-assays>)

As Mie theory is only applicable to spherical nanoparticles, further modification of the formula would need to be done to account for nonspherical nanoparticles. Gans et. al. adjusted Mie's formula to nanoparticles of any aspect ratio according to the following formula [34]:

$$C_{ext} = \frac{\omega}{3c} \epsilon_m^{3/2} R \sum \frac{(1/P_j^2) \epsilon_i}{\{\epsilon_r + [(1 - P_j)/P_j] \epsilon_m\}^2 + \epsilon_i^2}$$

where  $\omega$  is the plasma frequency and  $P_j$  is the depolarization factors across the three dimensions or axis. Based on the equation, nonspherical nanoparticles will have two absorbance peaks, one corresponding to the sum of the transverse SPR which is contributed by the  $x$  and  $y$  axis, and the other corresponding to the longitudinal SPR contributed by the  $z$  axis, which appears at higher wavelengths (figure 8). TEM images of gold nanorods can be found in appendix A.

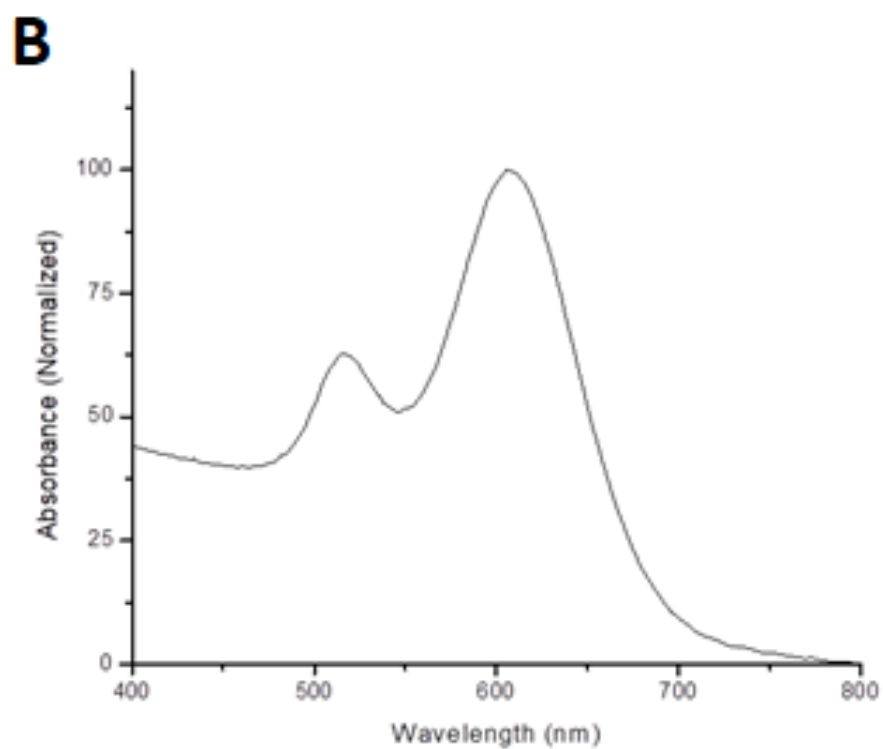
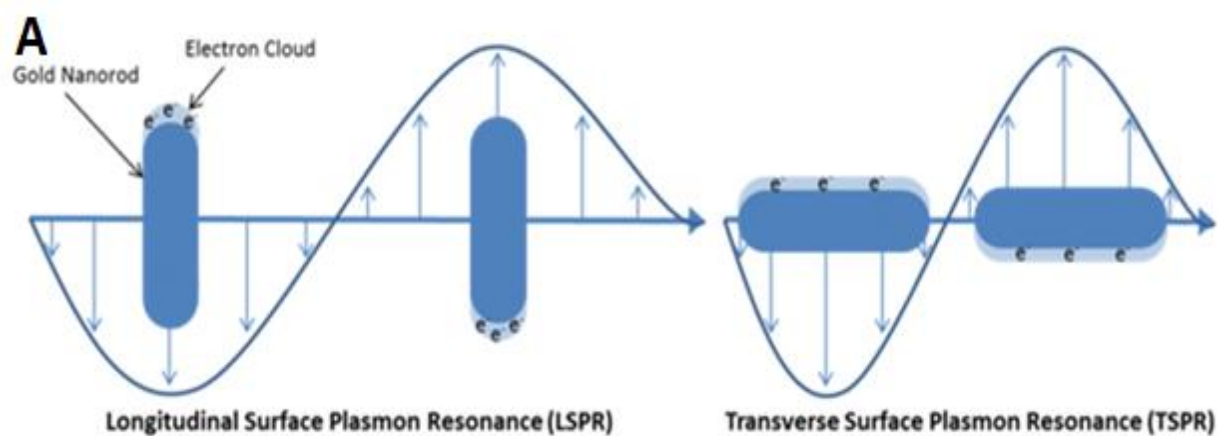


Figure 8. (A) Schematic diagram of the two localized surface plasmon resonance modes of a metal nanorod (B) Absorbance spectrum of gold nanorods suspended in solution with a transversal SPR absorbance signal at 520 nm and a longitudinal SPR signal at 615 nm

### **1.3.2 Mercury Sensor using Surface Plasmon Resonance of Gold Nanorods**

Metallic gold possesses remarkable chemical stability and resistance to oxidation compared to other metal nanoparticles such as silver or copper, which are easily oxidized. Gold nanoparticles also have a strong plasmon resonance, with silver nanoparticles having the strongest and palladium and platinum nanoparticles having weak plasmon resonance [35]. The strong plasmon resonance combined with its chemical stability makes gold nanoparticles suitable as a sensor. Gold nanorods in particular are ideal sensors as they have two localized surface plasmon resonance absorbance peaks due to their nonspherical shape. As with other nanoparticles, gold nanorods require a surfactant in order to prevent aggregation and allow the nanorods to remain suspended in solution. In the seed mediated growth method developed by Al-Sayed et. al., the surfactant cetyltrimethylammonium bromide (CTAB) is used, which forms a bilayer around the gold nanorod [36]. The longitudinal SPR of gold nanorods is tunable based on their aspect ratio, with larger aspect ratios corresponding to higher wavelengths (Figure 9). Gold nanorods have been studied due to their strong surface enhanced Raman scattering (SERS) of adsorbed molecules, allowing them to be used as a SERS-based sensor [37-38], as well as their sensitivity to the refractive index of the surrounding medium, allowing them to be used to detect biomolecular binding [39-41].



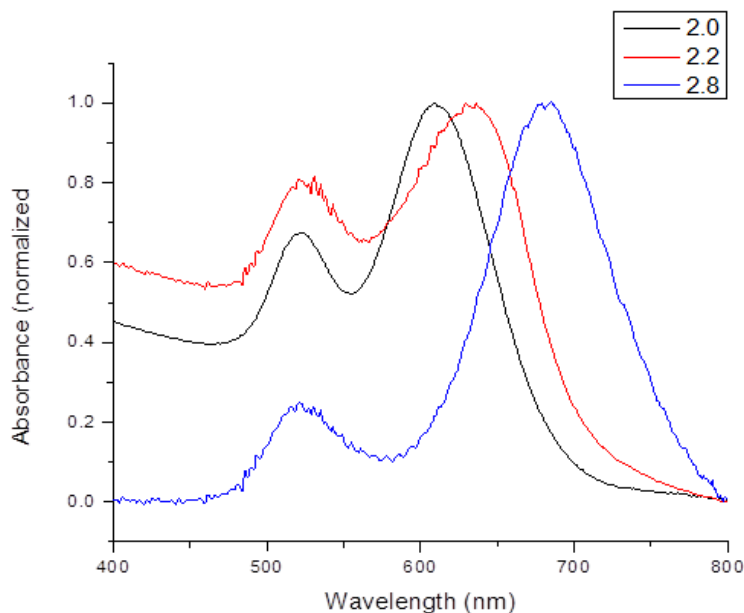
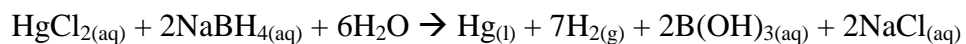


Figure 9. Absorbance spectra of gold nanorods with varying aspect ratios (length/diameter) in aqueous solution

This work focuses on the use of gold nanorods as a SPR based sensor for mercury, taking advantage of the well-known amalgamation process between elemental gold and mercury.

Previous work done by Rex et. al. presented a direct method of inorganic mercury determination in tap water through the addition of gold nanorods suspended in solution [42]. Oxidized mercury was reduced through the use of sodium borohydride, a strong reducing agent capable of reducing all forms of oxidized mercury to elemental mercury to allow for the amalgamation process to take place based on the following reactions:



The CTAB bilayer preferably binds to the longitudinal sides of the nanorods rather than the end surfaces, effectively shielding the nanorods on that side. As such, the active sites where the mercury amalgamation takes place are at the ends of the nanorods which have fewer CTAB molecules [43-44]. Upon amalgamation, the Au-Hg alloy is no longer optically active, causing the effective aspect ratio of the gold nanorod to decrease (figure 10), thereby causing a measurable decrease in the longitudinal SPR maximum wavelength. The decrease is linearly proportional to the concentration of mercury, allowing for quantification through the least squares method with the limit of detection of 0.153 ppb [42].

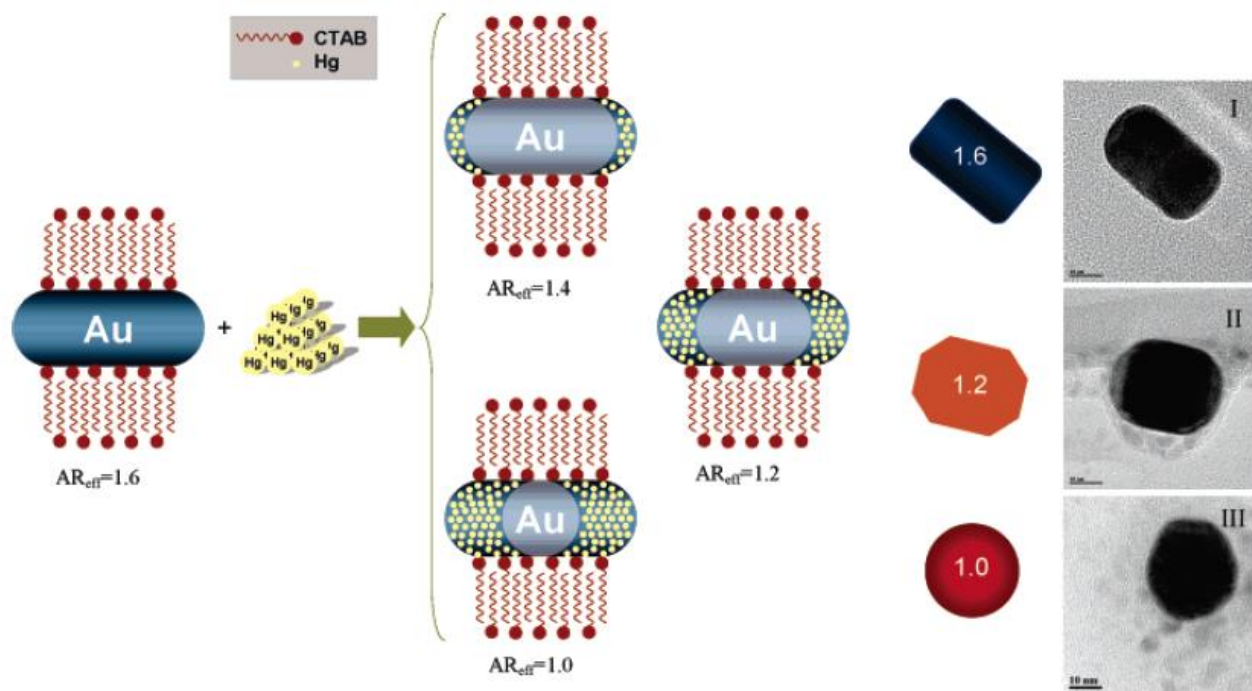


Figure 10. Schematic diagram of the amalgamation process of the gold nanorods with mercury and TEM images in the absence (I) and presence (II and III) of reduced mercury. [42]

## **CHAPTER 2: PORTABLE MERCURY SENSOR FOR TAP WATER USING SURFACE PLASMON RESONANCE OF IMMOBILIZED GOLD NANORODS**

Published in Talanta (Elsevier) vol 99 (2012) pg 180-185

### **2.1 Introduction**

While gold nanorods have high chemical stability, the main challenge to their use as a sensor is the aggregation of the nanorods due to the degradation of the CTAB bilayer due to the sample matrix. Upon aggregation, there is a drastic decrease in the spectral resolution of the SPR peaks due to the formation of macromolecules (figure 11). While the controlled aggregation of gold nanoparticles can be used as a colorimetric sensor [45-48], the loss of the longitudinal SPR wavelength prevents use of the sensor for the purposes of mercury detection as described herein. There are two main factors that contribute to the degradation of the bilayer and subsequent aggregation. The first is the presence of natural organic matter (NOM) which can adsorb onto the nanorod surface and displace the CTAB bilayer [49-50]. The second is ionic strength, particularly of negatively charged ions that can be attracted by the positively charged CTAB bilayer and effectively cancel out the electrostatic repulsion between the nanorods, leading to aggregation at high concentrations [51-52]. Water as a sample matrix can contain both high concentrations of organic matter as well as a high ionic strength that would make SPR based gold nanorod sensing difficult. The effects of NOM and ionic strength will be discussed further in chapter 4.

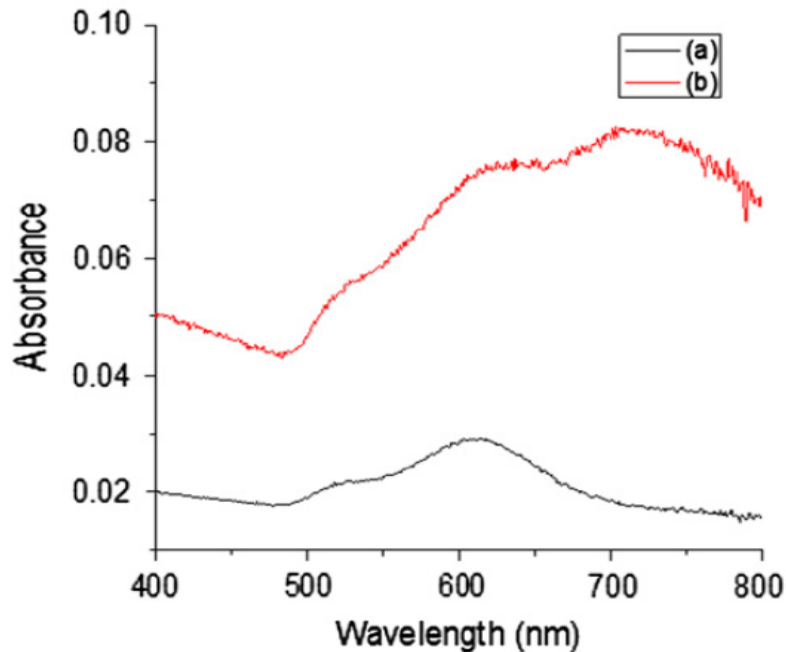


Figure 11. UV-Vis spectra of gold nanorods with longitudinal SPR peak at 615 nm without (a) and with (b) aggregation

In this chapter, an extension of the work done by Rex et. al. is presented [42]. A solution to prevent the aggregation of gold nanorods is proposed through the immobilization of the nanorods onto a solid silica substrate treated with (3-mercaptopropyl)trimethoxysilane (MPTMS). The thiol moiety of the MPTMS provides a capture surface for the gold nanorods, effectively adhering them to the solid substrate preventing aggregation even in the presence of NOM or high ionic strength. The characterization and experimental optimization of the substrate as well as the analytical figures of merit for the quantification of mercury for the sensor will be described herein [53].

## **2.2 Experimental**

### **2.2.1 Chemical and Reagents**

All experiments used analytical-reagent grade chemicals. Hydrogen peroxide (30%), hexadecyltrimethylammonium bromide (CTAB) and (3-mercaptopropyl)trimethoxysilane (MPTMS) were purchased at Sigma-Aldrich. Gold nanorods with peak longitudinal SPR wavelengths 615 nm ( $6.29 \times 10^{11}$  nanorods/mL), and 750 nm ( $5.77 \times 10^{10}$  nanorods/mL) were purchased from Nanopartz, Inc. According to the manufacturer, their average dimensions were 25×51 nm and 25×71 nm. Ethanol, sodium borohydride, mercury (II) chloride, sodium nitrate, lead (II) nitrate, copper sulfate, arsenic pentoxide, and sodium chloride were purchased from Fisher Scientific. Water (18 MΩ cm) was purified using a Barnstead Infinity Filter.

### **2.2.2 Instrumentation**

A Cary 50 (Varian) single beam spectrometer was used to record absorbance measurements. The illumination source was a 75-Watt pulsed xenon lamp with 2-nm fixed band-pass. Instrumental performance was monitored with a commercial standard (Photon Technology International) consisting of a single crystal of dysprosium-activated yttrium aluminum garnet mounted in a cuvette-sized holder with a well-characterized quasi-line absorption spectrum. Wavelength accuracy was evaluated periodically by comparing the recorded position of several spectral lines to the maximum wavelengths provided by the manufacturer. The standard deviations of the average maximum wavelengths obtained from repetitive scans within 300–800 nm confirmed the performance of the spectrometer according to specifications ( $\pm 0.02$  nm). When testing solutions, a 600  $\mu$ L quartz cuvette was used with 1-cm

path length. To examine the absorbance of the Gold nanorod-modified substrates, the substrates were placed against the face of a 1 cm quartz cuvette in the optical path.

Bright field images were acquired using a Nikon TE-2000U microscope equipped with a mercury lamp and 0.52 numerical aperture (NA) condenser. A Plan-Fluor 60X air objective (0.70 NA) collected the light that was imaged using a Retiga 1300i Fast 1394 CCD detector and QImaging software.

A Zeiss-ULTRA-55 FEG SEM was used to acquire images with an in-lens detector. An electron acceleration voltage of 2 kV was used to minimize charging the sample surface. Prior to imaging, surfaces were coated with a graphite layer using vacuum deposition.

### **2.2.3 Gold Nanorod Immobilization**

Glass cover slides were functionalized using the procedure detailed by Okamoto and Yamaguchi [54]. The cover slides were first cleaned using piranha solution (30% H<sub>2</sub>O<sub>2</sub> mixed in a 1:4 ratio with concentrated H<sub>2</sub>SO<sub>4</sub>) for twenty minutes and rinsed with copious amounts of water. The slides were dried and then immersed in a solution containing 10% ethanol and 90% MPTMS (volume percent) for 10 min. The slides were again rinsed with copious quantities of methanol before being immersed in the colloidal Au nanoparticle solutions for two hours. Prior to immobilization, the gold nanorod solutions were chemically reduced using 0.100 M sodium borohydride as a reducing agent. The concentrations of the nanoparticle solutions varied based on the solution provided by the supplier, for the nanoparticles with 615 nm LSPR maximum, the concentration was  $2.2 \times 10^{11}$  nanoparticles/mL.

#### **2.2.4 Mercury Detection Measurements**

Chemically functionalized glass cover-slides with immobilized gold nanorods on the surface were immersed in water and placed in a cuvette in the beam path of a UV–Vis spectrophotometer. Since the amalgam formation between mercury and Au forms only with metallic Hg,  $2.22 \times 10^{-4}$  M  $\text{HgCl}_2$  was chemically reduced using 0.100 M sodium borohydride. The mercury was reduced prior to addition to the cuvette containing the Au NR sensor. Small volumes of mercury were added to the cuvette and allowed to react (10 min for immobilized nanorods and 4 min for nanorods in solution) and the absorbance spectra were measured after the additions, yielding a range of Hg concentrations from 1.0–50.0  $\mu\text{M}$ .

### **2.3 Results and Discussion**

#### **2.3.1 Immobilization of Gold Nanorods onto a Solid Substrate**

The functionalization of the silica substrate is possible through the conversion of the silica on the surface to silanol using a strong oxidizer such as the piranha solution. The methoxy groups of the MPTMS are hydrolyzed to the silanol groups which – upon condensation with each other and with the silanol groups of the glass – form a layer of MPTMS on the silica substrate [55-56]. The high affinity of the thiol moiety on the MPTMS provides a capture surface for gold nanorods, which then form a monolayer of immobilized nanorods along the surface of the substrate (figure 12).

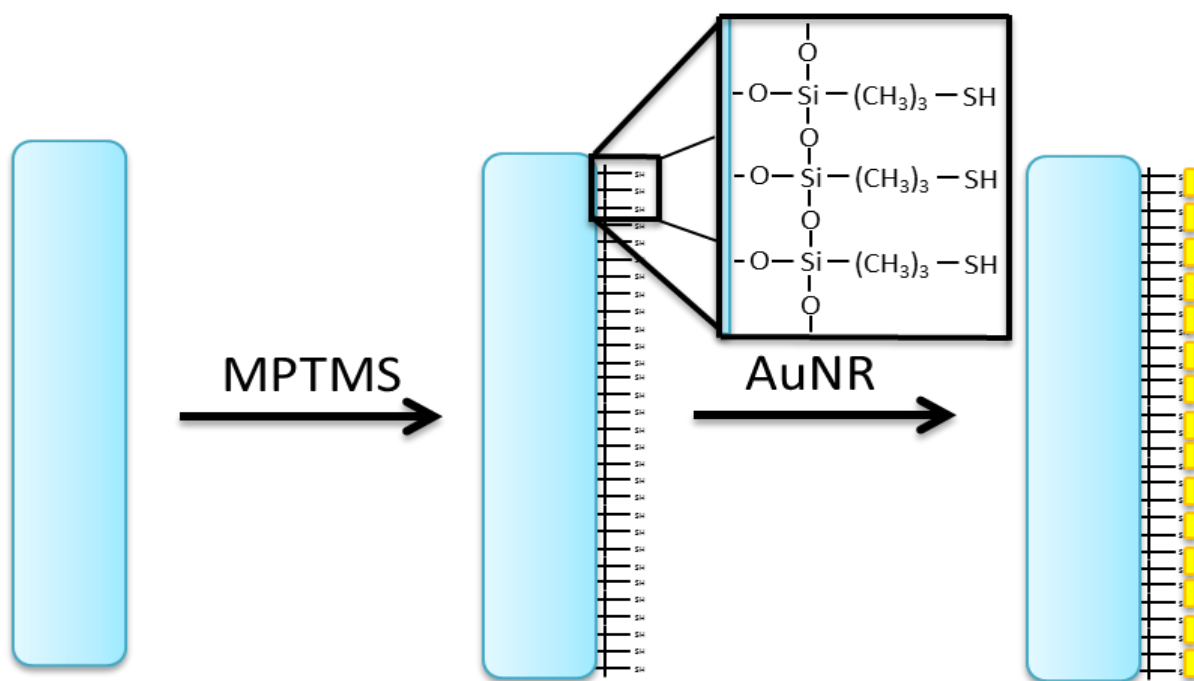


Figure 12. Schematic diagram of the procedure for the functionalization of a silica substrate with MPTMS and gold nanorods

Images of the gold nanorod functionalized solid substrates were acquired using scanning electron microscopy (SEM). The images show that the functionalization procedure causes a small amount of nanorod aggregation on the substrate surface with most of the gold nanorods flat on the surface of the substrate (figure 13). Longer immersion times resulted in greater number of nanoparticles up to a certain coverage. Optimization of the immersion time found that 2 hours was sufficient to deposit enough nanorods for a strong SPR absorbance signal. Increasing the immersion time beyond that point resulted in aggregation.



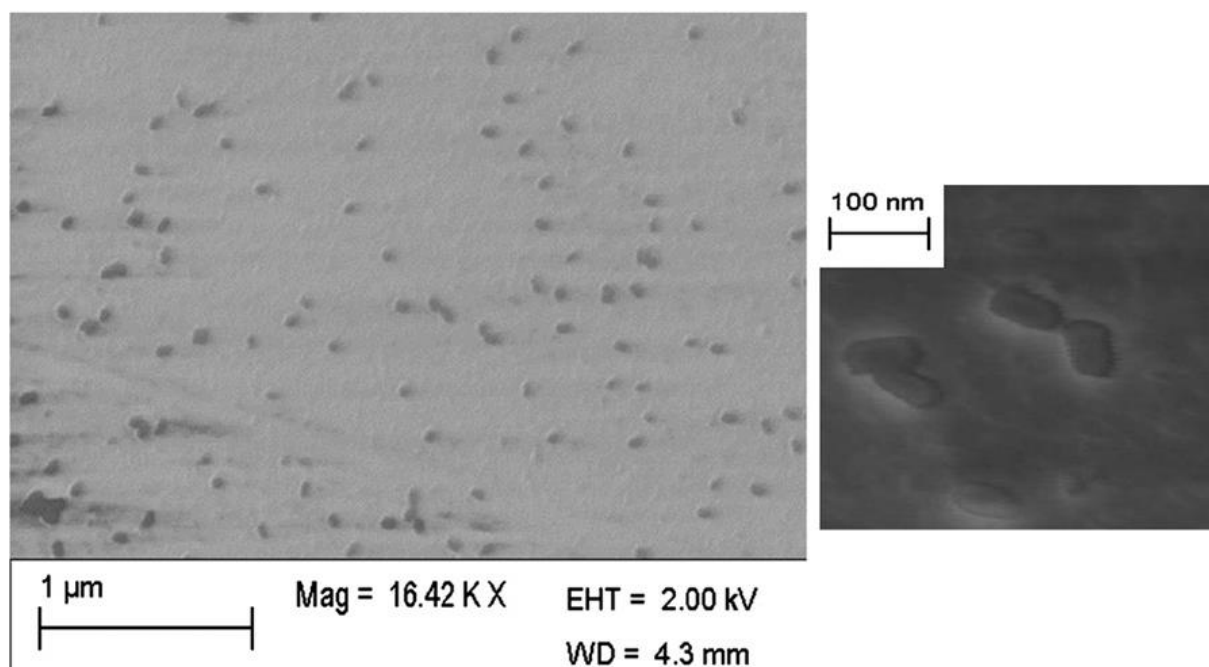


Figure 13. Scanning electron microscope images of gold nanorod functionalized solid silica substrates at varying magnifications

### **2.3.2 Mercury Detection**

As discussed in section 1.3.2, the SPR absorbance wavelength of the gold nanorods in solution is affected by two factors: the aspect ratio and the refractive index of the surrounding medium. The same phenomenon is observed with the immobilized gold nanorods, with a change in the SPR maximum wavelength due the surround medium including contact with the thiol surface due to the immobilization as well. As such, the nanorod response to mercury must be measured in a way that the changes in refractive index are not present or negligible in order to accurately quantify the mercury concentration through the shift in the SPR wavelength. The shift due to refractive index are most noticeable when the functionalized substrate is exposed to air ( $n = 1.00$ ) as opposed to when the substrate is immersed in water ( $n = 1.33$ ), wherein the there

is only a slight difference in the SPR maximum when compared to gold nanorods in solution (figure 14).

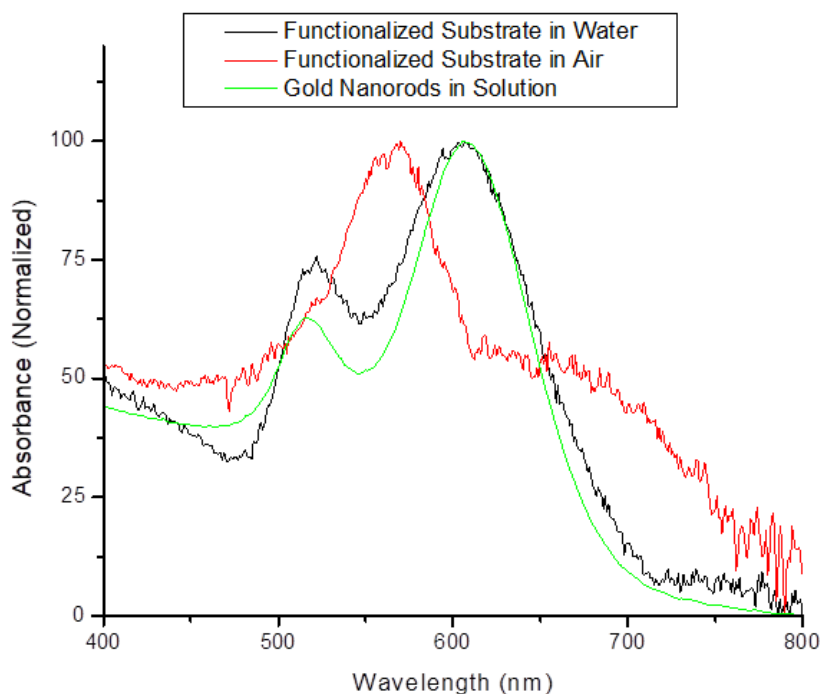
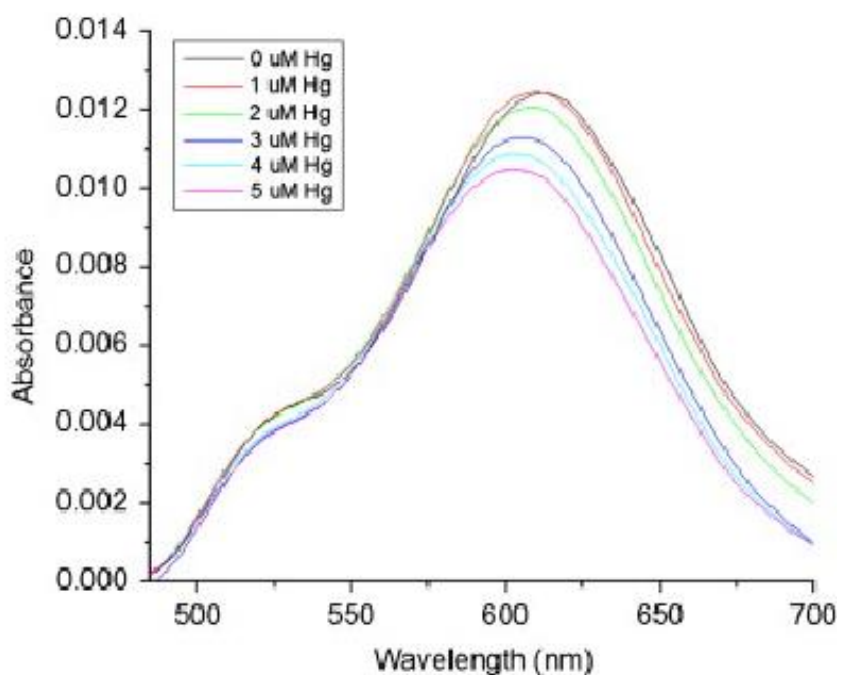


Figure 14. UV-Vis spectra of gold nanorods with longitudinal SPR peak at 615 nm in solution (green), immobilized onto a solid substrate exposed to water (black) or air (red)

In order to attribute the shifting SPR wavelength response to the mercury amalgamation process rather than the change in the refractive index, the solid substrate is kept in an aqueous solution and the spectra of the immobilized gold nanorods is recorded prior to mercury additions to establish the starting wavelength. It is also important to note that the extent to which the aspect ratio of the nanorods changes upon amalgamation with mercury depends on the number of nanorods present or exposed to the mercury for a given concentration of mercury. Hence, the calibration for the quantification on mercury is calculated based on the change in wavelength per

nanorod. The number of nanorods in solution is proportional to the absorbance signal of the SPR, allowing for calculation of the number of nanorods immobilized on the surface by measuring the difference in absorbance of the nanorod solution used before and after functionalization with the solid substrate. Upon addition of the reduced mercury, a decrease in the SPR wavelength was observed in the spectra. The change in the wavelength max was plotted as a function of the ratio between the molar concentration of mercury and the number of nanorods on the substrate, leading to a linear calibration curve (figure 15).

A



B

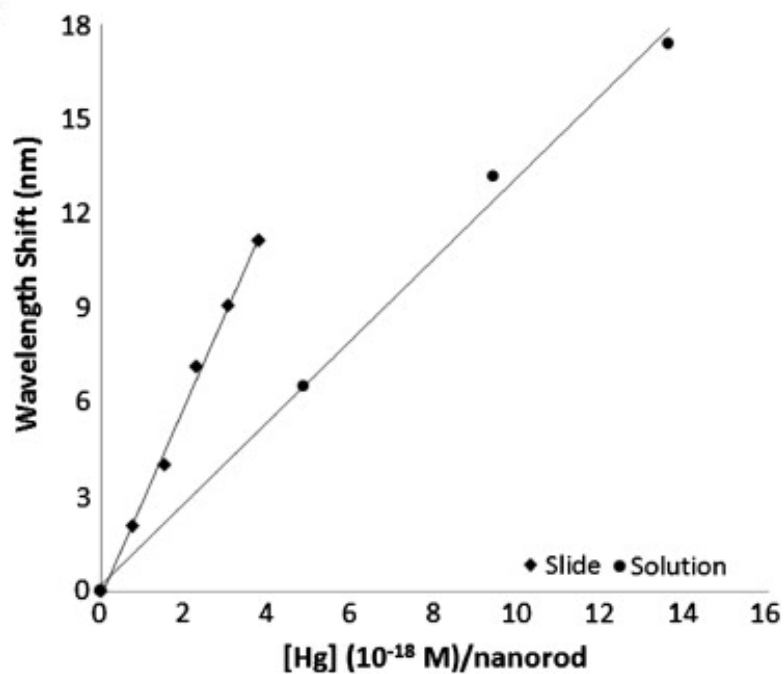


Figure 15. (A) Absorbance spectra of immobilized gold nanorods in aqueous solution with addition of reduced mercury. (B) Calibration curve showing the change in the SPR wavelength in the presence of mercury of the solid sensor and of gold nanorods in solution

### **2.3.3 Analytical Figures of Merit**

The analytical figures of merit were investigated for two types of sensors: immobilized gold nanorods on solid substrates and gold nanorods suspended in an aqueous solution. Both sensors used nanorods of the same aspect ratio (25 x 51 nm). After estimating the number of nanorods present on the surface or in solution, the SPR wavelength response of each sensor in the presence of mercury was plotted as a function of the concentration of mercury and the number of nanorods on the surface or in solution (table 2). Plotting the change in wavelength as a function of concentration of mercury per nanorod removes potential variations in sensitivity due to differences in nanorod density on the surface of the substrate or in solution. For each concentration plotted on the calibration graph, the change in SPR wavelength was the average of three measurements taken from three spectral runs. The linear fittings ( $\Delta\lambda = b \cdot [\text{Hg}]/\text{NR} + a$ ) and the statistics of the fittings ( $a \pm s_a$  and  $b \pm s_b$ ) were calculated with the least squares method. The correlation coefficients of the calibration curves are close to unity with a calculated F-value of 5.1 and a critical F-value of 19.1, indicating that the calibration curve is linear with a 95% confidence [57]. The sensitivity ( $\Delta\lambda \cdot \text{NR} / [\text{Hg}]$ ; units of  $\text{nm M}^{-1}$ ) of the sensors was calculated as the slope of the calibration curve. The limits of detection (LOD) were calculated using the equations recommended by the International Union of Pure and Applied Chemistry (IUPAC) [58].

Table 2. Analytical figures of merit for mercury detection using gold nanorods in solution or gold nanorods immobilized on a solid substrate

	<i>Gold Nanorod Solution</i>	<i>Immobilized Gold Nanorods</i>
$\Delta\lambda = b \cdot [\text{Hg}] / \text{NR} + a^a$	$\Delta\lambda = 1.30 \times 10^{18} \cdot [\text{Hg}] / \text{NR} + 0.2$	$\Delta\lambda = 2.99 \times 10^{18} \cdot [\text{Hg}] / \text{NR} - 0.1$
Correlation Coefficient	0.9952	0.9957
Sensitivity	$1.30 \times 10^{18} \text{ nm.NR.M}^{-1}$	$2.99 \times 10^{18} \text{ nm.NR.M}^{-1}$
Standard deviation of the slope <sup>b</sup>	$\pm 0.06 \times 10^{18} \text{ nm.NR.M}^{-1}$	$\pm 0.09 \times 10^{18} \text{ nm.NR.M}^{-1}$
Standard deviation of the intercept <sup>b</sup>	$\pm 0.6 \text{ nm}$	$\pm 0.2 \text{ nm}$
LOD (M/NR) <sup>c</sup>	$2.49 \times 10^{-18}$	$3.24 \times 10^{-19}$

<sup>a</sup>Equation for the linear best fit with b = slope/sensitivity and a = intercept

<sup>b</sup>Standard deviations calculated according to calibration guidelines [57]

<sup>c</sup>Limits of detection calculated according to IUPAC guidelines [58]

Comparison of the analytical figures of merit of the nanorods in solution with the immobilized nanorods shows sensitivities of the same order of magnitude, indicating that the chemical functionalization of the nanorods to the surface of a solid substrate does not significantly impact the surface area available for the mercury amalgamation to take place at the ends of the nanorods. The lower limit of detection with the immobilized gold nanorods results from the approximately two times higher sensitivity and the approximately three times lower standard deviation of the intercept. One possibility for the poorer reproducibility of measurements of the gold nanorods in solution is the scatter of resulting from a longer optical path length and the random motion of the nanorods.

### **2.3.4 Interference Studies**

The utility of a mercury sensor relies on its sensitivity for mercury without interferences from other potential species found within the sample matrix, which in this case are inorganic ions

that can be present and are also reduced by the sodium borohydride along with the mercury. The selection of potential interferences followed the EPA list of soluble inorganic ions (arsenic, barium, copper, sodium and lead) and a variety of counterions (oxide, acetate, sulfate, chloride and nitrate) commonly found in tap water composition [3]. Each ion was individually tested at 5  $\mu\text{M}$  concentration, i.e. a much higher concentration than what is presented as the maximum contamination level by the EPA in tap water samples, with the reference being the SPR wavelength of the immobilized gold nanorods immersed in Nanopure water before addition of the ion concentration (table 3). The standard deviations of the average shifts in SPR wavelength are within the experimental error of the reference signal ( $P = 95\%$ ;  $N = 3$ ), indicating that none of the ions tested caused significant spectral shifts that could interfere with the accuracy of the mercury detection.

Table 3. Shift in the SPR absorbance maximum wavelength for the immobilized gold nanorod sensor in the presence of 5  $\mu\text{M}$  concentration of a potentially interfering species

<i>Compound</i>	$\text{As}_2\text{O}_5$	$\text{Ba}(\text{C}_2\text{H}_3\text{O}_2)_2$	$\text{CuSO}_4$	$\text{NaCl}$	$\text{Pb}(\text{NO}_3)_2$
$\Delta\lambda_{\text{max}} \text{ (nm)}$	$0.5 \pm 0.1$	$-0.5 \pm 0.1$	$-0.5 \pm 0.1$	$0.0 \pm 0.3$	$-0.7 \pm 0.1$

### **2.3.5 Quantification of Mercury in Tap Water**

The ability of the immobilized gold nanorod sensor to detect mercury in tap water was evaluated by the multiple standard addition of mercury to a tap water sample. The immobilized gold nanorod sensor was immersed in a solution containing 2% (by volume) tap water reduced with 0.1 M  $\text{NaBH}_4$ , followed by additions of 5  $\mu\text{L}$  aliquots of 200.0  $\mu\text{M}$   $\text{HgCl}_2$  to the solution to construct a multiple standard addition curve (figure 16). The concentration of mercury in the tap water sample was calculated by extrapolation to the x-intercept of the standard addition curve,

obtaining a mercury concentration of  $9.5 \times 10^{-10}$  M, a value that is below the limit of detection of the sensor.

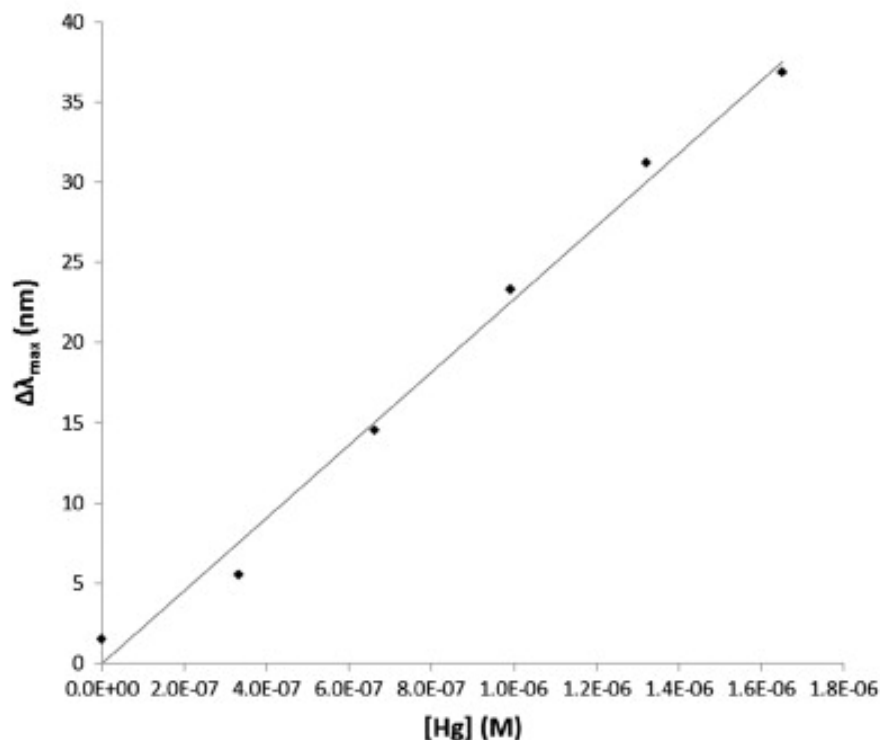


Figure 16. Multiple standard addition curve for the quantification of mercury in tap water

The quantification of capabilities of the sensor for mercury in contaminated tap water were also evaluated by creating a synthetic sample consisting of several EPA contaminants with a known and quantifiable concentration of mercury using the same multiple standard addition method. The experiment would reveal whether the mercury interaction with the potentially interfering species would result in erroneous quantification of mercury. The synthetic mixture contained all of the following species at their EPA limits: sodium chloride ( $7.0 \times 10^{-3}$  M), copper sulfate ( $2.1 \times 10^{-5}$  M), barium acetate ( $1.5 \times 10^{-5}$  M), arsenic (V) oxide ( $1.3 \times 10^{-7}$  M), and lead nitrate ( $7.2 \times 10^{-8}$  M). The mixture also contained mercury, spiked to a concentration of



$5.0 \times 10^{-7}$  M. The concentration determined from the standard addition plot was  $5.0 (\pm 1.6) \times 10^{-7}$  M, which found to be statistically indistinguishable (95% confidence) from the spiked concentration using the t-test (figure 17).

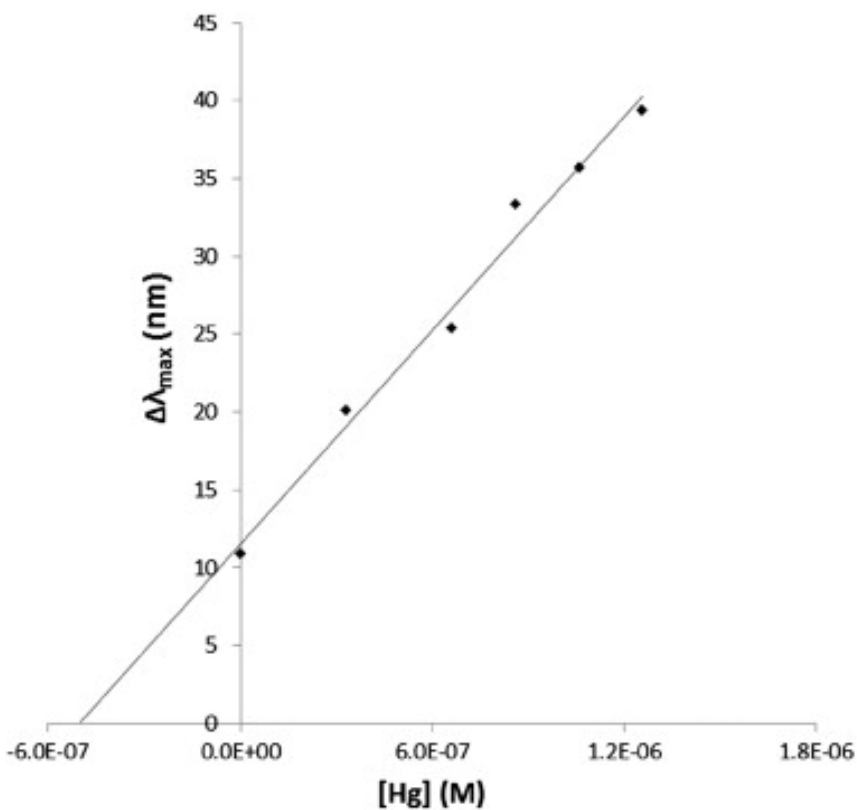


Figure 17. Multiple standard addition curve for the quantification of mercury in a synthetic contaminated tap water sample

## **2.4 Conclusion**

This chapter details the analytical capabilities of gold nanorods immobilized on a solid silica substrate for sensing mercury in water samples. In comparison to solution measurements, the immobilization of gold nanorods on a solid substrate improves both the sensitivity and the limit of detection. Immobilization of the gold nanorods also prevents aggregation from

degradation of the surfactant layer due to adsorption of organic matter or high ionic strength. No interference was observed from several inorganic ions commonly present in tap water samples, showing selectivity to mercury through the amalgamation with gold. The possibility of using solid substrates with immobilized gold nanorods is a step towards further functionalization of the sensor such as the conversion of the sensor to an electrochemical based sensor which will be discussed in chapter 3, or analysis of mercury in water flows using flow injection analysis which will be discussed in chapter 4.

## **CHAPTER 3: INDIUM TIN OXIDE ELECTRODE MODIFIED WITH GOLD NANORODS FOR POTENTIAL CONTROLLED SURFACE PLASMON RESONANCE STUDIES**

Published in *Microchimica Acta* (Springer Nature) vol 180 (2013) pg 1013-1020

### **3.1 Introduction**

This chapter presents an approach for the enhancement of the immobilized gold nanorod sensor through the introduction of potential control through the use of a silica substrate coated with a layer of indium tin oxide (ITO). ITO is a well-known ternary composition with a formulation of 74% indium, 18% oxygen, and 8% tin by weight. It has a high electrical conductivity with a similar optical transparency as glass. This modification will remove the need for a reducing agent, as well as open up possible avenues for other trace metal quantification as well as speciation due to the ability to control the reduction potential, though this chapter will be focusing on its use as a mercury sensor. The use of gold nanoparticle functionalized ITO coated glass slides is well documented. Its applications include but are not limited to enhancement of chemiluminescence [58-59], SPR based biosensors [60-62], or hydrogen peroxide sensors [63]. Herein, the combination of SPR sensing through UV-Vis spectroscopy with simultaneous electrochemical potential control will be investigated with mercury sensing as the model system.

However, the translation of the procedures used for the immobilization of gold nanorods onto a silica glass slide to immobilized gold nanorods onto ITO slides has proven difficult due to the difference in the surface of the substrate. The ITO thin film on the glass occupies the majority of the silica surface, making MTPMS functionalization and the subsequent gold nanorod immobilization difficult. Thus, a systematic investigation of the optimum parameters for the immobilization of gold nanorods onto ITO-coated glass slides using MPTMS was needed.

Optimization of MPTMS surface coverage through proper reaction times, solvent, and temperature conditions will be discussed [58,64-65], as well as CTAB removal, and ionic strength conditions needed for reproducible production of the gold nanorod-MPTMS-ITO electrodes [66].

## **3.2 Experimental**

### **3.2.1 Chemical and Reagents**

Indium tin oxide coated ( $70\text{--}100\ \Omega \cdot \text{sq}^{-1}$ ) glass cover slides were purchased from Sigma-Aldrich. Fisher Scientific supplied (3-mercaptopropyl) trimethoxysilane, concentrated ammonium hydroxide, sulfuric acid, potassium ferrocyanide, potassium nitrate, and sodium chloride. Gold nanorods with peak longitudinal SPR wavelength 615 nm ( $6.29 \times 10^{11}$  nanorods  $\cdot \text{mL}^{-1}$ ) and aspect ratio 1.9, were purchased from Nanopartz, Inc. Silver epoxy used to attach a lead to the ITO electrode was acquired from Ted Pella, Inc. Nanopure water ( $18\ \text{M}\Omega\text{-cm}$ ) was purified using a Barnstead Infinity Filter.

### **3.2.2 Instrumentation**

Absorbance spectra were acquired using an HR4000 UV–Vis spectrometer. The  $25 \times 25$  mm ITO slides were placed in an optical glass cuvette (Starna Cells) with dimensions large enough to accommodate the ITO working electrode, Ag/AgCl miniature reference electrode (eDAQ, Inc.) and platinum wire counter electrode. Potential control was attained using CH Instruments 400A potentiostat. For contact angle measurements, a Ramé-Hart Goniometer 100 was used with a  $10\ \mu\text{L}$  sessile drop imaged on the surface. SEM images were acquired using a

Zeiss-ULTRA-55 FEG. An in-lens detector and electron acceleration voltage of 2.00 kV were used to acquire images of Gold Nanorod-MPTMS-ITO electrodes.

### **3.2.3 Preparation of MPTMS-modified ITO Electrodes**

Commercially obtained ITO coated glass cover slides were cleaned by sonication for 20 min in each of the following solvents sequentially: soapy water, water, acetone, and methanol. The slides were then dried and treated with 1 % (v/v)  $\text{NH}_4\text{OH}$  in Nanopure water for 1 h at 80 °C. After the immersion in  $\text{NH}_4\text{OH}$ , the slides were rinsed with copious quantities of water and dried at room temperature for several hours.

Several methods for MPTMS self-assembly were tested to attain high surface coverage (table 4). After determining which concentration of MPMTS and reaction conditions (reflux or room temperature) was required, reaction times to prepare MPTMS-modified ITO slides were investigated. Elucidation of required reaction time was accomplished by immersing the hydroxide-treated ITO slides in 10 % (v/v) MPTMS in ethanol for varying lengths of time. MPTMS-ITO slides were subjected to a variety of reaction times with 15 min increments in the MPTMS reaction solution. After removing the slides from the MPTMS solutions, they were rinsed with copious quantities of methanol and allowed to dry at room temperature. The slides were then treated by heating to 110 °C in an oven for 60 min to allow Si-O-Si condensation. Slides were stored in methanol until they were used, either for contact angle and cyclic voltammetry characterization or for gold nanorod immobilization.

Table 4. Reaction conditions for MTPMS-ITO monolayer self-assembly

Method Designation	Volume % MTPMS	Solvent	Reaction Condition	Reaction Time
1	10%	Toluene	Reflux	60 minutes
2	10%	Ethanol	Room temp	0 – 60 minutes
3	2%	Ethanol	Room temp	24 hours

### **3.2.4 Attachment of Gold Nanorods to MPTMS-modified Electrodes**

Commercially produced gold nanorods were treated prior to immobilization on MPTMS-ITO cover slides by removal of excess CTAB from the nanorod solution and adjusting the ionic strength with NaCl. This was accomplished by subjecting 1.00 mL of nanorod solution to two centrifugation cycles at 6,000 rpm for 30 min each. After each centrifugation, 900  $\mu$ L supernatant volume was removed and replaced with the same volume of Nanopure water. Additional centrifugation steps caused precipitation of the gold nanorods. As described by Ferhan et al., the ionic strength of NR solutions can strongly affect the immobilization capabilities of the nanorods [67]. To control the ionic strength, a 0.01 M stock solution of NaCl was prepared and small aliquots added to the 1 mL of nanorod solution to attain the desired NaCl concentration (between 10  $\mu$ M and 100  $\mu$ M). Gold nanorods with low CTAB concentration and varying NaCl concentration were immobilized on the MPTMS-ITO surfaces by placing a 1 mL drop of the NaCl/Nanorod solution on the surface of the MPTMS-modified ITO for varying times (between 4 h and 17 h). ITO electrodes with gold nanorod modification were stable for up to 1 month when stored in Nanopure water.

### **3.2.5 Electrochemical Characterization**

Bare ITO, MPTMS-modified ITO and Gold Nanorod-MPTMS-ITO electrodes were examined using cyclic voltammetry with 1 mM ferrocyanide at  $100 \text{ mV} \cdot \text{sec}^{-1}$  scan rate. The supporting electrolyte was 0.1 M  $\text{KNO}_3$ , although other unreactive supporting electrolytes such as KCl would also be suitable. Verification of the presence of gold nanorods on the ITO surface was accomplished using cyclic voltammetry in 0.5 M  $\text{H}_2\text{SO}_4$  solution in the range of  $-0.15$  to  $1.4 \text{ V}$  at  $100 \text{ mV} \cdot \text{sec}^{-1}$  scan rate. To monitor the SPR signal in response to applied potential, Gold Nanorod-MPTMS-ITO electrodes were immersed in 0.1 M  $\text{KNO}_3$  with potential applied using a potential step procedure with simultaneous UV–Vis absorbance measurements.

## **3.3 Results and Discussion**

### **3.3.1 MPTMS Surface Modification and Characterization**

Producing an ITO electrode surface capable of capturing gold nanorods requires formation of an adequate MPTMS layer similar to the procedure done in chapter 2. Fractional monolayer coverage has two disadvantages. The first is that gaps in the MPTMS layer would allow diffusion of electrochemical species to the ITO surface, creating a competitive surface in addition to the nanorods at which electrochemical reactions can occur. Secondly, submonolayer coverage would result in a scarcity of thiol functionality. Abundant thiol moieties are required to allow multiple capture sites for the gold-thiol binding to occur, a necessary step in forming nanorod-modified electrodes that is already challenging due to the electrostatic repulsion between the positively charged nanorods due to the CTAB particles.

As such, multiple methods were investigated in order to determine the optimal reaction conditions needed for MTPMS self-assembly (table 4). To determine whether the reflux MPTMS modification method was superior to the room temperature preparation, cyclic voltammograms were obtained for the refluxed and room temperature MPTMS-modified ITO slides [68-69]. The voltammograms were obtained in 1 mM ferrocyanide with 0.1 M  $\text{KNO}_3$  as a supporting electrolyte. The bare ITO slide showed typical reversible CV shape with  $\sim 60$  mV  $\Delta E_{\text{peak}}$ , while ITO slides that had been treated with MPTMS with either reflux or room temperature treatment did not show peak currents (figure 18). The lack of the peak current is consistent with the formation of a monolayer preventing diffusion of the solution redox species to the ITO surface as MPTMS monolayer itself is non-conductive. The conductivity of the electrode will be reestablished after formation of the gold nanorod layer and will be further discussed in section 3.3.3. Both room temperature methods (10% MTPMS for 60 minutes or 2% MPTMS for 24 hours) showed similar results, as such, the 60 minute MPTMS immersion procedure will be used due to the significantly shorter reaction time needed.



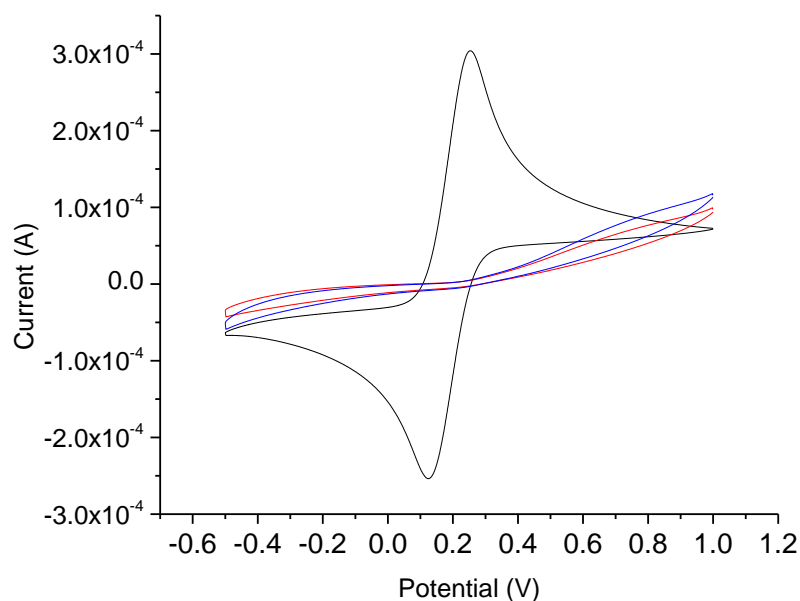


Figure 18. Cyclic voltammograms of a bare ITO slide (black line), ITO slide after reflux treatment (blue line), and room temperature treatment (red line)

Since both reflux and room temperature MPTMS modification method were successful, room temperature preparation methods were selected for simplicity. The time required to achieve an MPTMS monolayer was then investigated at room temperature. ITO slides were prepared using varying MPTMS reaction times and CVs measured for each (figure 19). The CVs revealed a reduction in anodic and reductive peak current and potential with reaction time, consistent with the formation of a monolayer that prevents diffusion of the solution redox species to the ITO surface. The change in peak potential is indicative of diminished rate of electron transfer and transition from reversible (bare ITO) to quasi-reversible (15–45 min reaction time) and irreversible (60 min) processes. The attenuation of redox peaks in CV experiments is consistent with the formation of highly ordered, compact self-assembled monolayers on ITO [70].

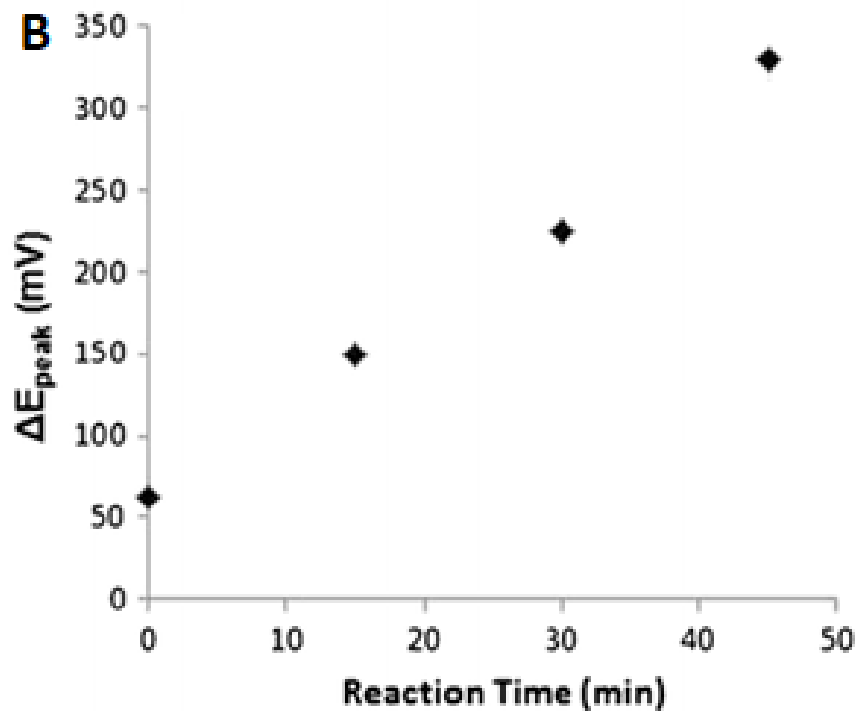
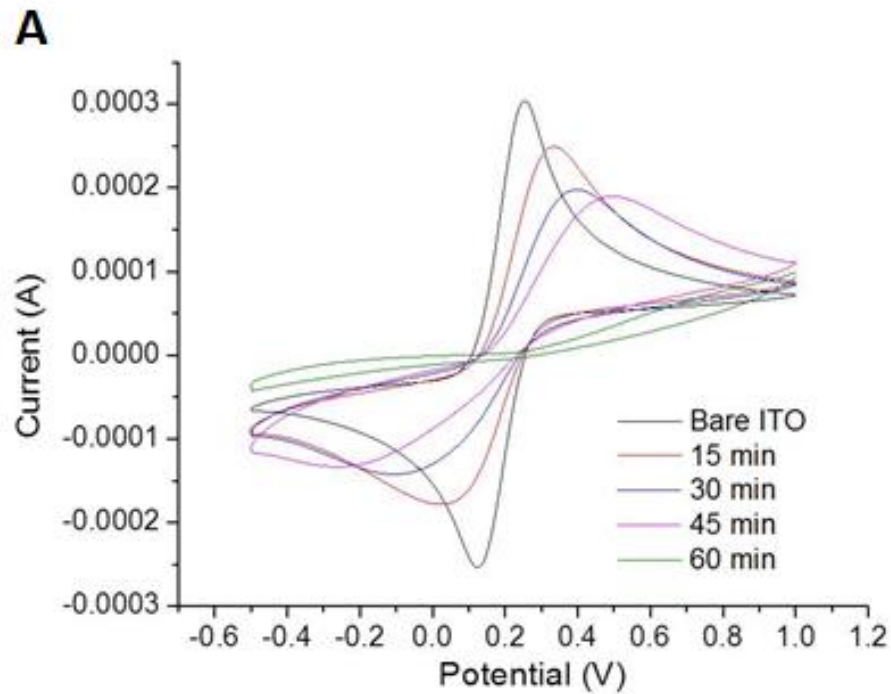


Figure 19. CV curves of bare ITO and MPTMS-modification with varying immersion times (a. 0 min, b. 15 min, c. 30 min, d. 45 min, e. 60 min). (B) Plot of the change in the anodic and reductive  $\Delta E_{\text{peak}}$  with MPTMS reaction time.

Further confirmation of the MPTMS monolayer formation was done through contact angle measurements as the bare ITO glass substrate is hydrophilic while the MPTMS monolayer is hydrophobic. The increasing contact angle of a sessile, 10  $\mu$ L drop of water on the MPTMS-ITO is consistent with the formation of a hydrophobic monolayer between the ITO and the water drop. When the contact angle is compared to the peak anodic current of the ITO slide in a ferrocyanide solution with respect to MPTMS reaction time, it is clear that the diminishing peak current with MPTMS reaction time is consistent with decreased access of the ferrocyanide to the ITO surface due to the formation of the MPTMS monolayer (figure 20). The 60 min MPTMS immersion was then used for all subsequent room temperature experiments as further immersion was not needed due to full MPTMS coverage.

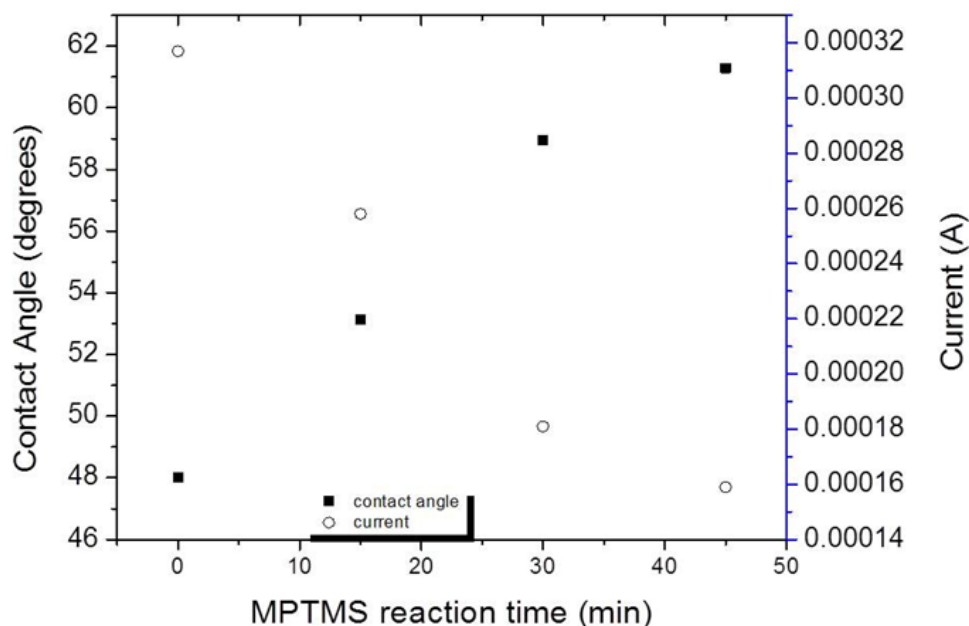


Figure 20. Contact angle of MPTMS-modified ITO slides and peak anodic current from CV curve with respect to MPTMS reaction time

### **3.3.2 Gold Nanorod Surface Modification and Characterization**

Despite adequate MPTMS surface coverage on the ITO slides, immersion of the slides in as-prepared commercial gold nanorod solution for 4 hours (twice the time needed for silica substrates) showed only limited success in attaching the nanorods to the thiols at the electrode surface (figure 21). The absorbance signal arising from the immobilized gold nanorods showed inadequate signal-to-noise for accurate SPR data acquisition with the electrode under potential control. Longer immersion times (up to 17 hours) in the nanorod solutions yielded similar results. It was concluded that the inadequate gold nanorod binding was due to electrostatic repulsion between positively charged CTAB bilayers surrounding the nanorods, such that the thiol sites at the surface remain unreacted. Unlike in silica substrates, the ITO surface seemed to contain significantly less available area for functionalization with the MPTMS, even after complete surface coverage, such that the thiol affinity for gold could not overcome the electrostatic repulsion between the nanorods.

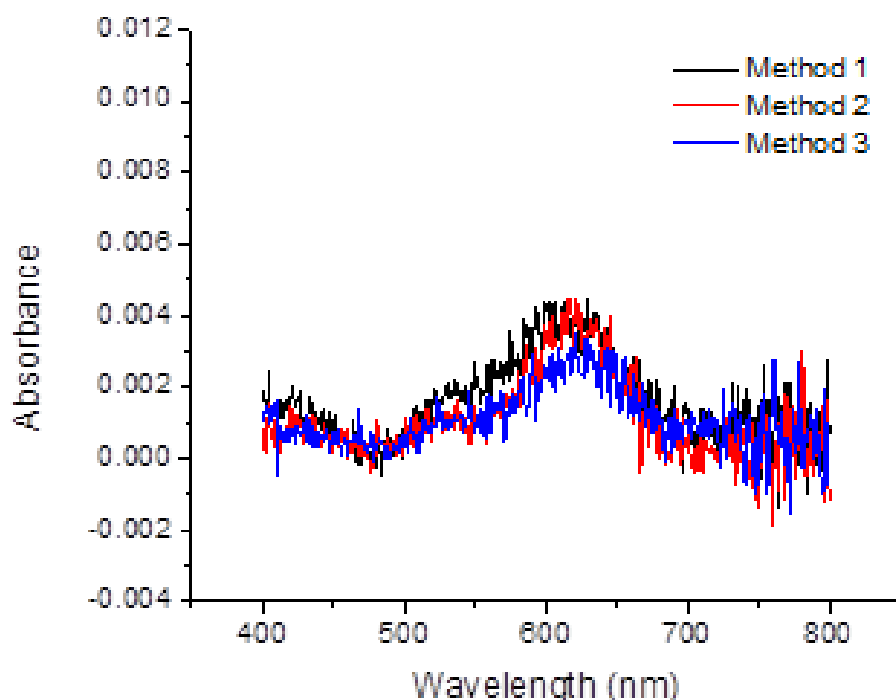


Figure 21. UV-Vis spectra of gold nanorods immobilized on ITO slides after functionalizing with MPTMS using methods 1-3 (table 4)

Ferhan et. al. detailed an approach to attenuate the excess CTAB in solution in concert with the addition of counter ions to minimize electrostatic repulsion and achieve higher surface coverage of NR on glass substrates [67] (figure 22). Although the thiol-gold immobilization approach here is different from that described by Ferhan et. al., the theory behind the adjustment in inter-nanorod forces in order to increase the favorability of nanorod deposition can be applied herein. Centrifugation to remove CTAB was attempted prior to immersing MPTMS-ITO slides in the gold nanorod solution. Two rounds of centrifugation and re-suspension showed improved nanorod immobilization (figure 23), tripling the absorbance of slides produced without centrifugation, but the signal-to-noise was still inadequate. Additional centrifugation resulted in the inability to re-suspend the nanorods due to insufficient CTAB available to form the bilayer,

resulting in aggregation. As such, alternative measures were required to diminish electrostatic repulsion further and enhance nanorod surface immobilization.

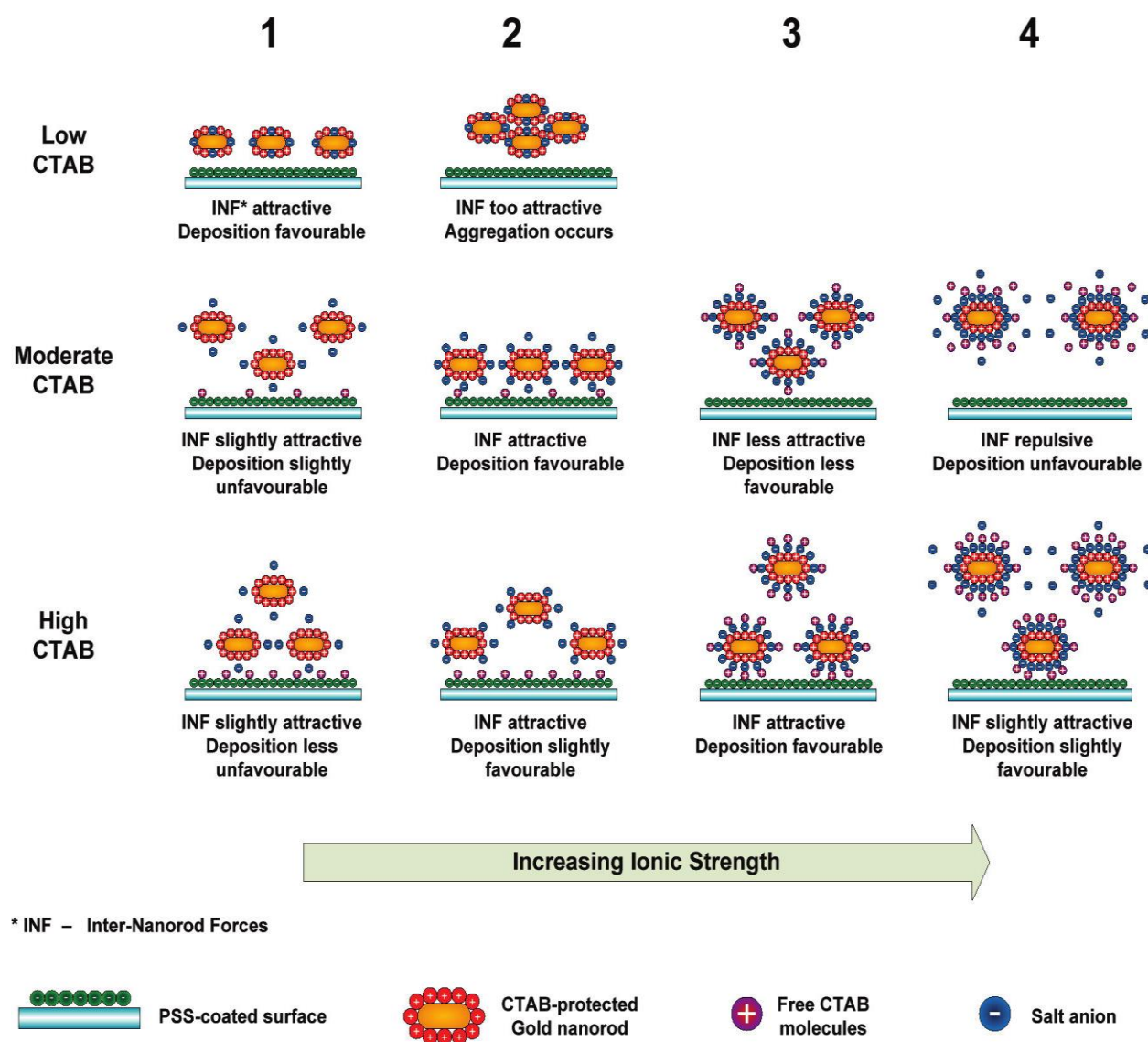


Figure 22. Schematics showing the inter-nanorod as well as nanorod-substrate interactions under increasing ionic strength at different CTAB concentrations [67]

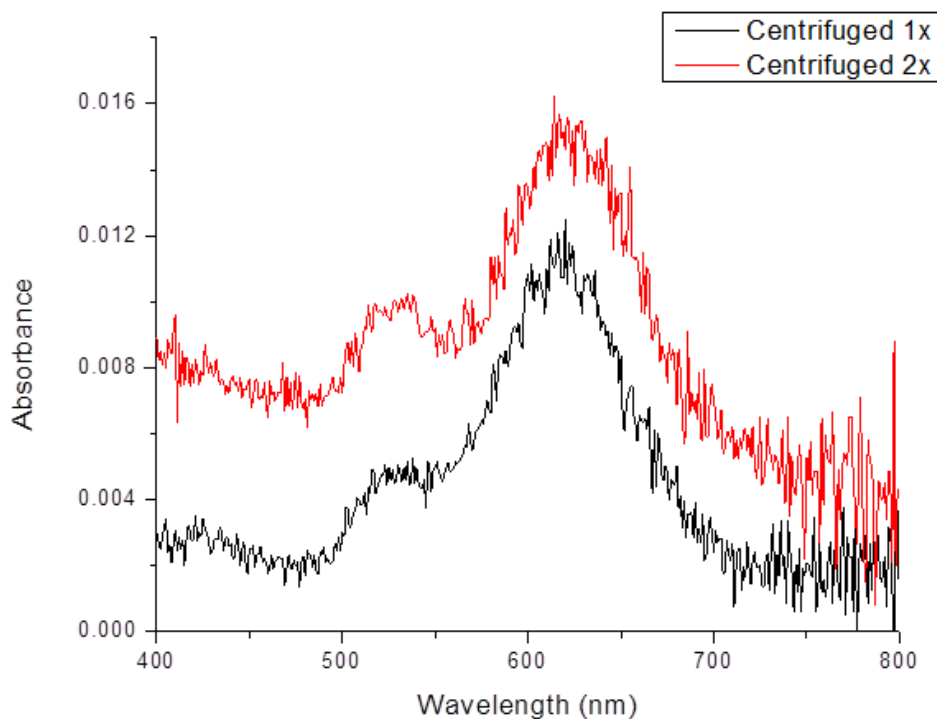


Figure 23. UV-Vis spectra of centrifuged gold nanorods immobilized on ITO slides

With the CTAB reduction showing improvement to the immobilization of the gold nanorods onto the MPTMS-ITO substrate, additional fine tuning of the electrostatic repulsion between nanorods was needed to further obtain acceptable coverage of the slide. This was accomplished through addition of ionic species to the nanorod solution to produce changes in the dispersion and aggregation behavior of the nanorods, ideally to reduce the electrostatic repulsion without causing significant aggregation. Sodium chloride was chosen as the model ion due to its simplicity, availability, and non-toxicity. Absorbance measurements of twice-centrifuged gold nanorod solution with addition of sodium chloride reveal a wide range of absorbance for solutions containing the same concentration of nanorods, varying only in the concentration of

sodium chloride (figure 24). It is apparent that the ionic strength changes the absorbance behavior of the nanorods in a nonlinear way, caused by repulsion or attraction of the nanorods.

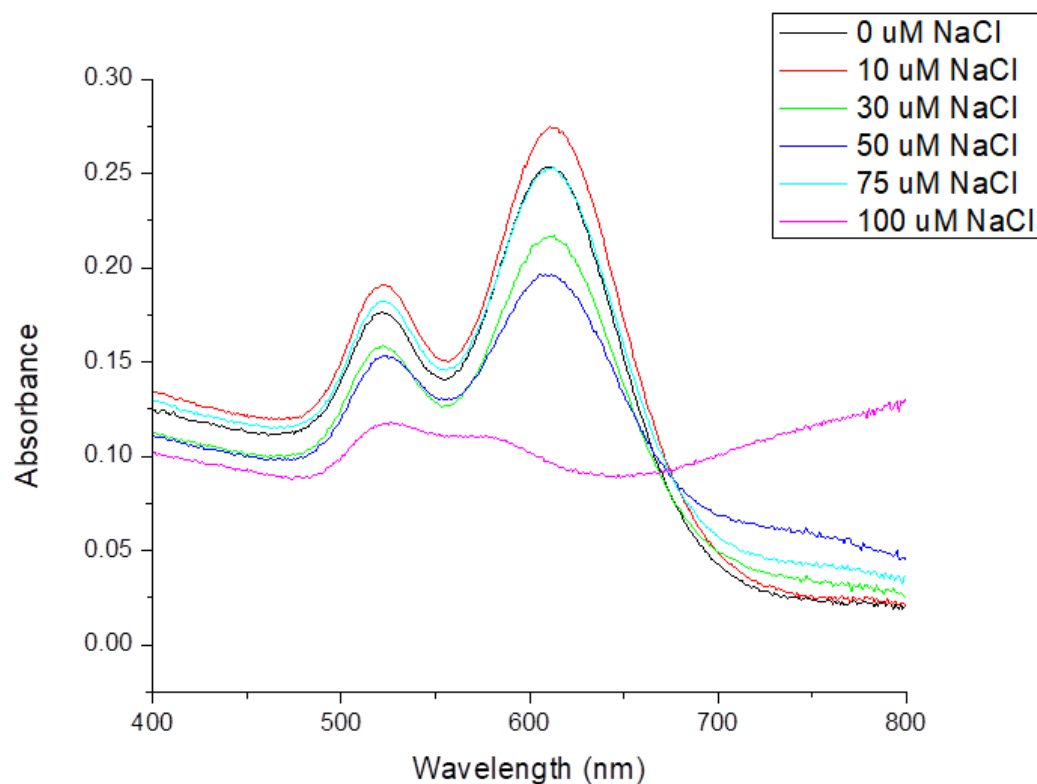


Figure 24. UV-Vis spectra of twice-centrifuged colloidal gold nanorods in solution in the presence of varying concentrations of sodium chloride

Addition of higher concentrations of sodium chloride can decrease the electrostatic repulsion between nanorods such that aggregation occurs and the signal is lost, as apparent in the weak absorbance of the 100  $\mu\text{M}$  NaCl solution. Nanorods in solution with lower NaCl concentrations may display diminished electrostatic repulsion which is exhibited in the solution nanorod SPR spectra by a slight decrease in absorbance. Moderate (50  $\mu\text{M}$ ) concentration of NaCl was selected for surface immobilization because this concentration yields reduced



electrostatic repulsion without resulting in aggregation. Using the moderate NaCl concentration combined with the centrifuged nanorods resulted in suitable conditions for minimal electrostatic repulsion, allowing for favorable deposition of the gold nanorods onto the MPTMS-ITO surface (figure 25). Comparison with the experiments with no NaCl added, the SPR absorbance of the immobilized nanorods increased eightfold with a 4 hour immersion time. Improved signal to noise of the absorbance spectra allowed selection of this procedure for all subsequent experiments in SPR measurements with potential control.

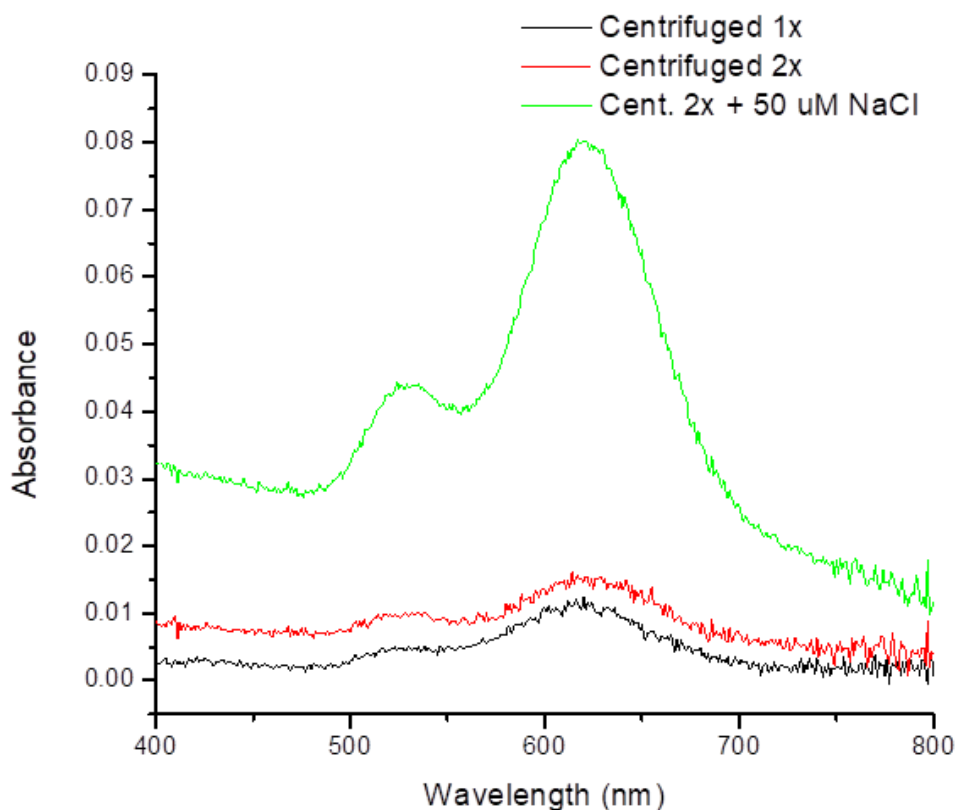


Figure 25. UV-Vis spectra of centrifuged gold nanorods with and without a moderate concentration of NaCl immobilized on ITO slides

Information about the distribution of individual nanorod and quantification of surface coverage was obtained through SEM images of the gold nanorod-MPTMS-ITO electrodes (figure 26). The well-dispersed particles are consistent with the absorbance spectral data, which showed no aggregation peaks in the spectra. Surface coverage of the nanorods was quantified by dividing the SEM images into sections with  $500\text{ nm} \times 500\text{ nm}$  dimensions and counting nanorods in 20 such sectors and dividing by the area of the region. The surface improved from 9 nanorods  $\cdot \mu\text{m}^{-2}$  in the absence of ionic strength control, to 15 nanorods  $\cdot \mu\text{m}^{-2}$  using a deposition solution containing  $50\text{ }\mu\text{M}$  NaCl.

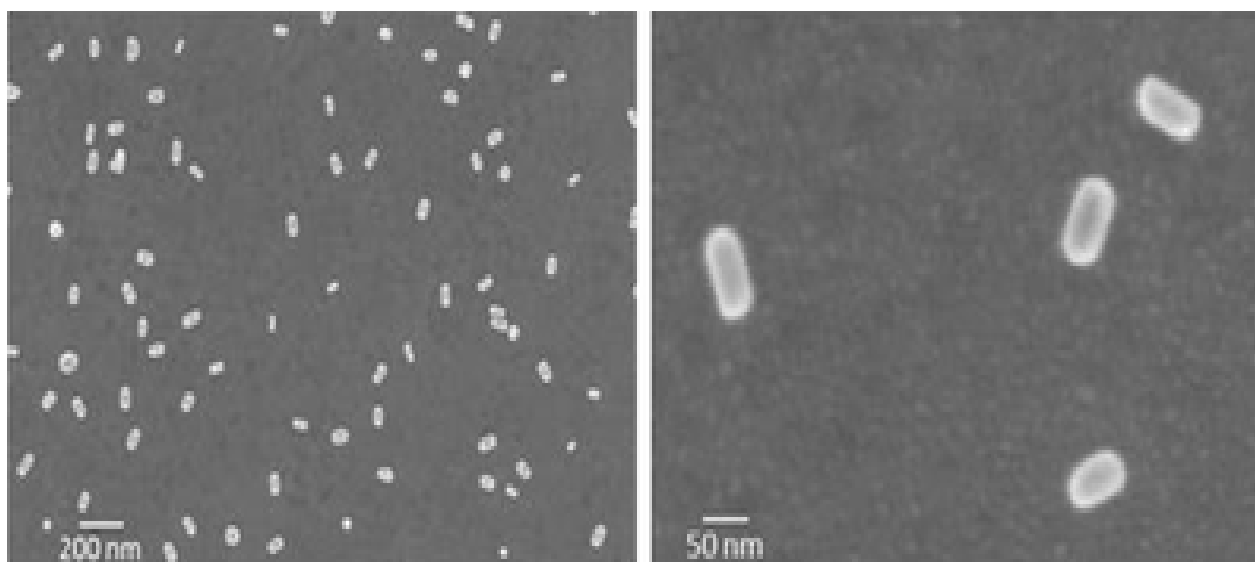


Figure 26. SEM images at different magnifications of gold nanorods immobilized on the MPTMS-ITO slide with surface coverage of 15 nanorods  $\cdot \mu\text{m}^{-2}$

### **3.3.3 Response of Gold Nanorod-MPTMS-ITO Electrodes under Potential Control**

The utility of combining SPR measurements with potential control has been previously investigated for applications such as metal detection with a gold electrode [71-72] and electric

field induced DNA hybridization [73]. Use of a gold nanorod-modified ITO electrode as an SPR sensor with conditions of applied potential requires characterization of the potential response of the nanorods as electrodes as well as the SPR response under potential control. As the conductivity of the ITO surface is effectively nullified after MPTMS functionalization, the potential control will be conducted on the gold nanorod surface, ensuring selectivity of the sensor to mercury. To confirm that the nanorods could act as sites for electrochemical reactions under potential control, the gold nanorod-modified electrodes were immersed in 0.5 M  $\text{H}_2\text{SO}_4$  and the CV response measured and compared to bare ITO and a bulk gold electrode under the same conditions (figure 27). The characteristic reductive peak at +0.84 V found on the gold electrode and similarly on the gold nanorod-ITO electrode can be attributed to the reduction of gold oxide that is formed after the anodic potential sweep [74-75], which confirms the presence of gold at the surface and that potential control over the nanorods separated through the silane-alkane-thiol layer can be achieved.

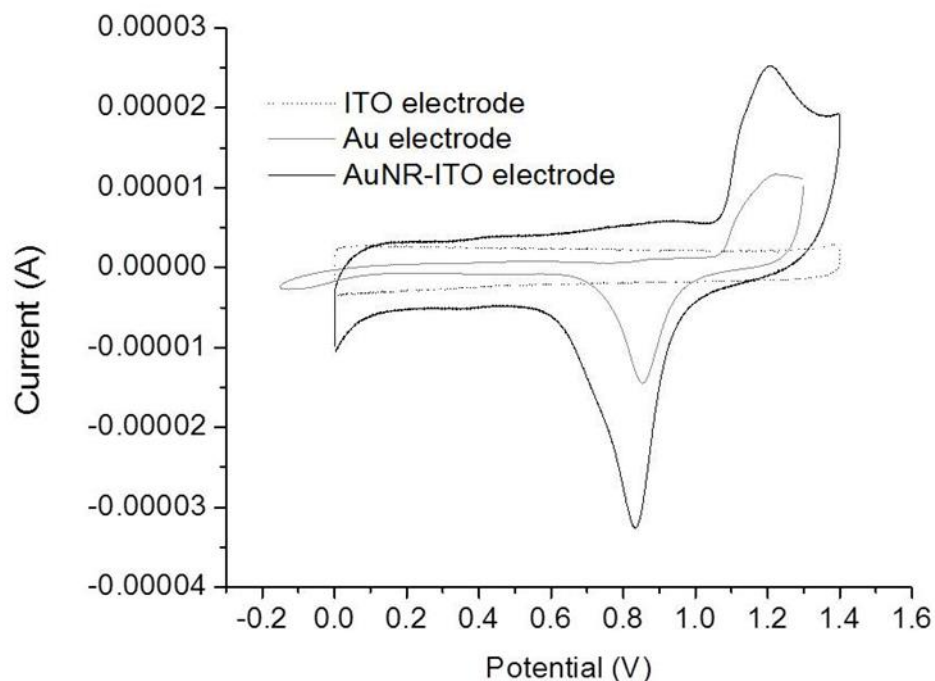


Figure 27. Cyclic voltammogram of a bare ITO slide (dashed line), bulk gold electrode (gray line), and gold nanorod-ITO electrode (black line) in 0.5 M H<sub>2</sub>SO<sub>4</sub>

The larger integrated area under the reductive peak for gold nanorod-MPTMS-ITO electrode relative to the bulk gold electrode arises from the difference in surface area between the two electrodes. The major contributions to the higher surface area of the gold nanorod-MPTMS-ITO electrode include the larger deposition area (25 x 25 cm ITO slide) compared to the smaller 2 mm gold electrode, as well as the higher surface area of the immobilized gold nanorods themselves due to higher surface roughness arising from microscopic features and the crystal structure of the gold nanorods compared to the bulk surface of the gold electrode. Gold oxide adsorption is among the most commonly used methods for surface roughness characterization [76]. The integrated gold oxide reductive peak area ( $5.9 \times 10^{-6}$  A) relative to the

peak area for the bulk gold electrode ( $2.2 \times 10^{-6}$  A) indicates that the gold surface area of the immobilized gold nanorods is a factor of ~2.6 times greater than that of the small gold working electrode.

With the voltammetric characterization of the gold nanorod-MPTMS-ITO electrode concluding the ability for potential control of the immobilized gold nanorods, characterizing the SPR response of the nanorods with applied potential is an essential control that must be performed prior to use of the electrode as a potential controlled SPR sensor. To determine the nanorod SPR response to different applied potentials, the electrode was immersed in 0.1 M  $\text{KNO}_3$  and the absorbance spectra recorded at a series of positive and negative potentials. This solution was selected to minimize the risk of redox reactions influencing the refractive index or gold structure at the nanorod surface, with the possible exception of the adsorption of ions within the double layer region. The longitudinal SPR peaks in the absorbance spectra are blue-shifted (lower wavelengths) under negative applied potential, while at positive potentials a red shift (higher wavelengths) is observed in the SPR peaks with respect to the wavelength with no potential applied (figure 28).

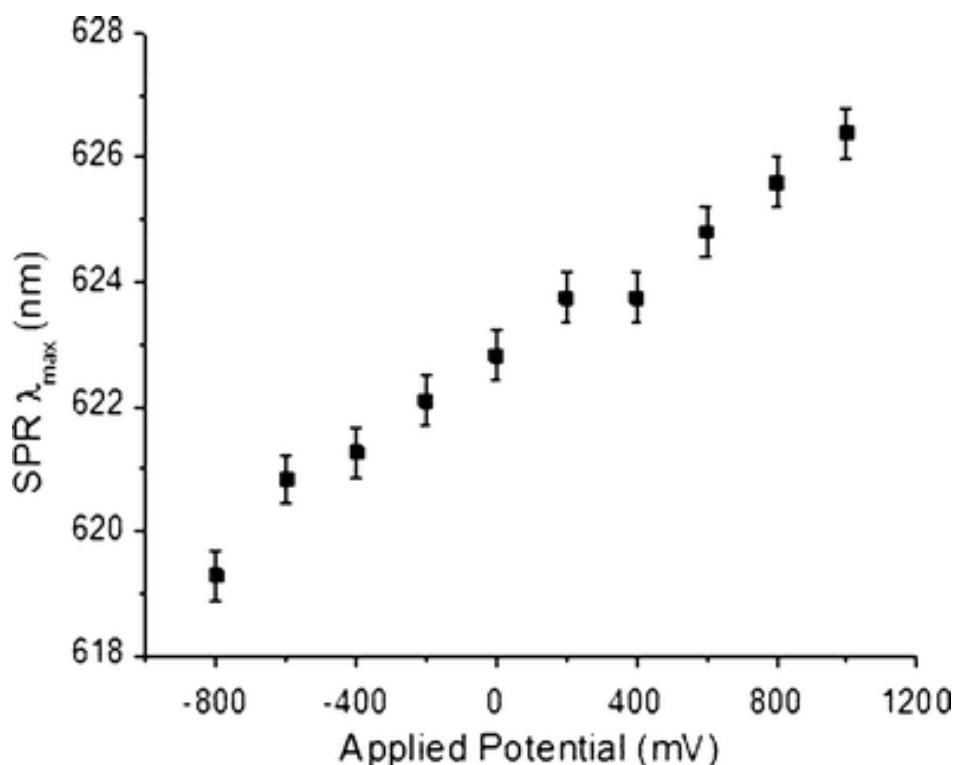


Figure 28. Plot of the SPR wavelength maximum under applied negative or positive potential

The linear response between wavelength shift and applied potential is due to the alteration in the electron density at the interface between the electrode and solution, particularly at the longitudinal surface plasmon mode of the nanorods, in a phenomenon known as electron charging [77-79]. However, this linear response deviates significantly if potentials were high enough to result in gold-oxide formation, which would cause irreversible difference in the refractive index of the surface of the gold electrode. As such, the upper limit of the applied potential should be the potential required for the gold-oxide formation which was seen in the gold nanorod-MPTMS-ITO electrodes at approximately +1.1 V. The reversible nature of the change in SPR response with potential, however, can be exploited to measure reversible changes in refractive index surrounding the nanorods. Alternatively, irreversible alterations in aspect

ratio of the nanorods resulting from reactions at the nanorod surface can be monitored after potential control is removed.

#### **3.3.4 Application of Gold Nanorod-MPTMS-ITO Electrodes to a Model System**

The potential application of the gold nanorod-MPTMS-ITO electrode as an SPR sensor was demonstrated with mercury as a model analyte system. The sensitivity and selectivity of gold nanorods to elemental mercury was discussed in section 1.3.2 and the same reactivity and amalgamation mechanism of mercury to the gold nanorods immobilized onto an ITO electrode is expected. Reduction of Hg(II) onto the immobilized gold nanorods was accomplished using potential sweep voltammetry (+1.0 V to -0.6 V at  $25 \text{ mV} \cdot \text{sec}^{-1}$ ) and with the peak for mercury reduction occurring at  $\sim 0.28 \text{ V}$  (figure 29). The resulting change in the SPR wavelength was recorded with a series of concentrations of  $\text{HgCl}_2$  in  $0.1 \text{ M KNO}_3$ . The absorbance spectra were recorded after the applied potential had been removed to ensure that the change in the SPR wavelength was due strictly to the change in the aspect ratio from the mercury amalgamation without any influence from the electron charging.

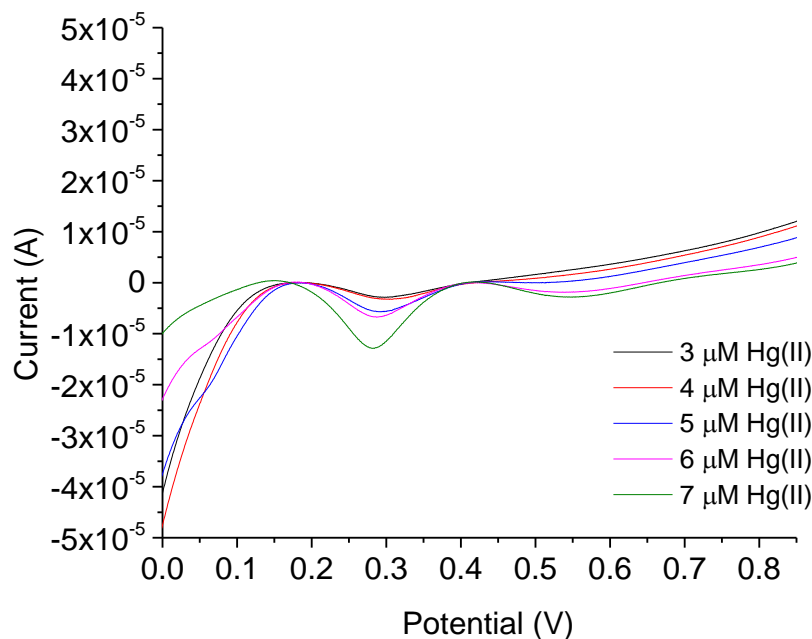


Figure 29. Cyclic voltammogram of the reduction of Hg(II) to mercury metal using the gold nanorod-MPTMS-ITO electrode

The linear response of the SPR signal (correlation coefficient 0.95 for linear least squares best fit) to the Hg(II) concentration per nanorod immersed in the solution indicates the applicability of gold nanorod-MPTMS-ITO electrodes for combined potential control-SPR quantification (figure 30). The limit of detection with the surface coverage reported ( $15 \text{ nanorods} \cdot \mu\text{m}^{-2}$ ) was  $8 \times 10^{-7} \text{ M}$ , but with different surface coverage the sensitivity and limit of detection could be altered. The limits of detection can also be improved through the use of anodic stripping voltammetry as opposed to cyclic voltammetry due to the preconcentration effect provided by the applied constant reduction potential, though at the cost of a considerably increased sample time and faster degradation of the gold nanorod layer through amalgamation.



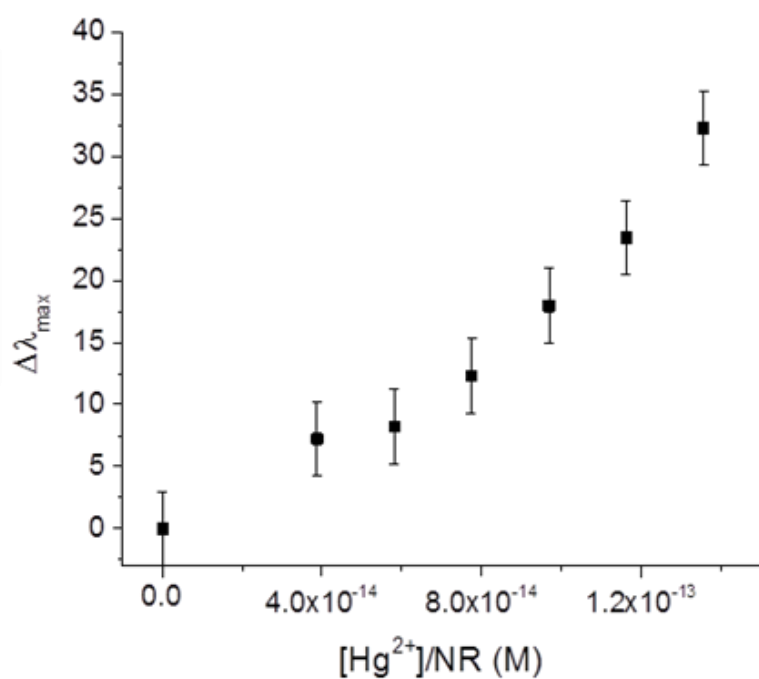
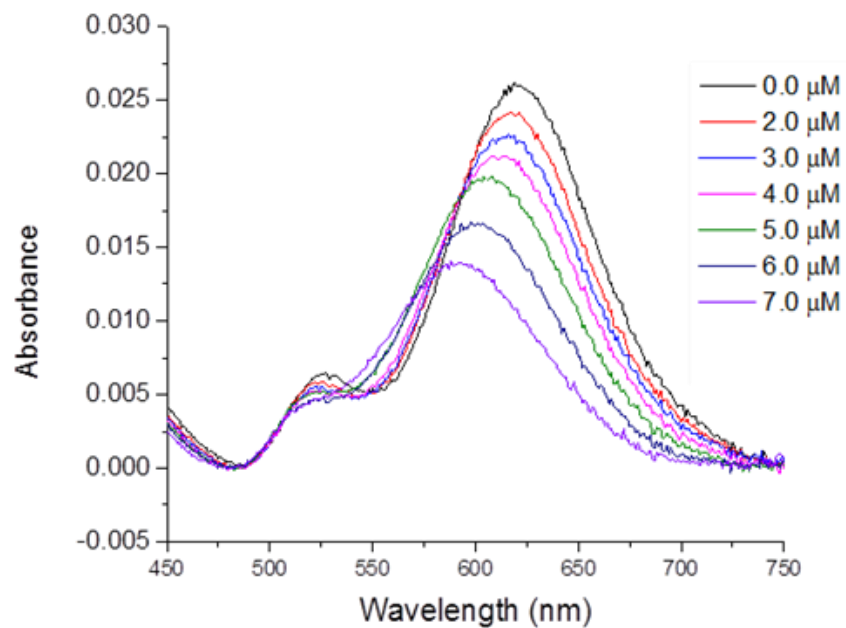


Figure 30. (A) SPR response of immobilized gold nanorods on an ITO electrode with addition of  $\text{HgCl}_2$  and reduction through potential sweep voltammetry (B) Calibration curve of the change in the SPR maximum absorbance wavelength with respect to concentration of mercury per nanorod

### **3.4 Conclusion**

The conditions for the fabrication of optically transparent gold nanorod functionalized ITO electrodes deviate from those required to functionalize silica substrates as seen in chapter 2. Pretreatment of the gold nanorods with CTAB removal procedures and increasing the ionic strength are essential for obtaining high absorbance signal-to-noise SPR substrates that can be subjected to potential control. The success of the procedure described here has been demonstrated using both cyclic voltammetry and SPR measurements coupled with potential sweep voltammetry in a model  $\text{HgCl}_2$  detection system. Although the electrodes cannot be regenerated after amalgamation with mercury, a single electrode can be used for a given calibration or standard addition procedure.

Possible applications of this technology include the as well as trace metals quantification and speciation due to the differing reduction potentials of each individual ion (figure 31) and their effect on the SPR wavelength of the immobilized gold nanorods. The mercury detection model can also be expanded with speciation between inorganic mercury ions and organic mercury compounds such as methylmercury, as each compound will also have a unique reduction potential (figure 32).

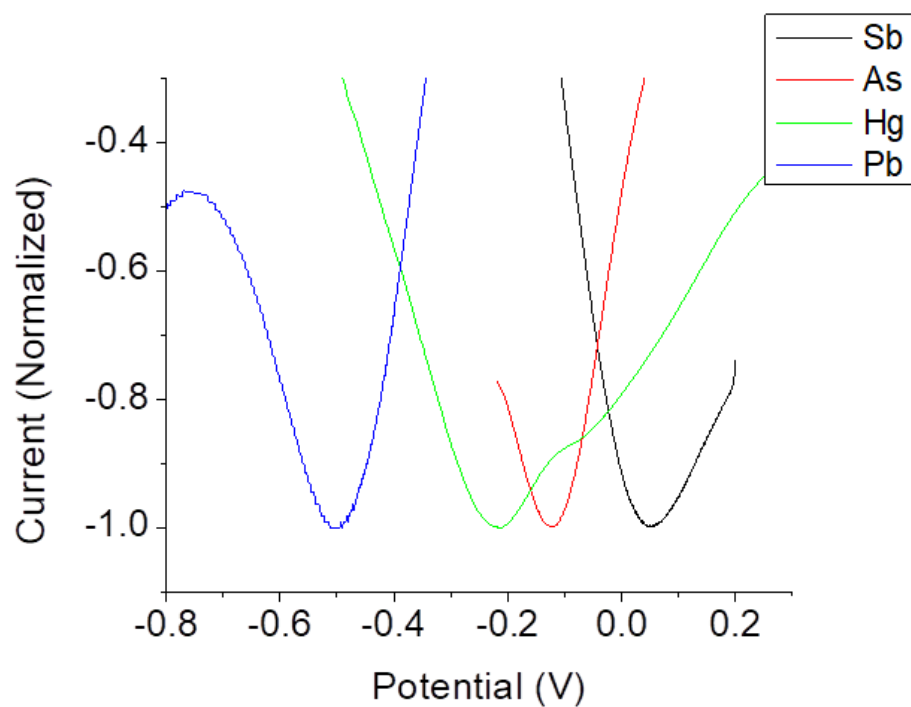


Figure 31. Cyclic voltammograms of the reduction of various metal ions metal using the gold nanorod-MPTMS-ITO electrode

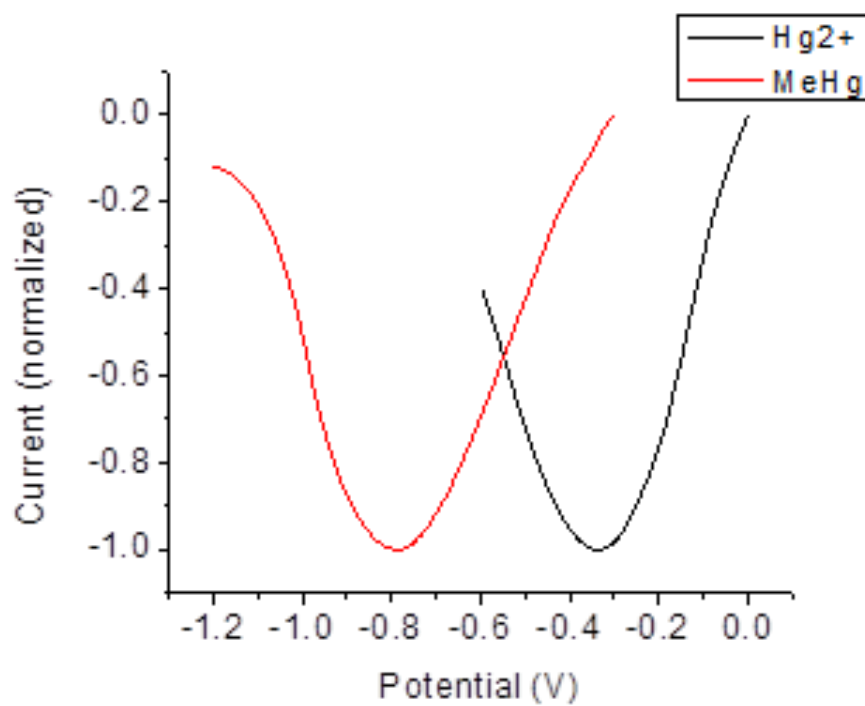


Figure 32. Cyclic voltammograms of the reduction of mercury ions and methylmercury using the gold nanorod-MPTMS-ITO electrode

## **CHAPTER 4: IMMOBILIZED GOLD NANORODS FOR SURFACE PLASMON RESONANCE DETECTION OF MERCURY IN FLOW INJECTION ANALYSIS**

Published in Talanta (Elsevier) vol 128 (2014) pg 196-202

### **4.1 Introduction**

In this chapter, flow injection analysis (FIA) is investigated as another approach to mercury detection with the use of the SPR based sensor via immobilized gold nanorods, effectively using a flow of a mercury sample to induce the amalgamation with the nanorods. This method seeks to further improve the sensitivity via the addition of FIA beyond the immobilization procedure which was proven in chapter 2 to increase the sensitivity of the sensor in static or batch conditions (figure 33). FIA methods have been used extensively since the 1970s when they were first utilized to achieve automation of serial assays and have since been used to determination of reaction rates, diffusion constants, and solubility products, among many other fundamental values [80-81]. FIA for mercury detection is often paired with another quantification method, most commonly atomic absorption [82-84].

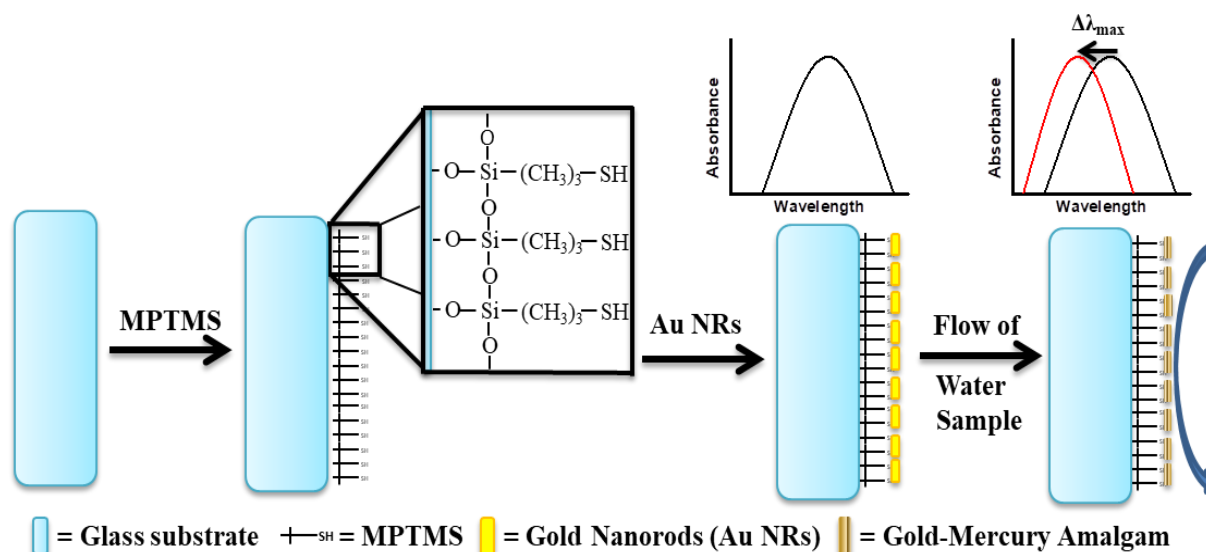


Figure 33. Simplified schematic diagram of the preparation and sensing method of immobilized gold nanorods used for mercury quantification

Investigation of two types of FIA modes is discussed herein, stopped flow and continuous flow modes [85]. Stopped flow involves the injection of the sample matrix and stopping the flow as it reaches the reaction cell containing the immobilized gold nanorods. The flow is stopped for an optimized time in order to allow the injected sample to fully react with the nanorods. Continuous flow involves the constant flow of sample through the reaction cell for a predetermined amount of time, allowing for an increasing build-up of the amalgamation process. Both methods have particular advantages and disadvantages for the determination that will be discussed in addition to their analytical figures of merit. In addition, the effect of ionic strength on the immobilized gold nanorods compared to their colloidal nanorod counterparts will be investigated due to its importance in mercury quantification using the SPR sensor in water samples.

## **4.2 Experimental**

### **4.2.1 Chemical and Reagents**

Bare gold nanorods with aspect ratio 1.9, nominal LSPR  $\lambda_{\text{max}}$  of 611 nm and capped with CTAB were purchased from Nanopartz, Inc. VWR Vistavision cover slides and glass slides were purchased from VWR International and cut to size. Reagents, including  $\text{HgCl}_2$ ,  $\text{NaCl}$ ,  $\text{H}_2\text{SO}_4$ , ethanol,  $\text{Al}(\text{NO}_3)_3$ ,  $\text{Co}(\text{NO}_3)_2$ ,  $\text{Cr}(\text{NO}_3)_3$ ,  $\text{Sr}(\text{NO}_3)_2$ ,  $\text{SnCl}_2$ ,  $\text{Pb}(\text{NO}_3)_2$ ,  $\text{Mn}(\text{CH}_3\text{COO})_2$ ,  $\text{MgSO}_4$ ,  $\text{H}_2\text{O}_2$  (30%),  $\text{NaBH}_4$ , and 85% (3-mercaptopropyl)trimethoxysilane (MPTMS) were acquired from Fisher Scientific. Otherwise noted, all solutions were prepared using 18 M $\Omega$  cm Nanopure water.

### **4.2.2 Immobilization of Gold Nanorods on a Glass Substrate**

Gold nanorods were immobilized on glass substrates according to a procedure slightly modified from chapter 2 to account for the discoveries (ionic strength control to minimize electrostatic repulsion between nanorods and favor deposition) discussed in chapter 3. Glass cover slides were cleaned by immersing them into a piranha solution – a 4:1 concentrated sulfuric acid to 30% hydrogen peroxide mixture – for 20 min. After rinsing with copious quantities of water and methanol, the clean substrates were stored in methanol until needed. A thiol-functionalized, self-assembled monolayer was deposited on the glass surface by immersing the clean slides into a MPTMS/ethanol mixture (10%/90% v/v) for 1 hour. The MPTMS functionalized substrates were rinsed copiously with methanol and then oven-heated to 110 °C for 3 hours.

With the aim of minimizing the electrostatic repulsion among the gold nanorods and achieve a better surface coverage on the MPTMS functionalized substrates, the commercial solution of nanorods was stripped from the excess of CTAB. This was accomplished by centrifuging 1 mL of Au NRs solution ( $2.23 \times 10^{11}$  NRs/mL) at 2033g for 30 minutes. After removing approximately 800  $\mu$ L of the supernatant from the sample vial, the gold nanorods were re-suspended in approximately the same volume of Nanopure water. This process was repeated twice. Additional rounds of centrifugation resulted in irreversible aggregation of the nanorods.

The nanorods were immobilized on the MPTMS substrates by placing 500  $\mu$ L of the gold nanorod solution on the functionalized surface for four hours. After removing the excess of un-reacted nanorods with water, the immobilized gold nanorod substrates were stored in Nanopure water until further use. Their absorption properties were found to remain constant within a six month period of substrate preparation. Longer time periods were not attempted.

#### **4.2.3 Instrumentation**

Flow injection analysis was carried out with a FIA-lab system (FIALab – 2000, Alitea Instruments USA, Inc.) operating in the single-line manifold configuration. The main components of the FIA-lab system consisted of a four channel peristaltic pump equipped with 0.75 mm internal diameter (i.d.) Teflon tubing, a sample injection valve, a T-piece, and a reaction coil (0.75 mm i.d. and 195 cm long). From the reaction coil, the sample was pumped to the flow- through detection cell and then to waste. For all experiments the sample loop injection volume was 150  $\mu$ L.

A custom demountable flow cell used to measure absorbance spectra from gold nanorods immobilized on solid substrates (figure 34). The basic unit (SL-5 EZ) was purchased from International Crystal Laboratories (Garfield, NJ) and modified in-house to fit the substrates. A silicon gasket was cut to the dimensions of the cell providing an inner cell volume equal to 15  $\mu$ L. Absorbance measurements were made with a double-beam Cary 50 spectrometer equipped with a 75-W pulsed Xenon lamp (spectral radiance from 190 to 1100 nm), a 1.5-nm fixed optical band-pass, a monochromator with a 24,000 nm/min maximum scan rate, a beam-splitter and two silicon photodiode detectors. Nonlinear peak fitting of spectral data was made with OriginLab 8.5 software.

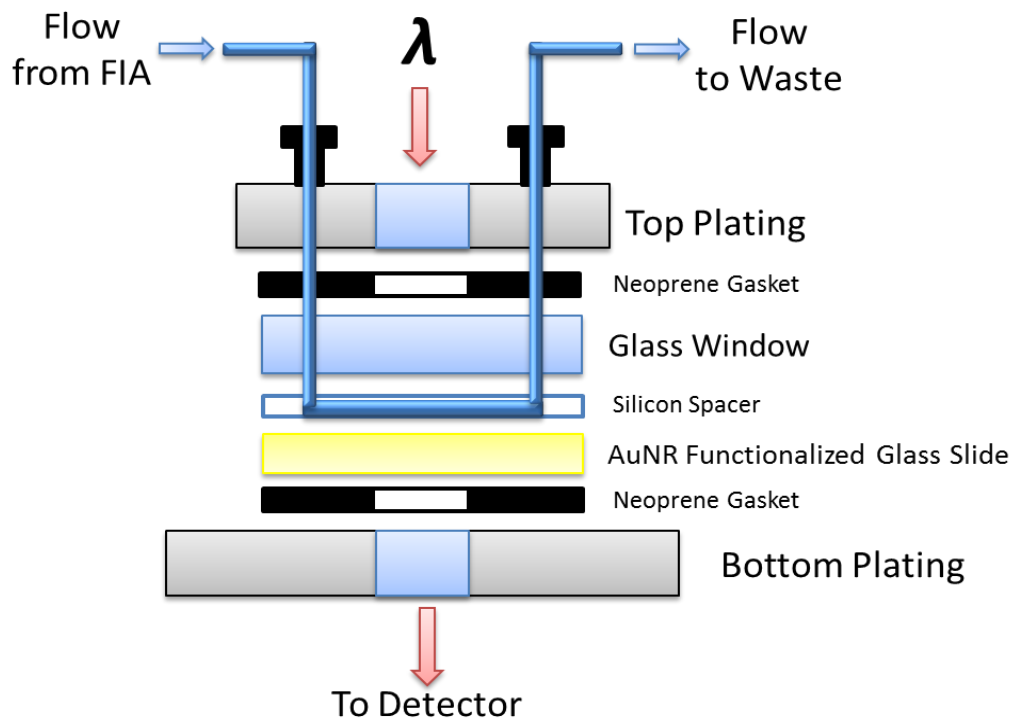


Figure 34. Schematic diagram of the flow cell used to measure absorbance from gold nanorod substrates



## **4.3 Results and Discussion**

### **4.3.1 Instrumental Performance and Spectral Fitting**

As the quantitation of mercury concentration with the immobilized gold nanorod sensor relies on the shifts of the SPR absorbance maximum wavelength, it is imperative to determine the reproducibility of the instrumental response. In the ideal case scenario – i.e., the absence of environmental noise – the ability to measuring reproducible wavelengths ultimately depends on the performance of the spectrometer. In order to test the reproducibility of the wavelength measurements acquired by the instrument, instrumental performance was monitored on a daily basis with a commercial standard (table 5). The standard consisted of a single crystal of dysprosium-activated yttrium aluminum garnet mounted in a cuvette-sized holder with a well-characterized, quasi-line absorption spectrum in the visible region. The wavelength and absorbance intensity accuracy of the instrument was verified by 10 measurements of the standard within 1 hour of use, and the position of the observed wavelengths compared with the wavelengths provided by the manufacturer. Performance of the FIA system is noted in appendix B.

Table 5. Reproducibility of measurements obtained with UV-Vis absorption spectrometer

$\lambda$ (nm)	Absorbance (a.u.)
$385.70 \pm 0.07$	$0.1858 \pm 0.0012$
$395.08 \pm 0.07$	$0.1410 \pm 0.00018$
$447.24 \pm 0.07$	$0.1303 \pm 0.0007$
$456.24 \pm 0.07$	$0.1039 \pm 0.0010$
$751.88 \pm 0.07$	$0.1433 \pm 0.0011$
$754.22 \pm 0.07$	$0.1358 \pm 0.0026$
$761.42 \pm 0.07$	$0.1043 \pm 0.0019$
$789.16 \pm 0.07$	$0.1084 \pm 0.0029$

Inaccuracies due to instrumental noise are dependent on the relative intensity of the SPR absorbance spectra, with the magnitude of the intensity proportional to the density of the gold nanorods immobilized on the surface. It is vital to be able to perform accurate analysis of trace concentrations of mercury through accurate measurements of the SPR maximum wavelength, which can be difficult if the signal-to-noise level is low. While it is possible to increase the absorbance intensity of the SPR signal through tuning of the ionic strength as discussed in section 3.3.2, the gold nanorod concentration on the surface has a substantial effect on the response of the sensor to mercury, as larger shifts per unit concentration of mercury are seen with relatively low concentrations of gold nanorods [86]. An alternative to facilitate the accurate measurement of the SPR maximum wavelength is through the nonlinear fitting of noisy spectral data to a Gram-Charlier (GCAS) function using a Levenberg Marquardt iteration algorithm [87] (figure 35). This approach was used to calculate the wavelength shift values used in this chapter. A tolerance ( $\chi^2$ ) of  $1 \times 10^{-9}$  was employed in all cases.

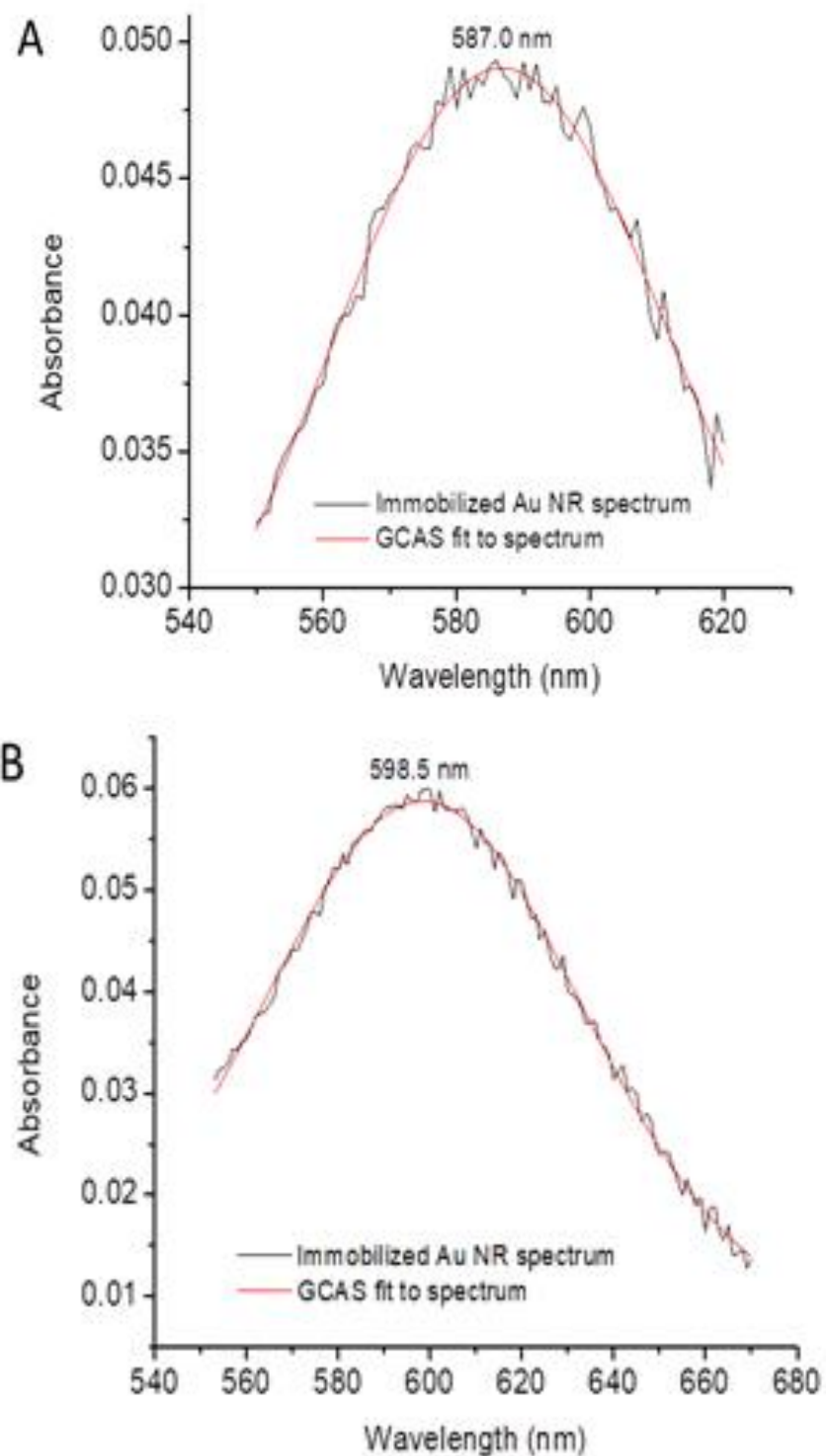


Figure 35. Absorbance spectra of immobilized gold nanorod substrates with curve fitting using the GCAS function. Spectra were recorded from glass substrates with different number of nanorods on their surface: (A)  $1.8 \times 10^{11}$  and (B)  $2.2 \times 10^{11}$  NRs.

### **4.3.2 Stabilization of Reference Wavelength with NaBH<sub>4</sub>**

As mentioned in previous studies by Rex et. al, in the presence of NaBH<sub>4</sub>, a blue shift in the SPR wavelength maximum is observed due to unreacted gold ions (Au<sup>3+</sup>) still present on the glass surface of the substrate [42]. Upon reduction to elemental gold and subsequent deposition on the immobilized nanorods increases the diameter of the nanorods and thereby reduces their aspect ratio. Kinetic experiments reveal the exposure time of approximately 6 needed for the reduction and deposition of the unreacted gold ions onto the immobilized gold nanorods (figure 36). In order to ensure the complete reduction and deposition process, a conservative time of 10 minutes of NaBH<sub>4</sub> exposure will be used before further experiments. Under these conditions, the statistics of the fittings of numerous absorption spectra recorded from individual substrates provided a  $\pm 1$  nm substrate-to-substrate variation of the average SPR wavelength maximum value.

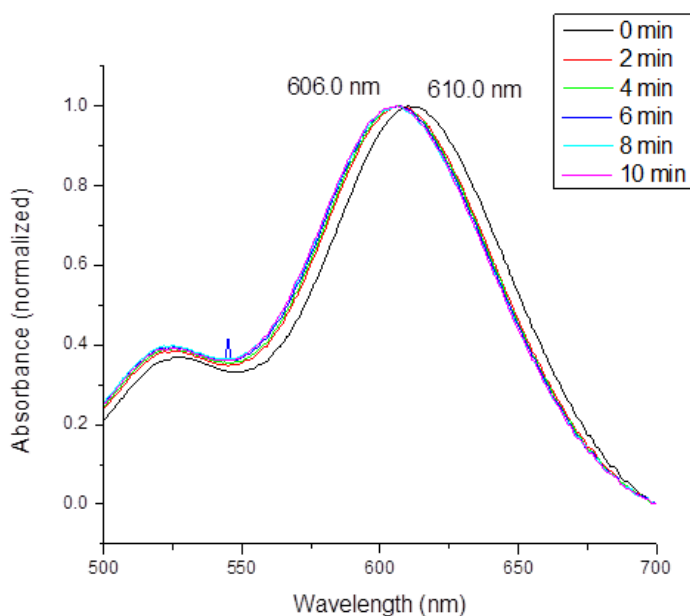


Figure 36. Absorbance spectra over time of the immobilized gold nanorod substrate immersed in a 10<sup>-3</sup> M NaBH<sub>4</sub> solution.

#### **4.3.3 Effect of Ionic Strength and NOM on the Spectral Features of Gold Nanorods**

Further studies were conducted to determine the full effect of ionic strength and natural organic matter on the immobilized gold nanorods compared to their colloidal counterparts. The sensor was first tested by exposing the immobilized nanorods to a tap water sample to determine if the sample matrix which contains significant concentrations of natural organic matter and ions capable of causing nanorod aggregation would affect the SPR absorbance signal of the sensor. Upon comparison with a gold nanorod solution exposed to the tap water sample matrix and a high concentration of sodium borohydride, the gold nanorods in solution clearly aggregated as indicated by the degradation of the SPR signal. The immobilized nanorods exposed to the same sample show some shift due to adsorption of organic molecules on the nanorod surface which slightly change the refractive index of the surrounding medium of the nanorods but no loss of the SPR signal (figure 37). The adsorption of the organic molecules occurs over approximately 10 minutes, after which the SPR signal becomes stable and no further shifts in the maximum SPR wavelength is noted with further exposure.

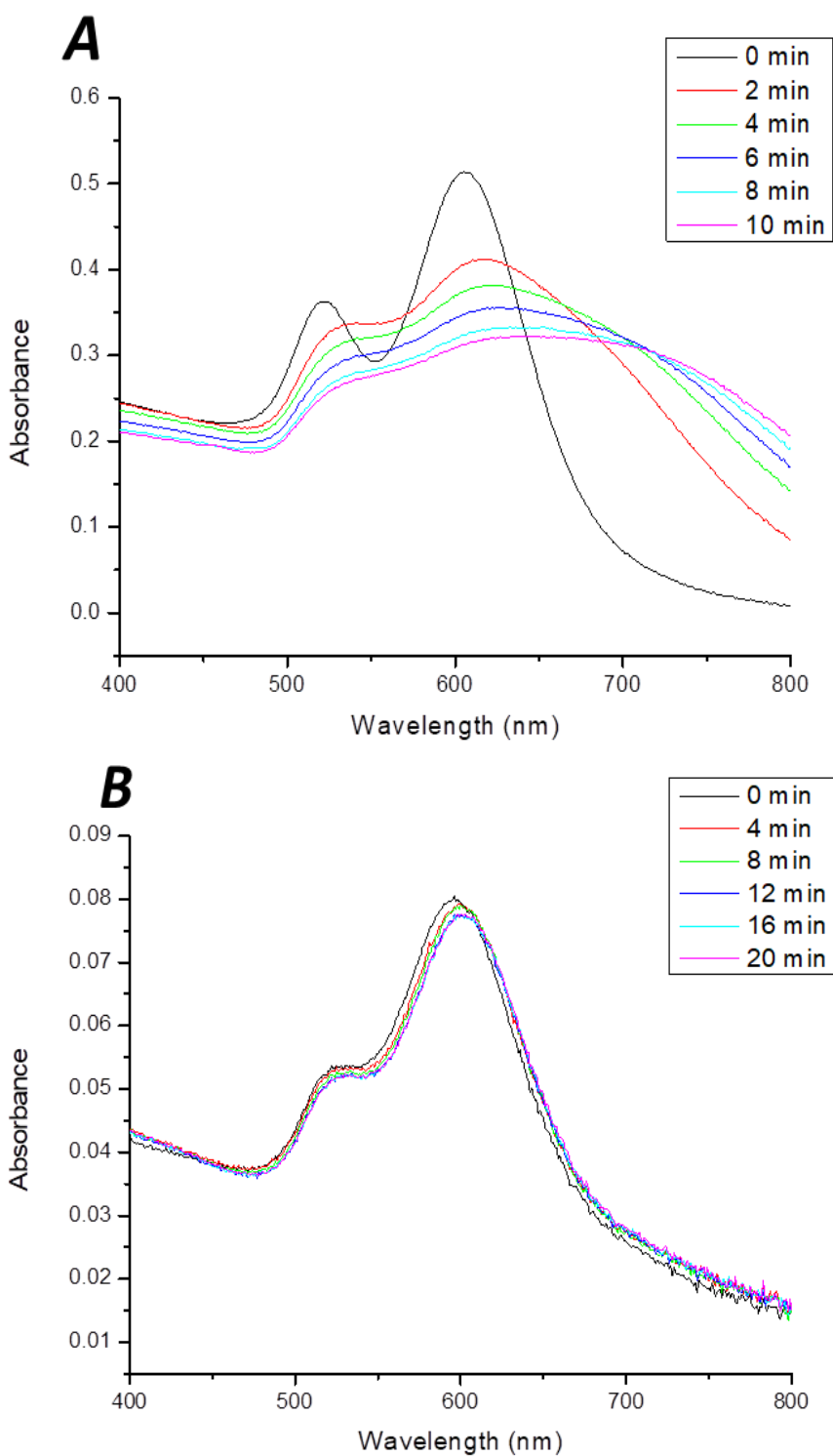


Figure 37. (A) Absorbance spectra over time of colloidal gold nanorods in the presence of a tap water sample and 0.01 M NaBH<sub>4</sub>. (B) Absorbance spectra over time of immobilized gold nanorods on a solid substrate in the presence of a tap water sample and 0.01 M NaBH<sub>4</sub>

In order to test the viability of the immobilized gold nanorods in potentially more contaminated species, the sensor was immersed in synthetic solutions of either high ionic strength or high concentrations of natural organic matter. In this case, a concentration of 0.5 M NaCl was used to imitate a high ionic strength and varying concentrations of humic acid was used to imitate the natural organic matter found in water samples (figure 38). As expected, the SPR absorbance spectra of the immobilized gold nanorods exhibited no change in the absorbance maximum as aggregation of the nanorods due to the loss of the CTAB bilayer is not possible due to their immobilization. Additions of increasing concentrations of humic acids displayed similar SPR wavelength shifts as seen in the tap water, verifying the SPR wavelength shift due to the adsorption of natural organic matter onto the nanorod surface.

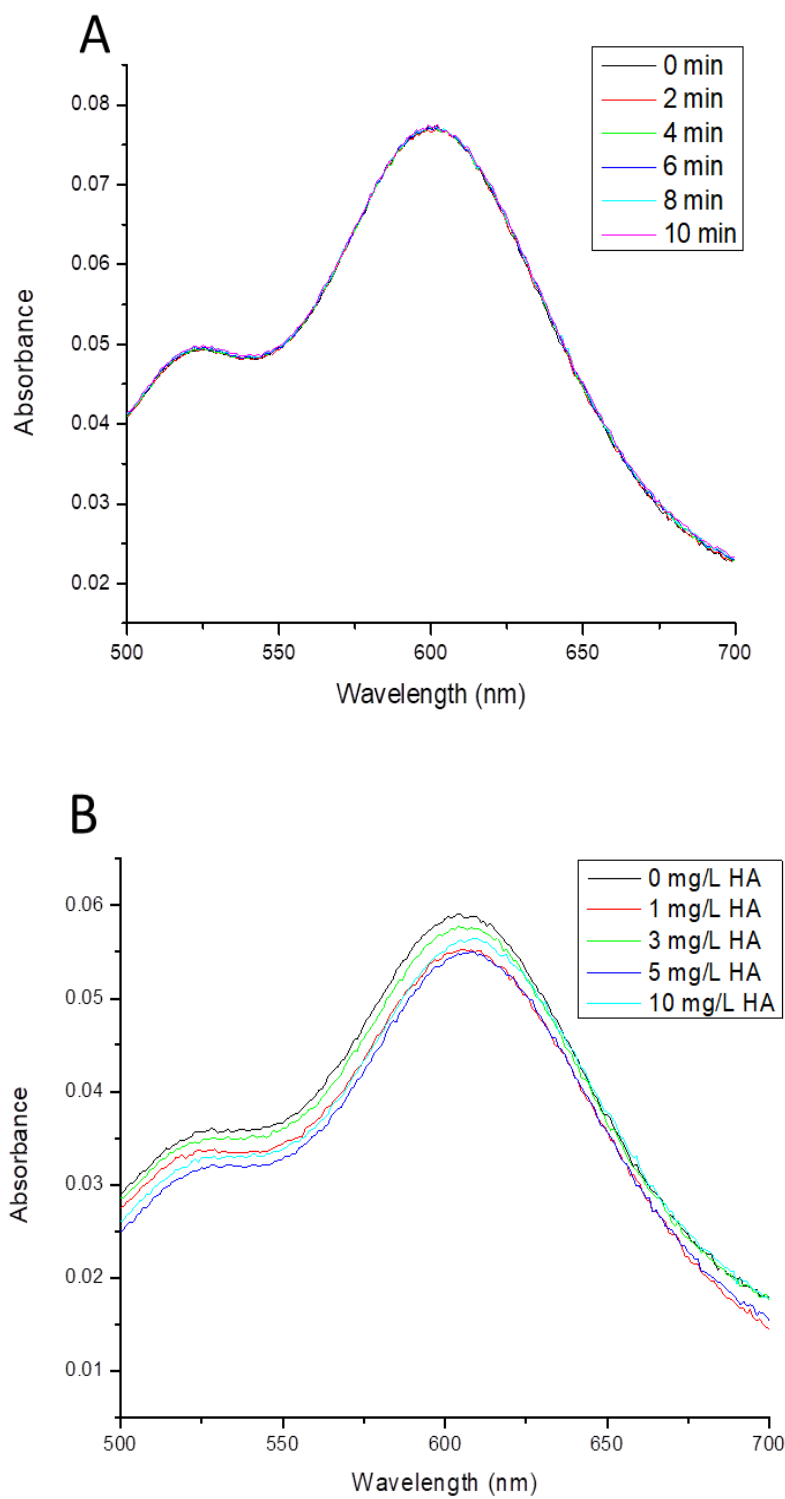


Figure 38. Absorbance spectra over time of immobilized gold nanorods on a solid substrate in the presence of (A) 0.5 M NaCl (B) increasing concentrations of humic acid (HA)



#### **4.3.4 Analytical Figures of Merit**

Two detection modes – stop and continuous flow – were investigated for the analysis of mercury in water samples. Stop flow experiments were carried out by pumping Nanopure water through the flow cell at a  $0.73 \text{ mL min}^{-1}$  rate followed by injection of the mercury sample. Standard solutions of  $\text{Hg}^{2+}$  were prepared in  $0.01 \text{ M NaBH}_4$ . After 30 seconds of sample injection, the carrier flow was stopped to allow for the interaction of the injected solution with the gold nanorod substrate. The 30 second period was the time observed to elapse between the injection of a color dye solution and its arrival at the sensing cavity of the flow cell. Within the micro-molar mercury concentration range, the amalgamation reaction was complete at approximately three minutes of substrate exposure time (figure 39).

Continuous flow experiments were carried out by pumping standard solutions of  $\text{Hg}^{2+}/10^{-3} \text{ M NaBH}_4$  at a  $0.73 \text{ mL min}^{-1}$  flow rate. In the nanomolar range, continuous flow exhibited wavelength shifts over time dependent on the concentration of the mercury sample flow, with higher concentrations requiring longer reaction times until equilibrium is reached and the wavelength remains constant (figure 40).

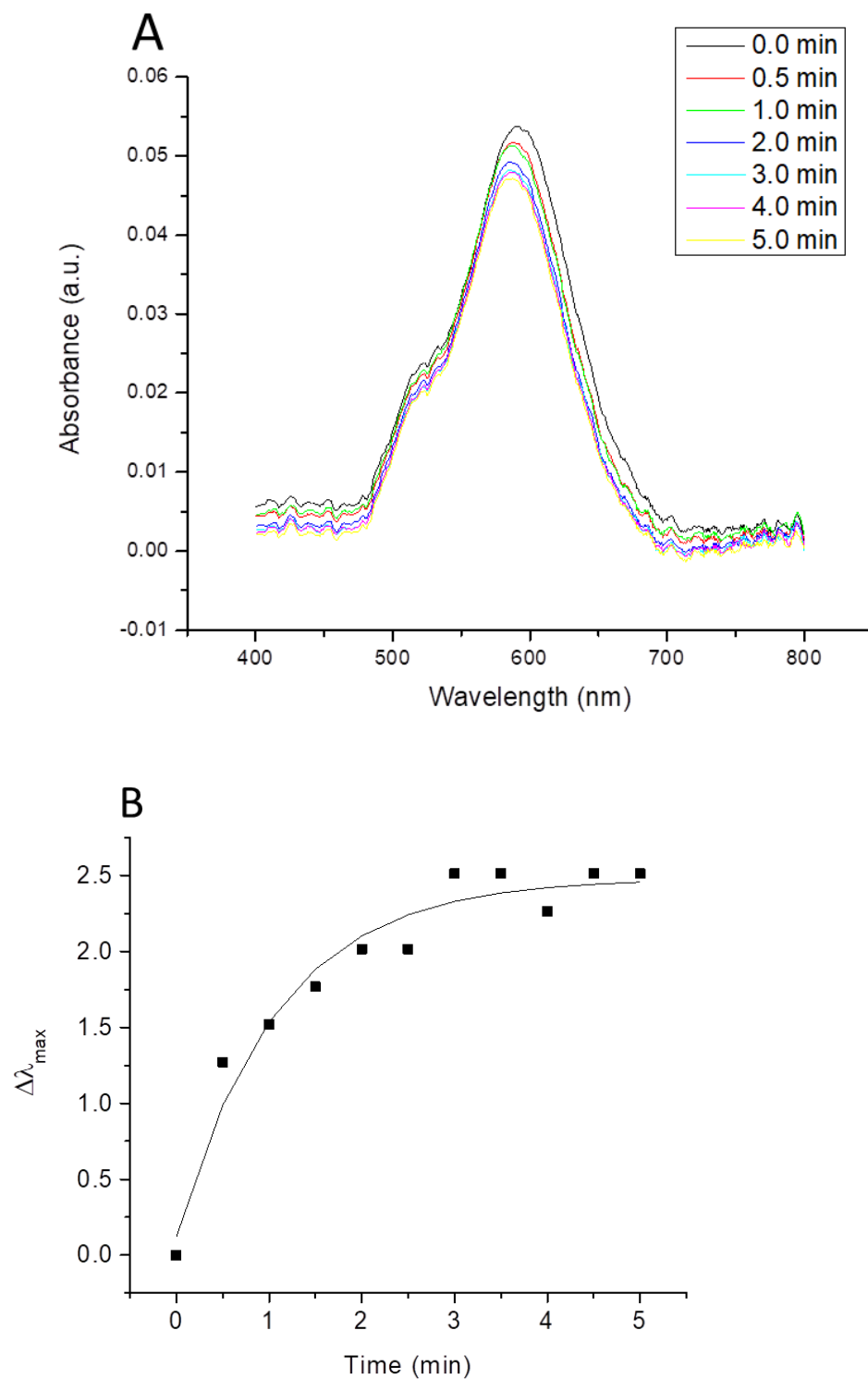


Figure 39. (A) Absorbance spectra of the SPR response of immobilized nanorods to Hg over time under stopped flow conditions. (B) Graph of the shift in the SPR maximum wavelength over time under stopped flow conditions

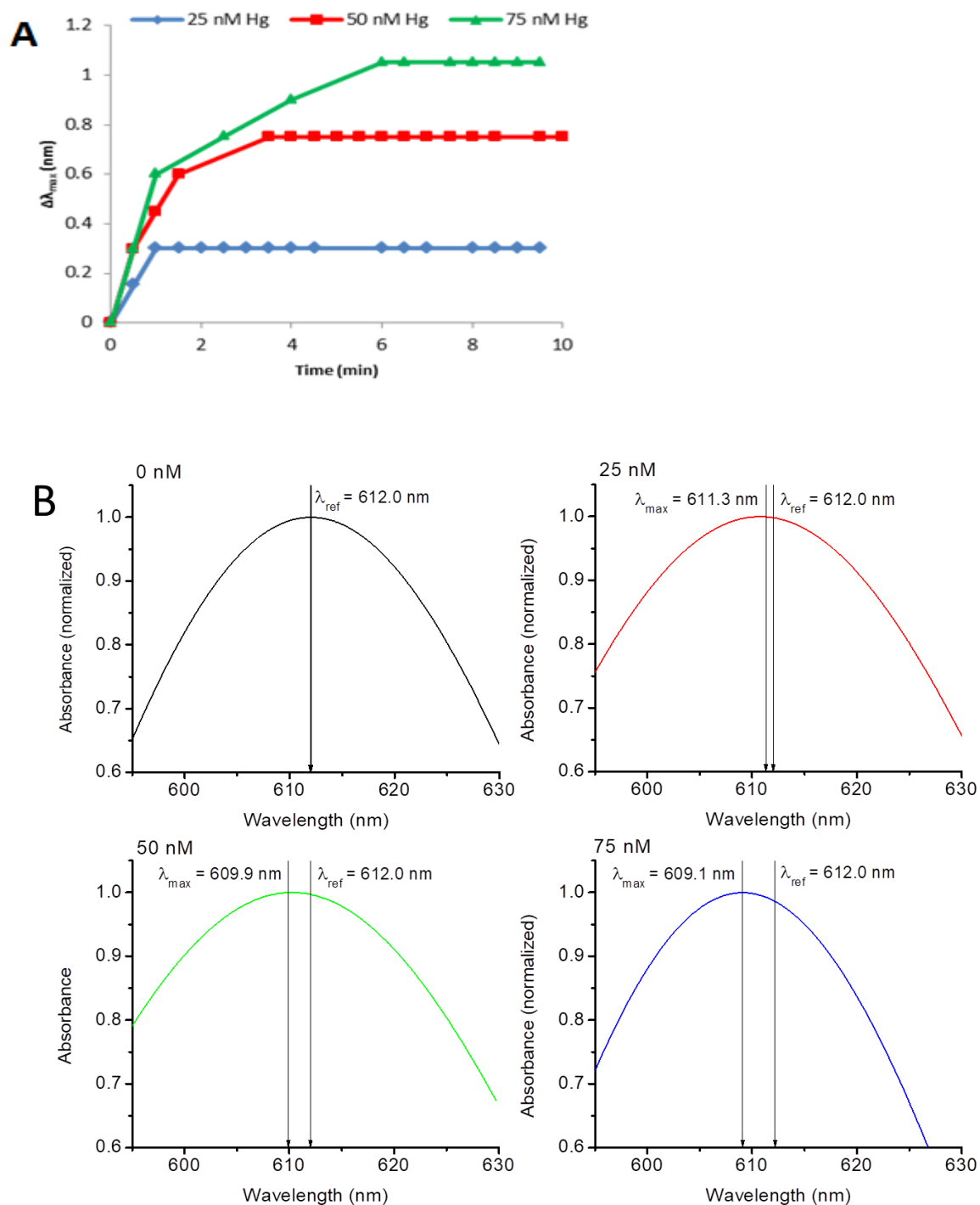


Figure 40(A) Graph (B) spectra of the SPR absorbance wavelength shifts over time of immobilized gold nanorods exposed to nanomolar concentrations of Hg in a continuous flow method

The linear dynamic ranges (LDR) of the calibration curves were based on five mercury concentrations. The entire set of stop flow data was obtained with one immobilized gold nanorod substrate, including the one substrate for blank measurements ( $10^{-3}$  M NaBH<sub>4</sub>/Nanopure water). Generating the entire set of continuous-flow data required the use of six substrates. The correlation coefficients obtained from the least squares fitting ( $\Delta\lambda_{\max}=b \cdot [\text{Hg}^{2+}] + a$ ) are close to unity, demonstrating the existence of a linear relationship between the SPR wavelength shift and mercury concentration. The limits of detection (LODs) were calculated as  $3 \times s_a/b$ ; where  $s_a$  is the standard deviation of the intercept ( $\Delta\lambda_{\max}=a \pm s_a$ ) when  $[\text{Hg}^{2+}] = \text{zero}$  and  $b$  is the slope (calibration sensitivity) of the linear plot. The limits of quantitation (LOQ) were calculated as  $10 \times s_a/b$  (table 6).

Table 6. Analytical Figures of Merit for mercury detection using immobilized gold nanorod substrates using either the stop flow or continuous flow methods.

	Stop Flow Method	Continuous Flow Method
Linear Dynamic Range <sup>a</sup>	$1.21 - 5.00 \times 10^{-6}$ M	$3.93 - 7.5 \times 10^{-8}$ M
Linear Fitting <sup>b</sup>	$\Delta\lambda_{\max} = (3.6 \times 10^6) \cdot [\text{Hg}] + 0.3$	$\Delta\lambda_{\max} = (4.0 \times 10^7) \cdot [\text{Hg}] - 0.1$
Standard Deviation of the Intercept <sup>c</sup>	$\pm 0.4$ nm	$\pm 0.2$ nm
Standard Deviation of the Slope <sup>c</sup>	$\pm 0.1 \times 10^6$ nm·M <sup>-1</sup>	$\pm 0.3 \times 10^7$ nm·M <sup>-1</sup>
Calibration Sensitivity	$3.6 \times 10^6$ nm·M <sup>-1</sup>	$4.0 \times 10^7$ nm·M <sup>-1</sup>
Correlation Coefficient	0.9969	0.9861
Limit of Detection <sup>d</sup>	$3.64 \times 10^{-7}$ M	$1.18 \times 10^{-8}$ M
Limit of Quantitation <sup>d</sup>	$1.21 \times 10^{-6}$ M	$3.93 \times 10^{-8}$ M

<sup>a</sup>Linear dynamic range = Limit of quantitation – Upper limit of detection

<sup>b</sup>Equation for the best linear fit:  $\Delta\lambda_{\max} = b \cdot [\text{Hg}] + a$  where  $b$  = calibration sensitivity and  $a$  = intercept

<sup>c</sup>Calculated according to [57]

<sup>d</sup>Limits of detection/quantification calculated according to IUPAC guidelines [58]

Upon comparison of the LOQ, the LOQ of the continuous flow method is shown to be approximately 30 times lower than the LOQ of the stopped flow method. The better LOQ result from the steeper slope of the continuous flow calibration curve (approximately 11 times higher) and the lower standard deviation of the intercept (approximately 3 times lower). The observed difference is due to the nature of the continuous flow, which exposes the gold nanorod substrate to significantly higher volumes of the sample, as opposed to the stopped flow which involves the single injection of 150  $\mu\text{L}$  of sample. As such, the stopped flow method requires a significantly higher concentration to expose the substrate to the same relative mass of mercury as the continuous flow which uses a high volume (7.3 mL) of low concentrations. The LOD obtained via the continuous flow approach (11.7 nM) is of the same order of magnitude of the maximum contamination level ( $\text{MCL} = 2 \text{ ppb} \equiv 9.97 \text{ nM}$ ) set for mercury by the EPA in drinking water samples.

#### **4.3.5 Analysis of Tap Water Samples**

While the sensing mechanism for the immobilized gold nanorod sensor relies on the amalgamation with mercury, gold is not the only element that mercury can form an amalgam with [88]. In particular, four methods have been shown to promote mercury amalgamation with a specific metal, namely (table 7): (1) direct physical contact with the other metal in the presence of a dilute acid; (2) immersion of the other metal in a liquid solution of a mercury salt; (3) immersion of Hg (0) in a liquid solution of a salt of the other metal; and (4) amalgamation via electrolysis. Within the reaction time used and the experimental conditions of the measurements, the only metal that forms an amalgam with elemental mercury is gold [89].

Table 7. Elements capable of forming an amalgam with Hg(0) under various conditions

Method	Elements
1 <sup>a</sup>	Sb, As, Bi, Cd, Au, Pb, Mg, K, Ag, Na, Te, Th, Sn and Zn
2 <sup>b</sup>	Cu, Au, Pt, Ag and Pd
3 <sup>c</sup>	Zn and Na
4 <sup>d</sup>	All of the above

<sup>a</sup>Method 1 = direct physical contact in dilute acid

<sup>b</sup>Method 2 = immersion of element in solution containing mercury salt

<sup>c</sup>Method 3 = immersion of Hg(0) in solution containing element

<sup>d</sup>Method 4 = electrolysis

Based on this information, the potential interferences will be due to interactions with the immobilized gold nanorods on the substrate surface, either through adsorption causing a change in the refractive index of the surrounding medium or through chemical reaction. The National Institute of Standards and Technology (NIST) has a standard reference material for trace elements in natural water [90] that presents a list of inorganic ions commonly found in fresh water samples that will be tested for potential interference due to their interaction with the immobilized gold nanorods (table 8). Each ion was tested at a 5.0  $\mu\text{M}$  concentration, a concentration significantly higher than the MCL reported with the exception of aluminum. Each wavelength shift was measured in the stop flow mode for 5 minutes after injection (figure 41). All measurements were made with the same substrate in the presence of  $10^{-3}$  M  $\text{NaBH}_4$ /Nanopure water. After measuring the wavelength shift caused by each inorganic salt, the cell was flushed for 5 min with  $10^{-3}$  M  $\text{NaBH}_4$ /Nanopure water at a  $0.73 \text{ mL min}^{-1}$  flow rate.

Table 8. Chemical species tested for interference with immobilized gold nanorod substrates using the stopped flow method.

Contaminant	Chemical Form	MCL <sup>a</sup>
Manganese	Mn(C <sub>2</sub> H <sub>3</sub> O <sub>2</sub> ) <sub>2</sub>	0.05 mg/L (0.91 μM)
Magnesium <sup>b</sup>	MgSO <sub>4</sub>	
Cadmium	Cd(NO <sub>3</sub> ) <sub>2</sub>	0.005 mg/L (0.04 μM)
Tin <sup>b</sup>	SnCl <sub>2</sub>	
Lead	Pb(NO <sub>3</sub> ) <sub>2</sub>	0.015 mg/L (0.07 μM)
Strontium <sup>b</sup>	Sr(NO <sub>3</sub> ) <sub>2</sub>	
Aluminum	Al(NO <sub>3</sub> ) <sub>3</sub>	0.2 mg/L (7.41 μM)
Chromium	Cr(NO <sub>3</sub> ) <sub>3</sub>	0.1 mg/L (1.92 μM)
Cobalt <sup>b</sup>	Co(NO <sub>3</sub> ) <sub>2</sub>	

<sup>a</sup>Maximum contamination level (MCL) as set by the EPA [3]

<sup>b</sup>No MCL was set by the EPA

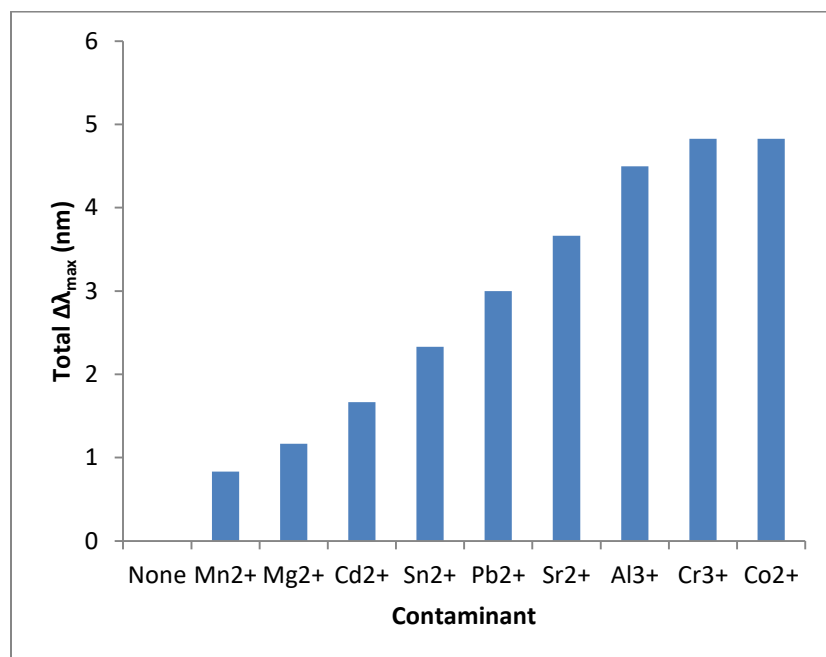


Figure 41. Graph of the shift of the SPR maximum wavelength recorded after 5 min of successive exposure to 5.0 μM concentrations of the inorganic salt

The sequential injections of high concentrations of inorganic ions cause a considerable shift in the SPR maximum wavelength that can affect the accuracy of the sensor. The plateau

that was reached after the addition of  $\text{Cr}(\text{NO}_3)_3$  is probably due to the surface saturation of the gold nanorods and the lack of available sites for further interactions with  $\text{Co}^{2+}$  ions. This assumption is supported by the wavelengths shift observed from a second substrate individually probed with  $5\ \mu\text{M}\ \text{Co}(\text{NO}_3)_2$ . While most tap water samples will have ion concentrations at orders of magnitude lower than what was tested, for more contaminated water samples, measures will need to be taken to account for high concentrations of interfering inorganic ions.

One possibility to account for the contribution of concomitant ions to the total wavelength shift is to measure the blank signal of a synthetic mixture tailored to mimic the typical composition of inorganic ions in fresh water samples and using the SPR wavelength maximum after exposure as the reference wavelength. The feasibility of this approach was tested with a tap water sample of unknown composition. Analysis was made under the continuous-flow mode via the calibration curve method. The SPR wavelength maximum of a substrate was monitored for 10 min under the flow of tap water ( $0.73\ \text{mL min}^{-1}$ ) in the presence of  $10^{-3}\ \text{M}\ \text{NaBH}_4$ . Since no change in the reference wavelength was observed, the tap water sample was fortified with  $\text{HgCl}_2$  to provide a final standard  $\text{Hg}^{2+}$  concentration (18 nM) above the LOD of the method (11.7 nM). After placing a new substrate in the flow cell and flowing the sample for 10 min at the same rate ( $0.73\ \text{mL min}^{-1}$ ), a  $[\text{Hg}^{2+}] = 20.5\ \text{nM}$  was obtained.

The high relative error ( $E_r = 13.9\%$ ) indicates the possible presence of unaccounted matrix interference, and thus a multiple standard addition method was employed instead to account for the potential interference of the unknown matrix (figure 42). One substrate was used to conduct the multiple standard addition experiment. The blank signal was estimated from the same standard mixture of inorganic ions used in the calibration curve procedure. The least-



squares fitting of the experimental data displays a linear correlation ( $R=0.9966$ ) for the equation

$$\Delta\lambda_{\max} = 0.042[\text{Hg}^{2+}] = 0.802. \text{ Extrapolation of the linear fitting yielded a } [\text{Hg}^{2+}] = 19.1 \text{ nM.}$$

This concentration presents a considerably lower relative error ( $E_r = 6.1\%$ ) than the one previously obtained by the calibration curve method.

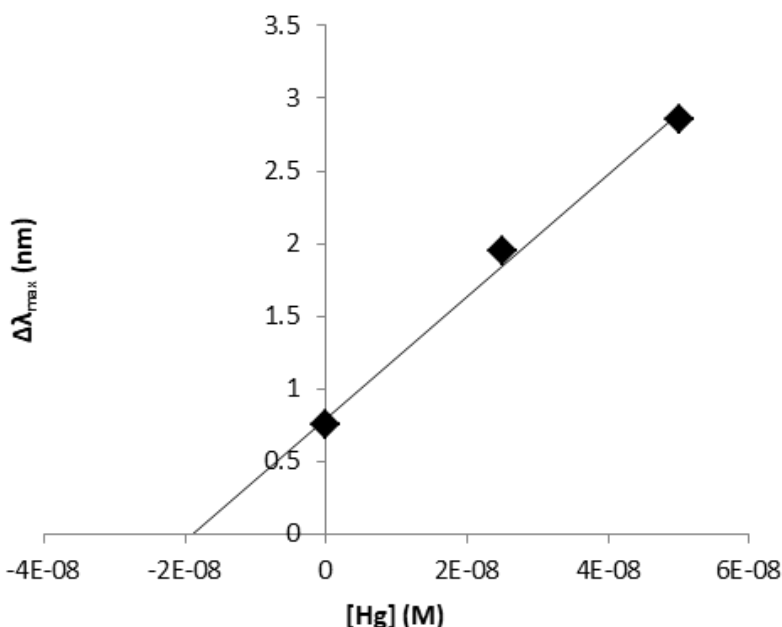


Figure 42. Graph of the shift of the SPR maximum wavelength recorded after multiple standard additions using the continuous flow method

#### **4.4 Conclusion**

This chapter expands on the original work done in chapter 2, integrating the ionic strength control for greater surface coverage of gold nanorods, as well as introducing flow injection analysis for improved limits of detection. The stability of the immobilized nanorods was also further realized, with experiments conducted on their resistance to aggregation in mediums of high ionic strength or high concentrations of natural organic matter. By restricting

their physical movement on the glass substrate, the immobilization of the nanorods prevents their aggregation in aqueous media, preserves their spectral features and provides a stable absorption spectrum for sensing purposes.

Comparison of the two FIA methods show the best LOD with the continuous flow method ( $11.7 \text{ nM} = 2.4 \text{ ng mL}^{-1}$ ), which is of the same order of magnitude as the MCL ( $2 \text{ ng mL}^{-1}$ ) stipulated by the EPA for drinking waters. With the current flow cell, an LOD improvement should be possible by increasing the volume of water flowed through the cell. The sample volume can be easily increased by using a faster flow rate, longer sample flowing times or both, allowing the continuous flow method to be easily modified to improve the method. LOD improvements via the stop flow method require a new cell design that optimizes the interaction of the gold nanorods with the small sample volumes injected in the FIA system. However, the sensitive detection of mercury via the stop flow method should prove useful in cases of limited volume availability of samples.

Independent of the detection mode, the accurate determination of mercury with the proposed sensor requires compensating for the interaction of concomitant ions with the substrate. In the case of tap water samples, accuracy of analysis was accomplished by measuring the blank signal of a synthetic mixture tailored to mimic the typical composition of inorganic ions in fresh water samples followed by multiple standard additions to account for any other unknown matrix effects. Another possible solution to the potential interferents is the adaptation of potential control as discussed in chapter 3 to the FIA system, allowing for more selective reduction, though this will require significant adjustments to the custom flow cell described herein to allow for electrode placement within the sample cavity.

## CHAPTER 5: CONCLUSIONS AND FUTURE STUDIES

Mercury remains a constant threat to human and environmental health, requiring constant monitoring. The methods presented herein provide an alternative to the traditional methods of mercury detection through the use of a portable sensor based on the localized SPR of gold nanorods. The gold nanorods were successfully immobilized onto two different substrates, silica glass and ITO film on glass. The immobilization of the gold nanorods provided physical stability, allowing for use in water samples containing high ionic strength or high concentrations of organic matter in which would cause aggregation in gold nanorods in solution by degradation of the stabilizing surfactant layer. The immobilized gold nanorods were further functionalized to allow not only batch experiments, but potential control or flow injection analysis in order to improve the selectivity and sensitivity of the sensor.

Future studies can include the combination of the potential control capabilities of the gold nanorod-ITO substrate with the flow injection analysis. This can be done through a custom flow cell that can accommodate the reference and counter electrodes within sample flow, and replacing the standard immobilized gold nanorod substrate with the ITO substrate as the working electrode. Anodic stripping voltammetry will also greatly increase the sensitivity of the method when combined with the flow conditions through a constant deposition and amalgamation of the gold nanorods. Potential control will also allow for speciation when combined with the FIA system, as previously discussed on section 3.4.

Optimization of the gold nanorod coverage onto the substrate is also under consideration in order to increase the sensitivity of the method. While the current studies recognize the importance of the number of nanorods on the surface to the sensitivity of the sensor, they do not

take into account the relative area in which the absorbed light passes through the substrate.

Optimization can be done by reducing the overall area of the immobilized gold nanorods on the substrate and confining the gold nanorods to the relative area illuminated by the instrument light source. For example, the Cary50 UV-Vis absorbance spectrometer illuminates a rectangular area with dimensions approximately 0.5 x 1.0 mm. By confining the immobilized gold nanorods to the area of illumination, the overall number of nanorods on the solid substrate will decrease drastically without having any effect on the absorbance signal of the SPR.

## **APPENDIX A: GOLD NANOROD TEM IMAGES**

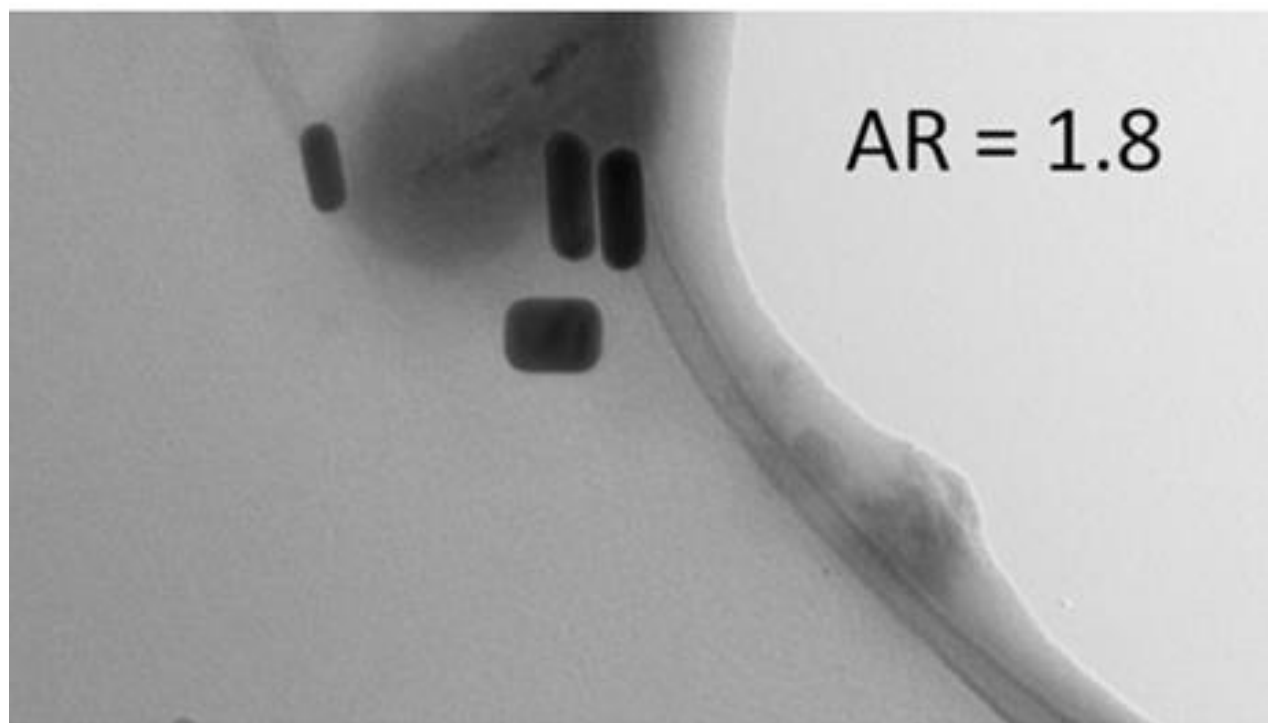


Figure A1. TEM image of gold nanorods with an aspect ratio of 1.8

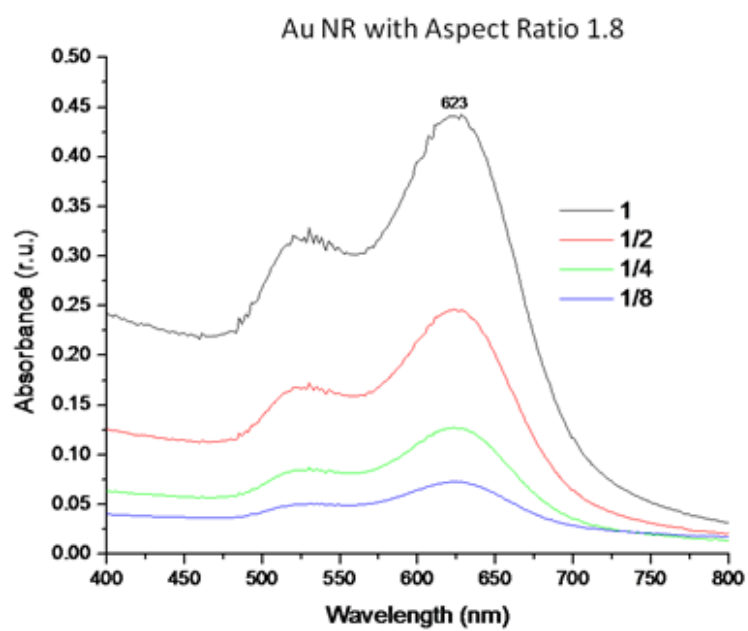


Figure A2. Absorbance spectra of gold nanorods with an aspect ratio of 1.8 at differing dilution factors

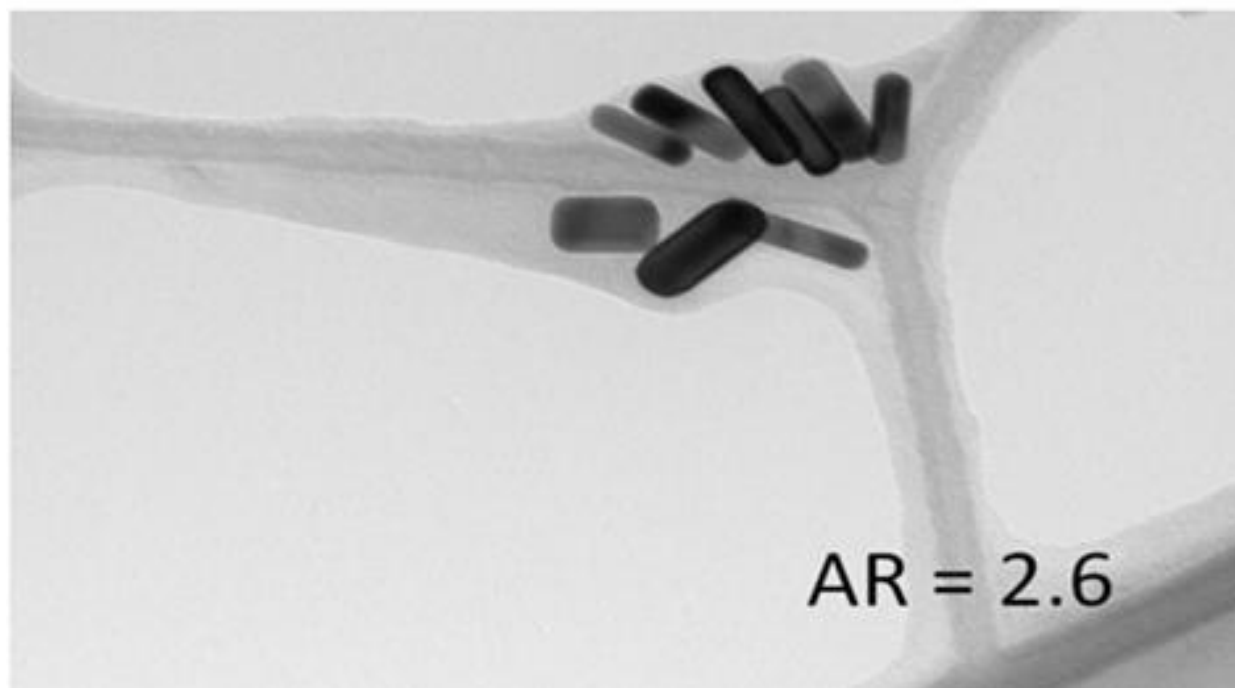


Figure A3. TEM image of gold nanorods with an aspect ratio of 2.6

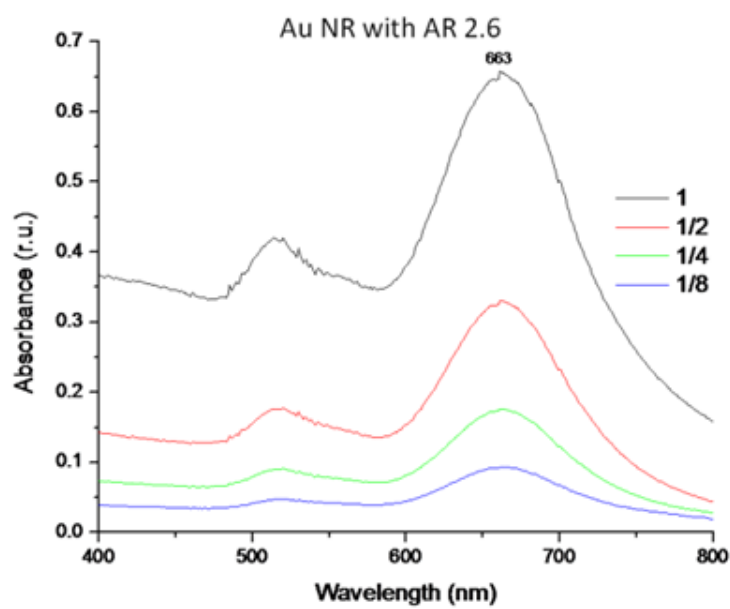


Figure A4. Absorbance spectra of gold nanorods with an aspect ratio of 1.8 at differing dilution factors

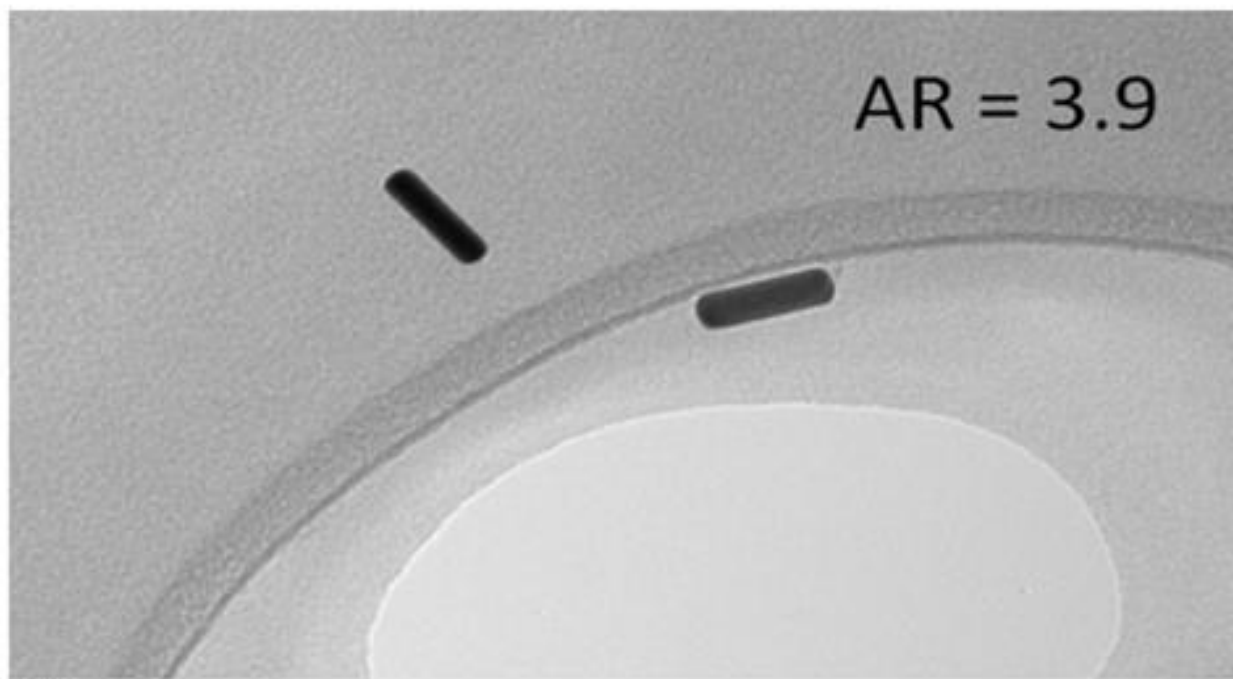


Figure A3. TEM image of gold nanorods with an aspect ratio of 3.9



## **APPENDIX B: FIA PERFORMANCE**

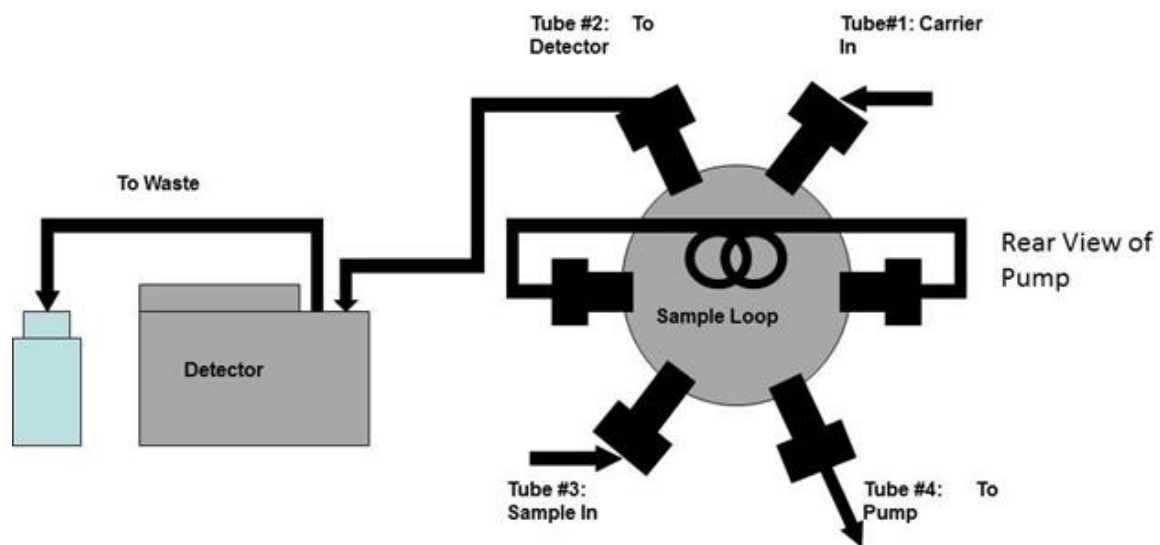


Figure A1. Instrumental setup for FIA analysis

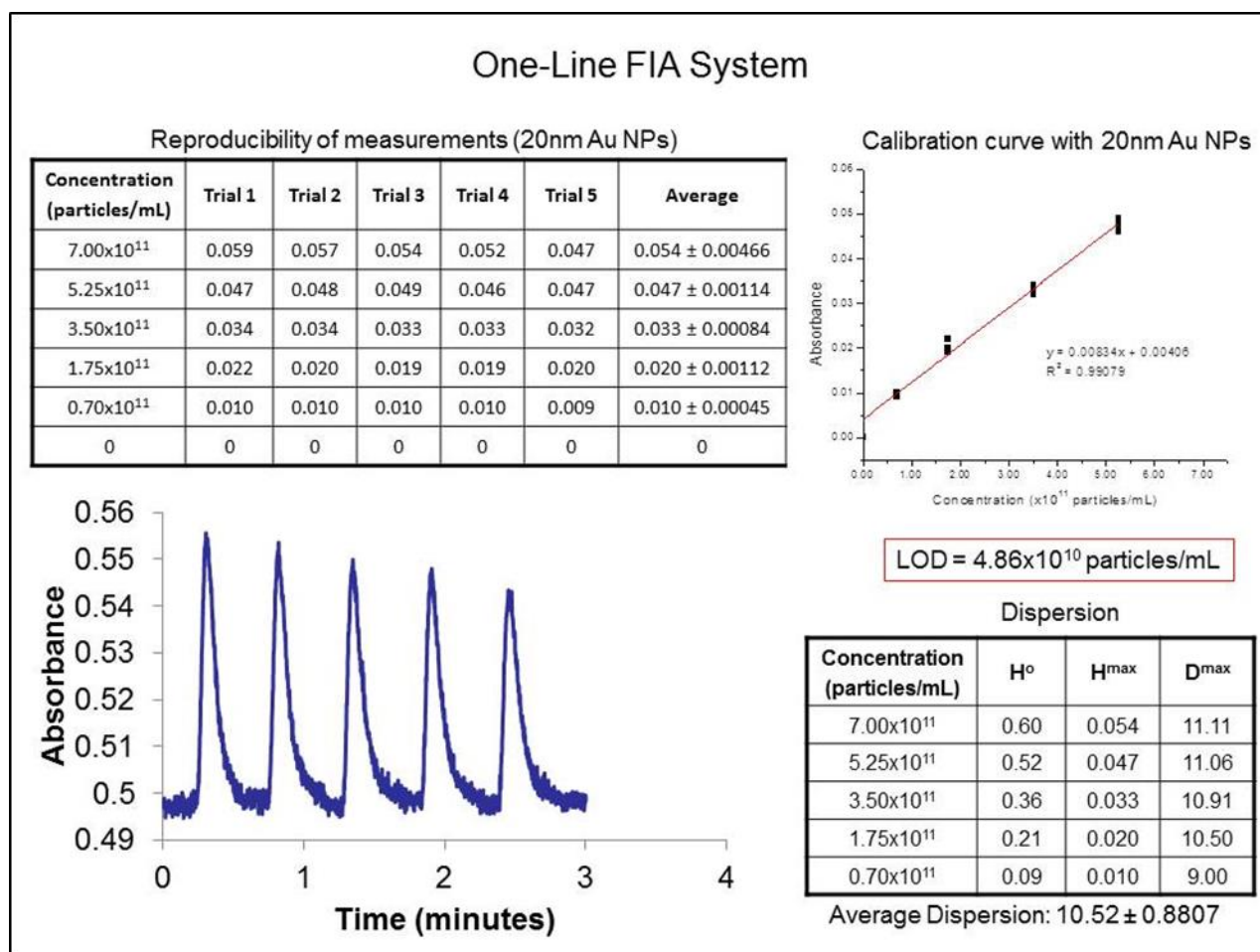


Figure A2. Analytical Figures of Merit of a one-line FIA system using gold nanoparticles as an analyte for performance testing.

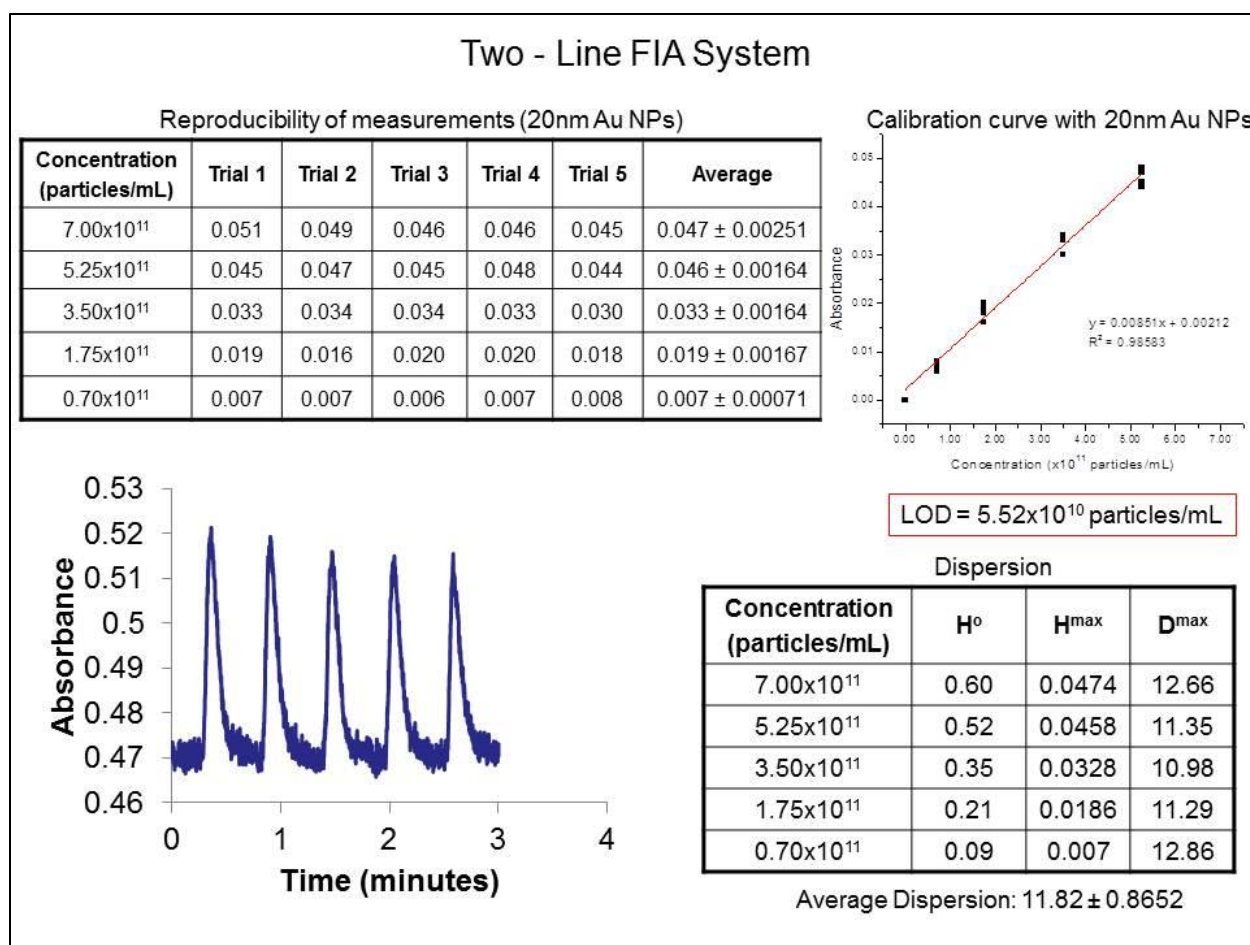


Figure A3. Analytical Figures of Merit of a two-line FIA system using gold nanoparticles as an analyte for performance testing.

## **APPENDIX C: PUBLISHER PERMISSIONS**

**SPRINGER NATURE LICENSE  
TERMS AND CONDITIONS**

Mar 21, 2019

---

This Agreement between Mr. Khang Trieu ("You") and Springer Nature ("Springer Nature") consists of your license details and the terms and conditions provided by Springer Nature and Copyright Clearance Center.

License Number	4553740690315
License date	Mar 21, 2019
Licensed Content Publisher	Springer Nature
Licensed Content Publication	Microchimica Acta
Licensed Content Title	An indium tin oxide electrode modified with gold nanorods for use in potential-controlled surface plasmon resonance studies
Licensed Content Author	Emily C. Heider, Khang Trieu, Victor M. Diaz et al
Licensed Content Date	Jan 1, 2013
Licensed Content Volume	180
Licensed Content Issue	11
Type of Use	Thesis/Dissertation
Requestor type	academic/university or research institute
Format	print and electronic
Portion	full article/chapter
Will you be translating?	no
Circulation/distribution	<501
Author of this Springer Nature content	yes
Title	DETECTION OF MERCURY THROUGH SURFACE PLASMON RESONANCE OF IMMOBILIZED GOLD NANORODS
Institution name	University of Central Florida
Expected presentation date	Apr 2019
Requestor Location	Mr. Khang Trieu 9209 Amity Court  ORLANDO, FL 32817 United States Attn: Mr. Khang Trieu
Total	0.00 USD
Terms and Conditions	

**Springer Nature Terms and Conditions for RightsLink Permissions**  
**Springer Nature Customer Service Centre GmbH (the Licensor)** hereby grants you a non-exclusive, world-wide licence to reproduce the material and for the purpose and requirements specified in the attached copy of your order form, and for no other use, subject to the conditions below:

1. The Licensor warrants that it has, to the best of its knowledge, the rights to license reuse of this material. However, you should ensure that the material you are requesting is original to the Licensor and does not carry the copyright of another entity (as credited in the published version).

If the credit line on any part of the material you have requested indicates that it was reprinted or adapted with permission from another source, then you should also seek permission from that source to reuse the material.

2. Where **print only** permission has been granted for a fee, separate permission must be obtained for any additional electronic re-use.
3. Permission granted **free of charge** for material in print is also usually granted for any electronic version of that work, provided that the material is incidental to your work as a whole and that the electronic version is essentially equivalent to, or substitutes for, the print version.
4. A licence for 'post on a website' is valid for 12 months from the licence date. This licence does not cover use of full text articles on websites.
5. Where '**reuse in a dissertation/thesis**' has been selected the following terms apply: Print rights of the final author's accepted manuscript (for clarity, NOT the published version) for up to 100 copies, electronic rights for use only on a personal website or institutional repository as defined by the Sherpa guideline ([www.sherpa.ac.uk/romeo/](http://www.sherpa.ac.uk/romeo/)).
6. Permission granted for books and journals is granted for the lifetime of the first edition and does not apply to second and subsequent editions (except where the first edition permission was granted free of charge or for signatories to the STM Permissions Guidelines <http://www.stm-assoc.org/copyright-legal-affairs/permissions/permissions-guidelines/>), and does not apply for editions in other languages unless additional translation rights have been granted separately in the licence.
7. Rights for additional components such as custom editions and derivatives require additional permission and may be subject to an additional fee. Please apply to [Journalpermissions@springernature.com](mailto:Journalpermissions@springernature.com)/[bookpermissions@springernature.com](mailto:bookpermissions@springernature.com) for these rights.
8. The Licensor's permission must be acknowledged next to the licensed material in print. In electronic form, this acknowledgement must be visible at the same time as the figures/tables/illustrations or abstract, and must be hyperlinked to the journal/book's homepage. Our required acknowledgement format is in the Appendix below.
9. Use of the material for incidental promotional use, minor editing privileges (this does not include cropping, adapting, omitting material or any other changes that affect the meaning, intention or moral rights of the author) and copies for the disabled are permitted under this licence.
10. Minor adaptations of single figures (changes of format, colour and style) do not require the Licensor's approval. However, the adaptation should be credited as shown in Appendix below.



**Title:** Portable mercury sensor for tap water using surface plasmon resonance of immobilized gold nanorods

**Author:** Emily C. Heider, Khang Trieu, Anthony F.T. Moore, Andres D. Campiglia

**Publication:** Talanta

**Publisher:** Elsevier

**Date:** 15 September 2012

Copyright © 2012 Elsevier B.V. All rights reserved.

Logged in as:

Khang Trieu

LOGOUT

Please note that, as the author of this Elsevier article, you retain the right to include it in a thesis or dissertation, provided it is not published commercially. Permission is not required, but please ensure that you reference the journal as the original source. For more information on this and on your other retained rights, please visit: <https://www.elsevier.com/about/our-business/policies/copyright#Author-rights>



**Title:** Gold nanorods for surface Plasmon resonance detection of mercury (II) in flow injection analysis

**Author:** Khang Trieu, Emily C. Heider, Scott C. Brooks, Fernando Barbosa, Andres D. Campiglia

**Publication:** Talanta

**Publisher:** Elsevier

**Date:** 1 October 2014

Copyright © 2014 Elsevier B.V. Published by Elsevier B.V. All rights reserved.

Logged in as:

Khang Trieu

LOGOUT

Please note that, as the author of this Elsevier article, you retain the right to include it in a thesis or dissertation, provided it is not published commercially. Permission is not required, but please ensure that you reference the journal as the original source. For more information on this and on your other retained rights, please visit: <https://www.elsevier.com/about/our-business/policies/copyright#Author-rights>



## REFERENCES

- [1] Wang, Q.; Kim, D.; Dionysiou, D.D.; Sorial, G.A.; Timberlake, D. Sources and remediation for mercury contamination in aquatic systems--a literature review. *Environmental Pollution*, **2004**, 131(2), 323.
- [2] Taylor, D.L.; Kutil, N.J.; Malek, A.J.; Collie, J.S. Mercury bioaccumulation in cartilaginous fishes from Southern New England coastal waters: Contamination from a trophic ecology and human health perspective. *Marine Environmental Research*, **2014**, 99, 20-33.
- [3] [https://www.epa.gov/sites/production/files/2016-06/documents/npwdr\\_complete\\_table.pdf](https://www.epa.gov/sites/production/files/2016-06/documents/npwdr_complete_table.pdf)
- [4] Gad, S.C.; Pham, T. Mercury. *Encyclopedia of Toxicology*, 3rd ed.; Oxford Academic Press: Oxford, UK, **2014**.
- [5] Tchounwou, P.B.; Ayensu, W.K.; Ninashvili, N.; Sutton, D. Environmental Exposure to Mercury and its Toxicopathologic Implication for Public Health. *Environmental Toxicology*, **2003**, 18, 149.
- [6] National Research Council. *Toxicological Effects of Methylmercury*; The National Academies Press: Washington, DC, **2000**.
- [7] Ke, J.; Li, X.; Zhao, Q.; Hou, Y.; Chen, J. Ultrasensitive Quantum Dot Fluorescence Quenching Array for Selective Detection of Mercury Ions in Drinking Water. *Scientific Reports*, **2014**, 4, 5624.
- [8] Gil, D.; Rodriguez-Caceres, M.; Hurtado-Sanchez, M.; De La Pena, A. Fluorescence Determination of  $\text{Hg}^{2+}$  in Water and Fish Samples using a Chemodosimeter based in a Rhodamine 6G Derivative and a Portable Fiber-Optic Spectrofluorimeter. *Applied Spectroscopy*, **2010**, 64, 520.
- [9] Powell, M.J.; Quan, E.S.; Boomer, D.W. Inductively Coupled Plasma Mass Spectroscopy with Direct Injection Nebulization for Mercury Analysis of Drinking Water. *Analytical Chemistry*, **1992**, 64, 2253.

- [10] WHO, 2004. Guidelines for Drinking-water Quality. Vol. 1: 3rd ed., Geneva, World Health Organization
- [11] Asante, K.A.; Agusa, T.; Subramanian, A.; Ansa-Asare, O.D.; Biney, C.A.; Tanabe, S. Contamination Status of Arsenic and other Trace Elements in Drinking Water and Residents from Tarkwa, a Historic Mining Township in Ghana. *Chemosphere*, **2007**, 66, 1513.
- [12] Jakhu, R.; Mehra, R. Risk Estimation and Multivariate Statistical Analysis of the Heavy Metal Content of Drinking Water Samples. *Toxicology and Industrial Health*, **2018**, 34, 714.
- [13] Cuculic, V.; Cukrov, N.; Kwokal, Z.; Strmecki, S.; Plavsic, M. Assessing Trace Metal Contamination and Organic Matter in the Brackish Lakes as a Major Source of Potable Water. *Environmental Geochemistry and Health*, **2018**, 40, 489.
- [14] Hatch and Ott reference W.R. Hatch and W.L. Ott, *Anal. Chim. Acta* **40**, 2085–7
- [15] Girard, J.E. *Principles of Environmental Chemistry*; Jones and Bartlett Publishers: Sudbury, MA, **2005**.
- [16] Ziaei, E.; Mehdinia, A.; Jabbari, A. A Novel Hierarchical Nanobiocomposite of Graphene Oxide-Magnetic Chitosan Grafted with Mercapto as a Solid Phase Extraction Sorbent for the Determination of Mercury Ions in Environmental Water Samples. *Analytica Chimica Acta*, **2014**, 850, 49.
- [17] Shabani, A.M.; Dadfarnia, S.; Nasirizadeh, N. Speciation Analysis of Mercury in Water Samples by Cold Vapor Atomic Absorption Spectrometry after Preconcentration with Dithizone Immobilized on Microcrystalline Napthalene. *Analytical and Bioanalytical Chemistry*, **2004**, 378, 1388.
- [18] Yordanova, T.; Dakova, I.; Balashev, K.; Karadjova, I. Polymeric Ion-imprinted Nanoparticles for Mercury Speciation in Surface Waters. *Microchemical Journal*, **2014**, 113, 42.
- [19] Stanis, E.; Werner, J.; Matusiewicz, H. Mercury Species Determination by Task Specific Ionic Liquid-based Ultrasound-assisted Dispersive Liquid-liquid Microextraction

- Combined with Cold Vapor Atomic Absorption Spectrometry. *Microchemical Journal*, **2013**, *110*, 28.
- [20] Kallithrakas-Kontos, N.; Foteinis, S. Recent Advances in the Analysis of Mercury in Water – Review. *Current Analytical Chemistry*, **2016**, *12*, 22.
- [21] Chen, X.; Han, C.; Cheng, H.; Wang, Y.; Liu, J.; Xu, Z.; Hu, L. Rapid Speciation of Mercury in Seawater and Marine Fish by Cation Exchange Chromatography Hyphenated with Inductively Coupled Plasma Mass Spectrometry. *Journal of Chromatography A*, **2013**, *1314*, 86.
- [22] Cheng, H.; Wu, C.; Shen, L.; Liu, J.; Xu, Z. Online Anion Exchange Column Preconcentration and High Performance Liquid Chromatographic Separation with Inductively Coupled Plasma Mass Spectroscopy for Mercury Speciation Analysis. *Analytica Chimica Acta*, **2014**, 828, 9.
- [23] Jia, X.Y.; Gong, D.R.; Han, Y.; Wei, C.; Duan, T.C.; Chen, H.T. Fast Speciation of Mercury in Seawater by Short-column High Performance Liquid Chromatography Hyphenated to Inductively Coupled Plasma Spectrometry after On-line Cation Exchange Column Preconcentration. *Talanta*, **2012**, *88*, 724.
- [24] Wu, Y.; Lee, Y.; Wu, L.; Hou, X. Simple Mercury Speciation Analysis by CVG-ICP-MS Following TMAH Pre-treatment and Microwave-assisted Digestion. *Microchemical Journal*, **2012**, *103*, 105.
- [25] Zhao, Y.; Zheng, J.; Fang, L.; Lin, Q.; Wu, Y.; Xue, Z.; Fu, F. Speciation Analysis of Mercury in Natural Water and Fish Samples by using Capillary Electrophoresis-inductively Coupled Plasma Mass Spectrometry. *Talanta*, **2012**, *89*, 280.
- [26] Kempegowda, R.G.; Malingappa, P. Diazonium Functionalized Exfoliated Graphitic Carbon as a Binderless and Covalently Modified Electrochemical Interface for Mercury Sensing. *Sensors and Actuators B*, **2013**, *186*, 478.
- [27] Gong, J.; Zhou, T.; Song, D.; Zhang, L.; Hu, X. Stripping Voltammetric Detection of Mercury(II) based on a Bimetallic Au-Pt Inorganic-Organic Hybrid Nanocomposite Modified Glassy Carbon Electrode. *Analytical Chemistry*, **2010**, *82*, 567.

- [28] Punrat, E.; Chuanuwatanakul, S.; Kaneta, T.; Motomizu, S.; Chailapakul, O. Method Development for the Determination of Mercury(II) by Sequential Injection/Anodic Stripping Voltammetry using an *in situ* Gold-film Screen-printed Carbon Electrode. *Journal of Electroanalytical Chemistry*, **2014**, 727, 78.
- [29] Faraday M. The Bakerian Lecture: Experimental Relations of Gold (and Other Metals) to Light. *Philosophical Transactions of the Royal Society London*, **1847**, 147, 159.
- [30] Rycenga, M.; Cobley, C.M.; Zeng, J.; Li, W.; Moran, C.H.; Zhang, Q.; Qin, D.; Xia, Y. Controlling the Synthesis and Assembly of Silver Nanostructures for Plasmonic Applications. *Chemical Reviews*, **2011**, 111, 3669.
- [31] Mie, G. Beiträge zur Optik trüber Medien, speziell kolloidaler Metallösungen. *Annalen der Physik*, **1908**, 25, 377.
- [32] Kelly, K.L.; Coronado, E.; Zhao, L.L.; Schatz, G.C. The Optical Properties of Metal Nanoparticles: The Influence of Size, Shape, and Dielectric Environment. *The Journal of Physical Chemistry B*, **2003**, 107, 668.
- [33] Zeman, E.; Schatz, G.C. An Accurate Electromagnetic Theory Study of Surface Enhancement Factors for Silver, Gold, Copper, Lithium, Sodium, Aluminum, Gallium, Indium, Zinc, and Cadmium. *The Journal of Physical Chemistry*, **1987**, 91, 634.
- [34] Gans, G. Über die Form ultramikroskopischer Goldteilchen. *Annalen der Physik*, **1912**, 342, 881.
- [35] Ru, E. L.; Etchegoin, P. *Principles of Surface Enhanced Raman Spectroscopy*; Elsevier: Oxford, UK, **2009**.
- [36] Nikoobakht B.; El-Sayed M.A. Preparation and Growth Mechanism of Gold Nanorods (NRs) Using Seed-mediated Growth Method. *Chemistry of Materials*, **2003**, 15, 1957.
- [37] Alvarez-Puebla R.A.; Agarwal A.; Manna P.; Khanal B.P.; Aldeanueva-Potl P.; Carbo-Argibay E.; Pazos-Perez N.; Viggderman L.; Zubarev E.R.; Kotov N.A.; Liz-Marzan L.M.

Gold Nanorods 3D-Supercrystals as Surface Enhanced Raman Scattering Spectroscopy Substrates for the Rapid Detection of Scrambled Prions. *PNAS*, **2011**, *108*, 8157.

- [38] Nikoobakht B.; El-Sayed M.A. Surface-Enhanced Raman Scattering Studies on Aggregated Gold Nanorods. *The Journal of Physical Chemistry A*, **2003**, *107*, 3372.
- [39] Nusz G.J.; Marinakos S.M.; Curry A.C.; Dahlin A.; Hook F.; Wax A.; Chilkoti A. Label-Free Plasmonic Detection of Biomolecular Binding by a Single Gold Nanorod. *Analytical Chemistry*, **2008**, *80*, 984.
- [40] Caswell K.K.; Wilson J.N.; Bunz U.H.F.; Murphy C.J. Preferential End-to-End Assembly of Gold Nanorods by Biotin–Streptavidin Connectors. *Journal of the American Chemical Society*, **2003**, *125*, 13914.
- [41] Chang, J.; Wu, H.; Chen, H.; Ling, Y.; Tan, W. Oriented Assembly of Au Nanorods Using Biorecognition System. *Chemical Communications*, **2005**, *8*, 1092.
- [42] Rex, M.; Hernandez, F.E.; Campiglia, A.D. Pushing the Limits of Mercury Sensors with Gold Nanorods. *Analytical Chemistry*, **2006**, *78*, 445.
- [43] Johnson, C.J.; Dujardin, E.; Davis, S.A.; Murphy, C.J.; Mann, S. Growth and Form of Gold Nanorods Prepared by Seed-mediated, Surfactant-directed Synthesis. *Journal of Materials Chemistry*, **2002**, *12*, 1765.
- [44] Gao, J.; Bender, C.M.; Murphy, C.J. Dependence of the Gold Nanorod Aspect Ratio on the Nature of the Directing Surfactant in Aqueous Solution. *Langmuir*, **2003**, *19*, 9065.
- [45] Wu, Y.; Liu, L.; Zhan, S.; Wang, F.; Zhou, P. Ultrasensitive Aptamer Biosensor for Arsenic(III) Detection in Aqueous Solution based on Surfactant-induced Aggregation of Gold Nanoparticles. *Analyst*, **2012**, *137*, 4171.
- [46] Ratnarathorn, N.; Chailapakul, O.; Dungchai, W. Highly Sensitive Colorimetric Detection of Lead using Maleic Acid Functionalized Gold Nanoparticles. *Talanta*, **2015**, *132*, 613.

- [47] Lakatos, M.; Matys, S.; Raff, J.; Pompe, W. Colorimetric As(V) Detection based on S-layer Functionalized Gold Nanoparticles. *Talanta*, **2015**, *144*, 241.
- [48] Cai, H.; Lin, D.; Wang, J.; Yang, P.; Cai, J. Controlled Side-by-side Assembly of Gold Nanorods: A Strategy for Lead Detection. *Sensors and Actuators B*, **2014**, *196*, 252.
- [49] Diegoli, S.; Manciuola, A.L.; Begum, S.; Jones, I.P.; Lead, J.R.; Preece, J.A. Interaction Between Manufactured Gold Nanoparticles and Naturally Occuring Organic Macromolecules. *Science of the Total Environment*, **2008**, *402*, 51.
- [50] Stankus, D.P.; Lohse, S.E.; Hutchison, J.E.; Nason, J.A. Interactions Between Natural Organic Matter and Gold Nanoparticles Stabilized with Different Organic Capping Agents. *Environmental Science and Technology*, **2011**, *45*, 3238.
- [51] Nikoobakht, B.; Wang, Z.L.; El-Sayed, M.A. Self-assembly of Gold Nanorods. *The Journal of Physical Chemistry B*, **2000**, *104*, 8635.
- [52] Sethi, M.; Joung, G.; Knecht, M.R. Stability and Electrostatic Assembly of Au Nanorods for Use in Biological Assays. *Langmuir*, **2009**, *25*, 317.
- [53] Heider, E.C.; Trieu, K.; Moore, A.F.; Campiglia, A.D. Portable Mercury Sensor for Tap Water using Surface Plasmon Resonance of Immobilized Gold Nanorods. *Talanta*, **2012**, *99*, 180.
- [54] Okamoto, T.; Yamaguchi, I. Local Plasmon Sensor with Gold Colloid Monolayers Deposited upon Glass Substrates. *Optics Letters*, **2000**, *25*, 372.
- [55] Westcott, S.L.; Oldenburg, S.J.; Lee, T.R.; Halas, N.J. Formation and Adsorption of Clusters of Gold Nanoparticles onto Functionalized Silica Nanoparticle Surfaces. *Langmuir*, **1998**, *14*, 5396.
- [56] Goss, C.A.; Charych, D.H.; Majda, M. Application of (3-Mercaptopropyl)trimethoxysilane as a Molecular Adhesive in the Fabrication of Vapor-Deposited Gold Electrodes on Glass Substrates. *Analytical Chemistry*, **1991**, *63*, 85.

- [57] Danzer, K.; Currie, L.A. Guideline for Calibration in Analytical Chemistry – Part 1. Fundamentals and Single Component Calibration. *Pure and Applied Chemistry*, **1998**, *70*, 993.
- [58] Currie, L.A. Nomenclature in Evaluation of Analytical Methods Including Detection and Quantification Capabilities – International Union of Pure and Applied Chemistry. *Pure and Applied Chemistry*, **1995**, *67*, 1699.
- [58] Wu, X.; Liu, L.; Yu, T.; Yu, L.; Xie, Z.; Mo, Y.; Xu, S. Ma. Y Gold Nanoparticles Modified ITO Anode for Enhanced PLEDs Brightness and Efficiency. *Journal of Materials Chemistry C*, **2013**, *1*, 7020.
- [59] Chen, Z.; Zu, Y. Gold Nanoparticle-Modified ITO Electrode for Electrogenenerated Chemiluminescence: Well-Preserved Transparency and Highly Enhanced Activity. *Langmuir*, **2007**, *23*, 11387.
- [60] Chen, F.; Fei, W.; Sun, L.; Li, Q.; Di, J.; Wu, Y. Direct Growth of Coupled Gold Nanoparticles on Indium Tin Oxide Substrate and Construction of Biosensor based on Localized Surface Plasmon Resonance. *Sensors and Actuators B*, **2014**, *191*, 337.
- [61] Hu, T.; Lin, Y.; Yan, J.; Di, J. Synthesis of Hollow Gold Nanoparticles on the Surface of Indium Tin Oxide Glass and their Application for Plasmonic Biosensor. *Spectrochimica Acta Part A*, **2013**, *110*, 72.
- [62] Yang, J.; Strickler, R.; Gunasekaran, S. Indium Tin Oxide-coated Glass Modified with Reduced Graphene Oxide Sheets and Gold Nanoparticles as Disposable Working Electrodes for Dopamine Sensing in Meat Samples. *Nanoscale*, **2012**, *4*, 4594.
- [63] Xiong, W.; Qu, Q.; Liu, S. Self-assembly of Ultra-small Gold Nanoparticles on an Indium Tin Oxide Electrode for the Enzyme-free Detection of Hydrogen Peroxide. *Microchimica Acta*, **2014**, *181*, 983.
- [64] Zhou, N.; Chen, H.; Li, J.; Chen, L. Highly Sensitive and Selective Voltammetric Detection of Mercury(II) using an ITO Electrode Modified with 5-methyl-2-thiouracil, Graphene Oxide and Gold Nanoparticles. *Microchimica Acta*, **2013**, *180*, 493.

- [65] Cheng, W.; Dong, S.; Wang, E. Gold Nanoparticles as Fine Tuners of Electrochemical Properties of the Electrode/Solution Interface. *Langmuir*, **2002**, *18*, 9947.
- [66] Heider, E.C.; Trieu, K.; Diaz, V.M.; Chumbimuni-Torres, K.Y.; Campiglia, A.D.; Duranceau, S.J. An Indium Tin Oxide Electrode Modified with Gold Nanorods for use in Potential-controlled Surface Plasmon Resonance Studies. *Microchimica Acta*, **2013**, *180*, 1013.
- [67] Ferhan, A.R.; Guo, L.; Kim, D. Influence of Ionic Strength and Surfactant Concentration on Electrostatic Surface Assembly of Cetyltrimethylammonium Bromide-capped Gold Nanorods on Fully Immersed Glass. *Langmuir*, **2010**, *26*, 12433.
- [68] Hillebrandt, H.; Tanaka, M. Electrochemical Characterization of Self-Assembled Alkylsiloxane Monolayers on Indium-Tin Oxide (ITO) Semiconductor Electrodes. *The Journal of Physical Chemistry B*, **2001**, *105*, 4270.
- [69] Ballarin, B.; Cassani, M.C.; Scavetta, E.; Tonelli, D. Self-assembled Gold Nanoparticles Modified ITO Electrodes: The Monolayer Binder Molecule Effect. *Electrochimica Acta*, **2008**, *53*, 8034.
- [70] Muthurasu, A.; Ganesh, V. Electrochemical Characterization of Self-assembled Monolayers (SAMs) of Silanes on Indium Tin Oxide (ITO) Electrodes – Tuning Electron Transfer Behavior Across Electrode-electrolyte Interface. *Journal of Colloid and Interface Science*, **2012**, *374*, 241.
- [71] Jung, C.C.; Saban, S.B.; Yee, S.S.; Darling, R.B. Chemical Electrode Surface Plasmon Resonance Sensor. *Sensors and Actuators B*, **1996**, *32*, 143.
- [72] Chinowsky, T.M.; Saban, S.B.; Yee, S.S. Experimental Data from a Trace Metal Sensor Combining Surface Plasmon Resonance with Anodic Stripping Voltammetry. *Sensors and Actuators B*, **1996**, *35*, 37.
- [73] Heaton, R.J.; Peterson, A.W.; Georgiadis, R.M. Electrostatic Surface Plasmon Resonance: Direct Electric Field-induced Hybridization and Denaturation in Monolayer Nucleic Acid Films and Label-free Discrimination of Base Mismatches. *PNAS*, **2001**, *98*, 3701.



- [74] Finot, M.O.; Braybrook, G.D.; McDermott, M.T. Characterization of Electrochemically Deposited Gold Nanocrystals on Glassy Carbon Electrodes. *Journal of Electroanalytical Chemistry*, **1999**, 466, 234.
- [75] Welch, C.M.; Nekrassova, O.; Dai, X.; Hyde, M.E.; Compton, R.G. Fabrication, Characterisation and Voltammetric Studies of Gold Amalgam Nanoparticle Modified Electrodes. *ChemPhysChem*, **2004**, 5, 1405.
- [76] Trasatti, S.; Petrii, O.A. Real Surface Area Measurements in Electrochemistry. *Pure and Applied Chemistry*, **1991**, 63, 711.
- [77] Iwasaki, Y.; Horiuchi, T.; Morita, M.; Niwa, O. Time Differential Surface Plasmon Resonance Measurements Applied for Electrochemical Analysis. *Electroanalysis*, **1997**, 9, 1239.
- [78] Mulvaney, P.; Perez-Juste, J.; Giersig, M.; Liz-Marzan, L.M.; Pecharroman, C. Drastic Surface Plasmon Mode Shifts in Gold Nanorods due to Electron Charging. *Plasmonics*, **2006**, 1, 61.
- [79] Novo, C.; Funston, A.M.; Gooding, A.K.; Mulvaney, P. Electrochemical Charging of Single Gold Nanorods. *Journal of the American Chemical Society*, **2009**, 131, 14664.
- [80] Růžička, J.; Hansen, H.J. *Flow Injection Analysis*; Wiley-Interscience: Hoboken, NJ, **1988**.
- [81] Valcarcel, M.; Luque de Castro, M.D. *Flow-Injection Analysis Principles and Applications*; Ellis Horwood Limited: Chichester, England, **1987**.
- [82] Hanna, C.P.; Tyson, J.F.; McIntosh, S. Determination of Total Mercury in Waters and Urine by Flow Injection Atomic Absorption Spectrometry Procedures Involving On- and Off-line Oxidation of Organomercury Species. *Analytical Chemistry*, **1993**, 65, 653.
- [83] Tao, G.; Willie, S.N. Determination of Total Mercury in Biological Tissues by Flow Injection Cold Vapour Generation Atomic Absorption Spectrometry Following Tetramethylammonium Hydroxide Digestion. *Analyst*, **1998**, 123, 1215.

- [84] Aduna de Paz, A.; Alegria, A.; Barbera, R.; Ferre, R.; Largada, M.J. Determination of Mercury in Dry-fish Samples by Microwave Digestion and Flow Injection Analysis Cold Vapor Atomic Absorption Spectrometry, *Food Chemistry*, **1997**, 58, 169.
- [85] Trieu, K.; Heider, E.C.; Brooks, S.C.; Barbosa, F.; Campiglia, A.D. Gold Nanorods for Surface Plasmon Resonance Detection of Mercury (II) in Flow Injection Analysis. *Talanta*, **2014**, 128, 196.
- [86] Perez-Juste, J.; Pastoriza-Santos, I.; Liz-Marzan, L.M.; Mulvaney, P. Gold Nanorods: Synthesis, Characterization and Applications. *Coordination Chemistry Reviews*, **2005**, 249, 1870.
- [87] Davis, A.; Kotz, S.; Read, C.B.; Balakrishnan, N.; Vidakovic, B. *Encyclopedia of Statistical Sciences*; John Wiley: New York, **1983**.
- [88] Habashi, Fathi. *Handbook of Extractive Metallurgy*; Wiley-Vch: Weinheim, Germany, **1997**.
- [89] Zaleski-Ejgierd, P.; Pyykko, P.  $\text{Au}_n\text{Hg}_m$  Clusters: Mercury Aurides, Gold Amalgams, or van der Waals Aggregates? *The Journal of Physical Chemistry A*, **2009**, 113, 12380.
- [90] <https://www-s.nist.gov/srmors/certificates/1640a.pdf>